DC Interruption Principle Using a Helical Arc Arrangement

A Thesis submitted to the University of Liverpool
for the degree of Doctor in Philosophy
in the Faculty of Engineering

By
Hassan Yousef Elzagzoug
Department of Electrical Engineering & Electronics

2013

Abstract

Electrical discharges have been used extensively in devices for interruption of fault currents. Much work has investigated the use of arc discharges for interrupting DC current. The problem with DC current is that there is no natural current zero where thermal losses from the arc dominate thus leading to arc extinction and the interruption of fault current.

Helical arc been arranged by using splitter blades to separate the arc turns.

The expansion of a helical arc confined between polymeric splitter blades is governed by both electromagnetic and aerodynamic forces. These arise due to the complex interaction between the individual arc turns, arc/ splitter blade interactions and surrounding media. These interactions can be exploited to control the rate of expansion. During this expansion stage there is a substantial increase in arc voltage which in low voltage systems can limit the current thereby causing current interruption providing the arc quenching conditions are suitable.

An experimental study has been undertaken to assess the fundamental characteristics of helical arcs confined between different arrangements of PTFE, PE and copper blades in three different sizes (180mm, 360mm and 500mm). Significant improvements in arc current limitation and interruption capability are observed when the arc voltage increases. A substantial increase in arc voltage was observed for all combinations of copper/ PTFE splitter blades. It was noted

that the prospective fault current is forced to near zero when copper blades are used in conjunction with PTFE blades. With the larger PTFE and PE blades sized 360mm and 500mm, it was observed that the arc stayed within the limit of blades, thus providing better arc control capability.

Simplified modelling of the forces acting on the arc (electromagnetic, aerodynamic) have been assessed. The electromagnetic forces act not only to produce radial expansion of the arc but also to keep alignment between the turns. The generation of the aerodynamic forces is very complex to model and indeed the modelling presented can only be used indicatively in any analysis at this stage. The work indicates that a compact DC interruption device may be possible based on the confinement of the plasma within the splitter blades and interaction with polymeric material.

Contents

List of Figures

List of Tables

Acknowledgement

During this PhD research project in the University of Liverpool has been my enjoyable and memorable experience. Here, I would like to appreciate the following:

I wish to express my sincere thanks to my supervisor, Prof. J. Spencer, for his steady support and patient guidance throughout the research period. He helped me to develop my background and provided the helpful suggestions till the last moment of my thesis.

I am very grateful to Mr J. Humphries, for his valuable assistance in setting up experiments and interpreting the results, practically when I first began this work.

Special thanks to Dr A. G. Deakin and Dr D. H. Smith, who gave me lots of valuable advice, suggestions and fruitful discussions, as well as help with proofreading.

I am also truly indebted and thankful to research group and my best friends, who were always willing to help. They gave me their best suggestions and help which made this work possible.

Last but not least, I wish to thank my parents as well as my uncle Dr Mohammad Al-Sharkawi for their warm encouragements, patience and support, which help me to complete this work.

Chapter 1

Background

1.1 Introduction

Electric arc discharges are utilised in AC circuit breakers to interrupt current in electrical networks [Flurscheim, 1982] [Ragaller, 1978]. The designs of these circuit breakers have been optimised to achieve arc extinction, thereby current interruption, as efficiently as possible to avoid excessive damage to electrodes and nozzles. As well as performing current interruption, which occurs when the current reaches zero, circuit breakers are also designed to withstand the rate of rise of recovery voltage (RRRV). However, in the case of DC current interruption [Shiba et al., 2011] [Ryan, 2012], the means of arc extinction is complicated by the lack of a natural current zero because the DC cycle consists of positive half-cycles compared with AC's positive followed by negative half cycles.

In DC circuit breakers a forced current zero is created either by the arc voltage exceeding the system voltage (for low voltage system) [Browne, 1984] or through an artificial current zero created by a resonant circuit close to the interrupter (for high voltage systems) [Ryan, 2001] [Garrard, 1976]. Traditionally for high

voltages, circuit breakers designed for AC current interruption have been modified and used alongside a resonant circuit [Gallagher and Pearmain, 1983]. However, such devices only have relatively short arc lengths and therefore have limited applications where there is a requirement to limit the DC fault level current prior to arc extinction in order to lessen the potential for damage. One of the aims of this research is therefore to investigate possibilities for DC circuit breakers.

Helical arc devices have been the subject of research [Ennis et al., 1995] [Afanasiev et al., 1981] as a possible means of limiting the potential for damage to a network when a DC fault develops. They achieve successful arc interruption and have the potential of withstanding the RRRV after current interruption due in part to the long arc lengths which can be produced in the helix.

In summary, the problems to be addressed in this thesis are that:

[A] DC interruption has no current zero. There is therefore a need to either force current to zero by increasing voltage or to use a resonant circuit. Also, arc length are too short to successfully interrupt the current.

[B] Helical blades may be used to extend the arc length but system developed so far have problems with inter-blade shorting, so extending arc length might assist with addressing the problem.

1.2 Literature Review

This section traces the development of circuit breaker evolution and reviews the properties of electric arcs that the breakers interrupt as well as arc modelling approaches (1.2.1 to 1.2.6). With direct current, there are additional problems in achieving arc extinction (1.2.7 to 1.2.8), i.e. current zero, even with different polymers (1.2.9). Two methods have been tried for DC interruption mainly,

namely arc elongation and decreasing arc diameter (1.2.8). This work examines a third method, namely arc shorting using helical blades, which combines aspects of the first two methods for arc elongation and constraining (helical) arc radius, together with two kinds of polymers separately, Polytetrafluoroethylene and polyethylene (PTFE and PE).

1.2.1 Circuit Breaker Evolution

Electromagnetic arc control can, disputably, be described as the oldest existing form of circuit interruption technique. In earlier times, the operator of manually-operated circuit breakers was required simply to pull two contacts apart using a long 'stick': the arc then moves along arcing horns until its elongation was sufficient to extinguish the current. Such devices were used to interrupt relatively small load currents, and it was around the turn of the century, the need to interrupt fault currents began to affect the course of circuit breaker development. The origin of the next step, the oil filled circuit breaker, is apparently still unknown [Lythall and Worth, 1972], but by around 1930 it was established as the pre-eminent circuit interruption technique. The principle behind the oil-filled interrupters is the arc vaporises the oil around it and the resulting gas blast causes the elongation of the arc, increasing its resistance. In the case of an alternating current supply, the current reduces to zero, fresh oil fills the extinction chamber, providing the material for the next blast and eventually the arc is extinguished. However, as electricity supply voltages and fault current levels increased, these self-generated gas blasts were unable to interrupt the resultant arcs and a more powerful gas blast was required.

Air blast circuit breakers were initially introduced, in the UK, only in applications where the voltage levels are very high because of the cost and complexity

of their associated compressors and pipe work. The arrival of SF_6 as an interrupting medium in the 1950's and 60's, and the consequent reduction in the gas pressures required, meant that gas blast techniques could become more cost competitive into oil, but the main motivation to abandon oil has been related to personnel safety. In a survey by Midlands Electricity [Carabok et al., 1994] they estimated that the risk of serious injury from oil-filled circuit breakers was from five to eight times greater than with SF_6 units. Moreover, the nature of the likely injuries such as severe burns makes oil increasingly unacceptable in modern industrial plant. However, a cheaper alternative to gas blast was still required, leading, in the 1970's to the gas puffer circuit breaker. In gas puffers, a hydraulic or pneumatic drive is required to move the contacts, but these too lead to both relatively high cost and complex mechanisms, so that they are too expensive to use at medium voltage levels. Rotating arcs were introduced to medium voltage circuit breakers in the late seventies/early eighties, and are now found at both 11 and 33kV, while increasingly they are being exploited within other types of interrupter, either to improve gas mixing, reduce contact wear or both [Plessl and Poole, 1987] [Bernard et al., 1990].

1.2.2 Electric Arcs

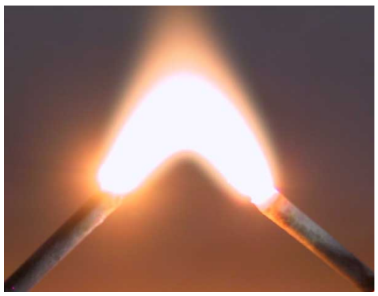

Figure 1.1: Electric arc

Generation of electrical arc results in electrical breakdown of a gas producing

ongoing plasma discharges, resulting from a current flowing through normally nonconductive media such as air. From the various shapes of electric arc, emergent properties of nonlinear patterns of current and electric field are obtained. The arc generally generates in the gas-filled space between two conductive electrodes and upon generation the temperature increases, and the rise in temperature is capable of melting or vaporizing most materials [Mendis et al., 1996] [Schupp et al., 2000]. An electric arc is a continuous discharge, while an electric spark is momentary discharge as shown in figure 1.1. An electric arc occurs in both direct current circuits and in alternating current circuits.

The unwanted or unintended electric arcing usually causes damage to electric power transmission and electronic equipment; e.g. melting of conductors, destruction of insulation, and fire. Example of devices which may result in arcing include switches, circuit breakers, relay contacts, fuses and poor cable terminations [Solver, 2002].

1.2.3 Properties of Electric Arcs

The arcing channel between two electrodes (anode and cathode) can be divided into an arc column with two regions, a cathode region and an anode region [Browne, 1984]. See figure 1.2 for more details.

1.2.3.1 Arc Column

The arc column temperatures are typically very high, between the range 5000 K to 20000 K [Jones and Fang, 1980], resulting in dissociation of gas molecules into free atoms. The electrons and atoms have high travel velocities resulting in ionization upon collision. Simultaneously, there is also a recombination process where electrons and positively charged ions form neutral atoms. At thermal

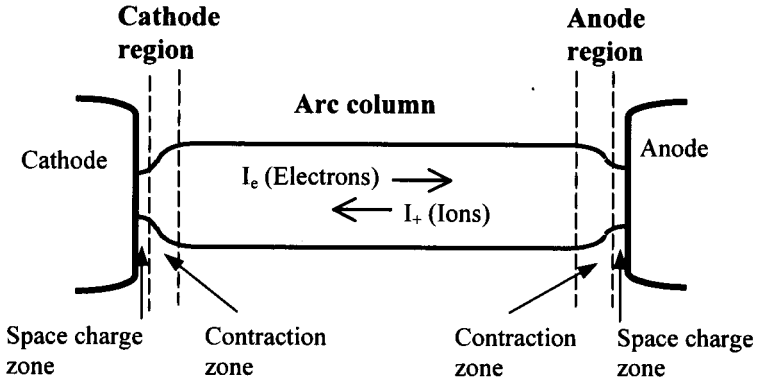

Figure 1.2: Regions of an arc channel [Browne, 1984]

equilibrium, the rate of ionization balances the rate of recombination; resulting in plasma state of gas and high number of free electrons and positive ions.

Presence of space charge can't be avoided even though the arc column is strongly ionized. Nevertheless, there is a balance between negative ion and positive ion charges. The electrons tend to have much higher (three orders of magnitude) mobility than the positive ions. Therefore, almost the entire current flow is due to the electrons. A high current arc is a relatively good electrical conductor due to the strong ionization. Typically, electrical conductivity of the arc plasma is in the range of 10-100 S/cm, which is comparable to the conductivity of e.g. carbon.

The total voltage and voltage gradient of the arc depend on the current magnitude, the type of gas, and the pressure [Browne, 1984]. When the arc reaches thermal equilibrium [Cobine, 1958], the arc column adjusts itself in such a way that the power supplied to the column (the ohmic heating) attains a minimum value. If there is a disturbance of this situation, the arc resistance increases, causing the ohmic heating to increase, then the temperature and/or diameter of the arc would increase [Djakov and Bakardjiev, 1976], and it automatically coun-

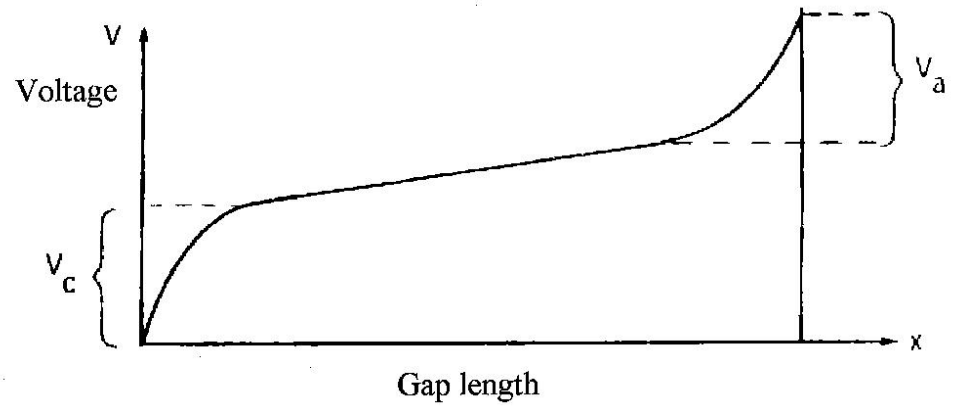

Figure 1.3: Typical potential distributions along an arc channel [Browne, 1948] Where Voltage (Vc): cathode region and Voltage (Va): anode region

teracts the disturbance. On the other hand disturbances that tend to increase the temperature or diameter of the arc result in increase of power losses. Figure 1.3 shows a typical potential distribution along an arc channel [Browne, 1984].

1.2.3.2 Pinch Effect

Magnetic forces are associated with the current that flows in the arc channel, and they lead to an internal overpressure in the arc channel, [Cullwick, 1966]. The phenomenon is often referred to as "pinch effect", and is illustrated in figure 1.4.

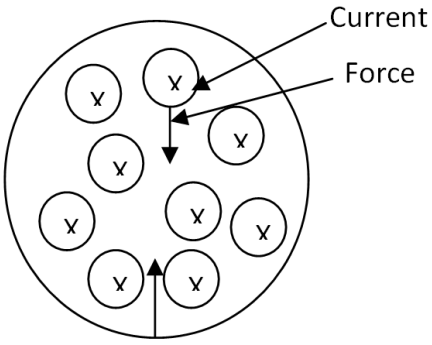

Figure 1.4: Magnetic forces in an arc column (simplified model)

The total current in the column may be imagined as consisting of a number of parallel current filaments which are shown in figure 1.4 as circles with crosses. Due

to the presence of internal magnetic force, separate filaments will be attracted to each other. The resultant overall force on each filament will be directed towards the centre of the column. In other words, the current that flows in the arc column upon interaction with the magnetic flux will result in a mechanical force that is directed toward the centre at each point of the column. Thus, the arc current filaments are radially constrained [Chen and Lieberman, 1984].

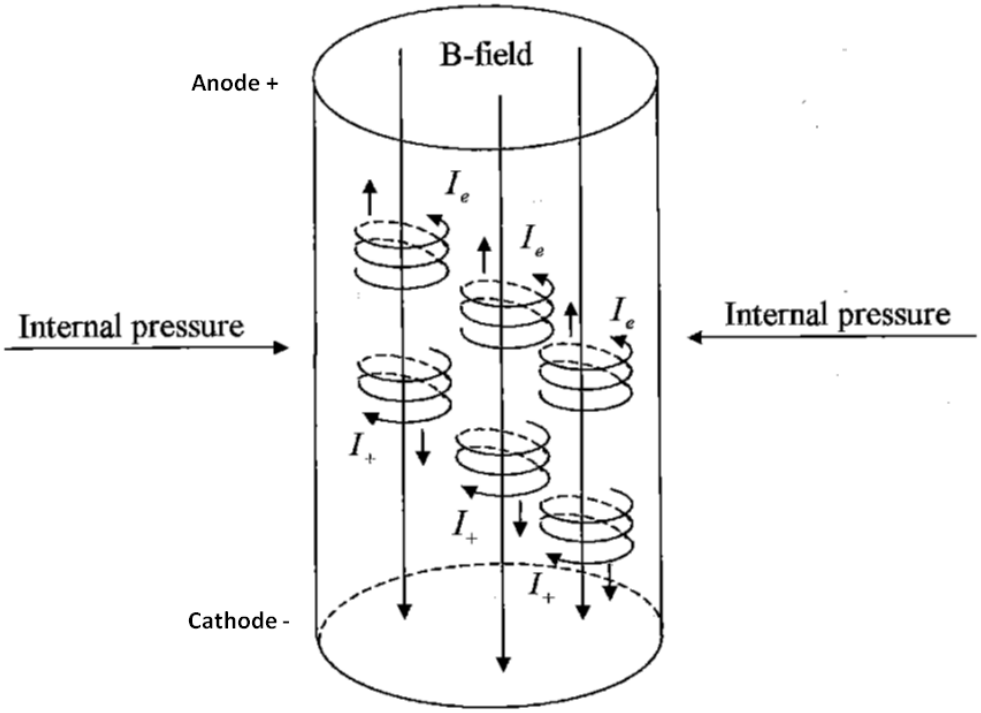

Figure 1.5: Arc column aligned with an external magnetic B field [Shpanin, 2006]

When placed in a strong magnetic field the properties of plasma as the electrical arc are radically altered and controlled, since the motion of the charged plasma particles is affected by the magnetic field. Electrons and ions cannot move freely in the direction perpendicular to the line of magnetic field force. Each particle has a trajectory in the form of helix, which is parallel to the magnetic field, and as a result particle motion is highly directed as shown on figure 1.5. Plasmas exhibit internal pressure when constrained by magnetic fields, and its value is

directly related to the magnitude of the external magnetic flux density B and the current density J flowing through the arc column. In fact, this pressure would immediately reduce and would lead to expansion of the column if there was no magnetic field, [Jones and Fang, 1980]

1.2.3.3 Contact Regions

Current carrying electrons are emitted into the arc column from the cathode [Browne, 1984]. It should be noted that some electrode materials have such a high boiling temperature that thermionic emission of electrons starts well below the evaporation temperature; example materials are carbon, tungsten and molybdenum [Browne, 1984]. With electrode materials having lower evaporation temperatures the major emission mechanism will be field emission, where electrons will be emitted due to the high electric field strength close to the surface [Cobine, 1958]. A typical example of such material is copper.

There will be an accumulation of positive ions, arriving from the arc column, which forms a space charge near the cathode region [Browne, 1984]. Because of this space charge effect, there will be high electric field strength close to the cathode surface (the cathode drop). Such high field strengths are essential for efficient field emission of electrons into the arc.

The main function of the anode is to collect electrons arriving from the cathode. The anode will gain energy upon interaction with the electrons arriving at a high speed, and therefore be kept at a high temperature. Close to the anode, there will be a lack of positive ions, since they tend to drift away from it [Cobine, 1958]. The surplus of electrons at the surface of the anode leads to high electric field strength (the anode drop). The arc diameter is often smaller when it is close to electrodes than further away from the electrodes, indicating that there will

be a gradient in current density that leads to strong heating contacts in the surrounding medium (air, oil, vacuum or SF_6). Therefore, the gradient in internal pressure is produced by electromagnetic compression due to the current density carrying within an arc channel. This pressure gradient contributes to the transport of plasma and metal vapour from the electrodes into the arc column [Cobine, 1958]

1.2.4 Types of Electrical Arc

Figure 1.6 describes the classification of the different types of electrical arcs along with their subdivisions.

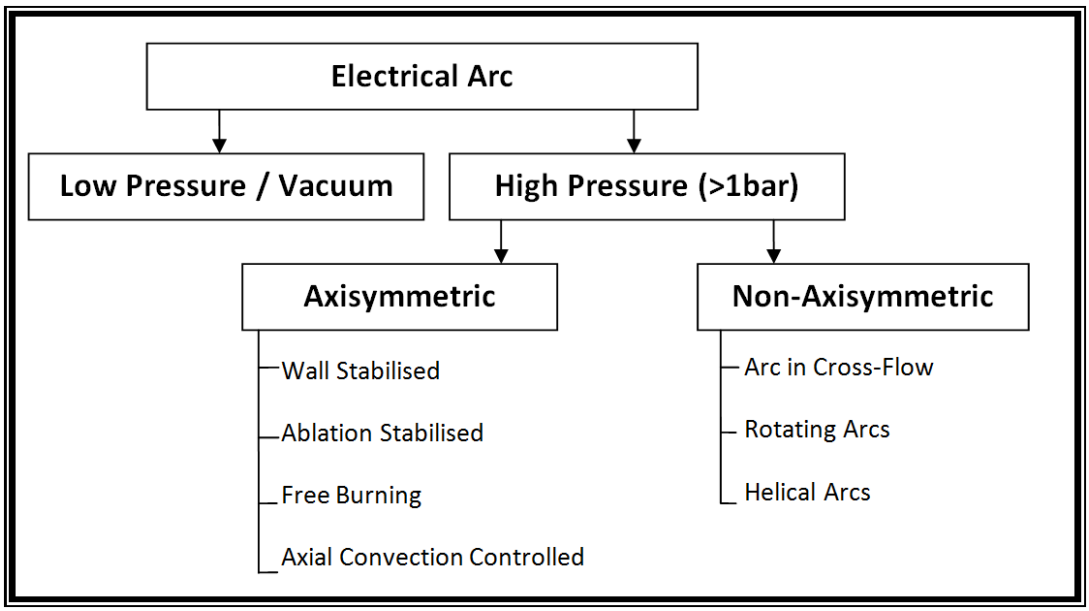

Figure 1.6: Electrical arc classification [Shpanin, 2006]

There are two fundamental classes of electrical arcs: high-pressure arcs (>1bar) and low pressure arcs. Low pressure arcs involve to current interruption applications successfully utilized at distribution level; while all transmission level circuit breakers involve interruption of a high-pressure arc [Jones, 1988]. Furthermore,

arcs can be classified as axisymmetric or non-axisymetric. The axisymmetric axial convection-controlled arc, used in two pressure circuit breakers, has found the most widespread use in circuit breaker technology and has received much theoretical investigation [Jones and Fang, 1980]. This type of arc burns within a flow of high-speed gas coaxial with the arc column and arc boundary due to the entrainment of cool gas formed by the flow. Non-axisymmetric arcs are also known as cross-flow arcs due of the nature of the studies conducted into them. Moreover, the rotating and helical arcs, that move under the action of Lorenz force produced by the cross arc current itself and an orthogonal electromagnetic field, comes under this class (Non-axisymmetric). They are used in present day rotary arc interrupters such as auto-puffer and self-pressurizing interrupters, and also in development of rotating-arc and auto-expansion combined circuit breakers [Ali, 2001].

1.2.5 Arc Modelling

Prediction of the electrical response of the arc through explicit or implicit knowledge of temporal thermal changes in the arc column is one of the main issues of arc modelling [Ryan and Jones, 1989]. Mathematical solutions of mass, momentum and energy conservation differential equations with Ohm's law and Maxwell's equations are sought simultaneously in axial, radial and time dimensions for axisymmetric arcs. Moreover, a number of additional phenomena (e.g. nozzle ablation, radiation transport, turbulence and electrode melting processes) during the arcing time complicate these [Fang, 1983]. Therefore, there is a need to make some arc modelling simplifications, in which these models may be used for accurate computations of parameters that could be measured in practice.

Cassie [Cassie, 1939], Mayr [Mayr, 1943] and Browne [Browne, 1948] derived

mathematical solution of arc models based on only a single ordinary differential equation. From the physical point of view, the Cassie model assumes that most loss of arc energy occurs by axial convection; whereas, the Mayr model considers that the radial contraction of the arc boundary dominates. However, these models suffer from limited accuracy in predicting circuit breaker performance since they do not take sufficient account of the detailed physical processes occurring within the arc column.

By solving the governing arc equations, the numerical solutions of the model of the physical processes occurring in the arc column may be used as analytical tools. Additionally, each model may be regarded as a special case of the boundary layer integral method [Cowley, 1974], which has been evaluated in further studies e.g. [Fang, 1983] and [Tuma, 1980]. The reported method describes the arc behaviour on the assumption of similarities between the radially integrated properties of various arc types. Consequently, a detailed knowledge of the radial arc structure becomes redundant, once the scaling laws relating the various radial integrals have been establish [Ryan and Jones, 1989]. To model the arc, governing equations describing the processes occurring during the arc interaction are used. Moreover, parameters appearing in the equations are measured experimentally (e.g. temperature, current density, gas pressure, radiation loss, velocity and electric field strength) in order to evaluate the accuracy of the solutions to the governing equations. Furthermore, the effects of chemical reacting species upon the material properties of the plasma need to be taken into account in the governing equations. The equation of conservation of momentum involves the uses of magnetic field interactions that may be either due to external sources or produced by the arc current itself. Energy conservation law is responsible for volumetric heat generation in the plasma via Ohm's law for resistive heat pro-

duction [Heberlein et al., 1984]. The radiation from the plasma produces a major mechanism of energy dissipation occurring under many conditions.

1.2.5.1 Arc Shape and Stability

The external magnetic field can control any arc column of sufficient length by producing a Lorenz driving force on the arc. An arc column rotating between two concentric electrodes (figure 1.7) has a complex convolute shape [Jones, 2001].

In 1963, Adams presented a simple model for a DC arc, that describes the behaviour of a rotary arc within a magnetic field and balanced by the aerodynamic drag force acting upon it. The theory states that the arc behaviour is governed by the following equation:

$$\frac{1}{2}\rho U^2 dC_D = BI \tag{1.1}$$

Where

ρ - gas density

U - arc velocity at given radius

d - arc diameter

C_D- drag coefficient

B - magnetic flux density

I - arc current

It should be noted that the arc velocity (perpendicular for each arc element) is constant for a given Lorenz force (Bi) but has a different direction because of the convolute shape. The shape of the arc column determined by the element of radial arc position (r) and angle (θ) with respect to the inner arc root is shown in (figure 1.7).

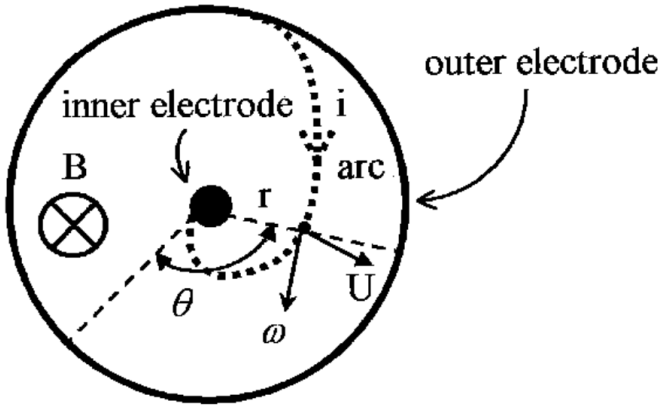

Figure 1.7: Arc shape between two concentric electrodes [Adam, 1963]

Estimation of the DC arc shape within the cross magnetic field is shown by Adam (1963) to be:

$$\theta = \sqrt{\frac{r^2}{c^2} - 1} - cos^{-1}\frac{c}{r} \tag{1.2}$$

Where c is a constant, which defined by:

$$c = \frac{1}{\omega}\sqrt{\frac{BI}{\frac{1}{2}\rho d C_D}} \tag{1.3}$$

and ω is the angular velocity of element of the rotary arc.

From this and equation 1.1

$$c\omega = U$$

$$c = U/\omega$$

Electromagnetic and aerodynamic forces do not affect the shape of the arc since the constant c is the ratio of these forces. The experimental result [Adam, 1963] obtained during arcing achieved reasonable agreement with theoretical prediction of the arc shape. However, the model suffers from a drawback for suffi-

ciently small arc gaps as the predication of the arc shape becomes difficult because electrode phenomena become important and are neglected.

1.2.6 Arc Interactions

1.2.6.1 Voltage Characteristic During Interruption

The voltage required to re-ignite the arc after it has been extinguished is higher than the arc burning voltage, and the process of re-ignition may be considered a race between the de-ionization process in the gap and the increasing recovery voltage determined by the external circuit. At this point, it is necessary to distinguish clearly between short and long arcs, [Cobine, 1958]. For short arcs, the phenomena at the electrodes of the normal arc consume a considerable part of the total voltage, and during re-ignition the regions near the electrodes become very important. For long arcs, the voltage drops at the electrodes are relatively small compared with the voltage required to sustain the column, in which regions the de-ionization phenomena are complicated.

1.2.6.2 Rate of Rise of Recovery Voltage (RRRV)

The voltage across the arc gap increases rapidly once the arc current stops flowing. The rate of rise of recovery voltage (RRRV) is important in determining whether the arc re-ignites. This situation is depicted in figure 1.8. The average gradient of the voltage rise from zero to its first peak with respect to time is higher when the frequency of the transient voltage across the arc contacts is higher. The RRRV across the arc gap is shown by the straight line shown in figure 1.8.

In practice the RRRV across an arc gap is directly related to the current decay rate before current zero; and this relationship measures severity of conditions imposed on an arc gap at different current interruption levels.

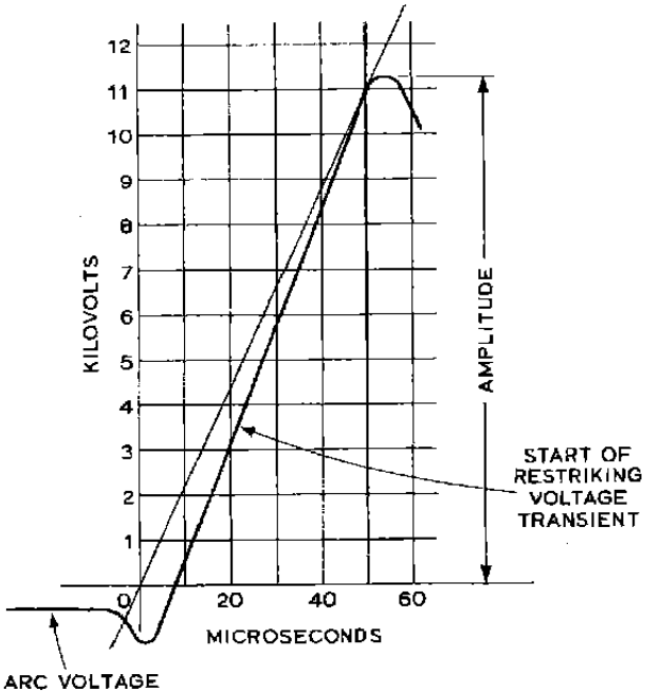

Figure 1.8: Determination of rate of rise recovery voltage (RRRV) [Lythall and Worth, 1972]

1.2.6.3 Influence of Gas Pressure on Arcing

The total pressure P in arc plasma can rise considerably above the original neutral gas pressure due to ionization [Von Engel, 1983]. According to Daltons law the total pressure of the gas in the chamber at the time of its ionisation is:

$$P = P_{gas} + P_{ion} + P_{electron} \tag{1.4}$$

Where

P = total pressure

P_{ion} = ionization pressure

$P_{electron}$ = electron pressure

Due to the formation of the heated (but electrically none conducting) gas sur-

rounding the arc column obeying the gas laws [Jones, 1984] pressure transients may arise. Although such pressure increases have advantages in electromagnetic arc rotation (rotary arc) and with helical arc, they also have disadvantages. For example aerodynamic resonance within the interrupter can occur during the arcing, which is likely at peak current, and this disturbs the gas-flow. This phenomenon can produce instabilities of the arc column itself, [Leclerc et al., 1980]. Because of ablation of the polymer by the arc leading to injection of additional mass into the polymer volume, which demands an additional mass-transport capability, additional pressure increases are produced. Clearly, pressurization effects during arc quenching are complex, but can be beneficial for assisting arc extinction.

1.2.7 Arc Extinction

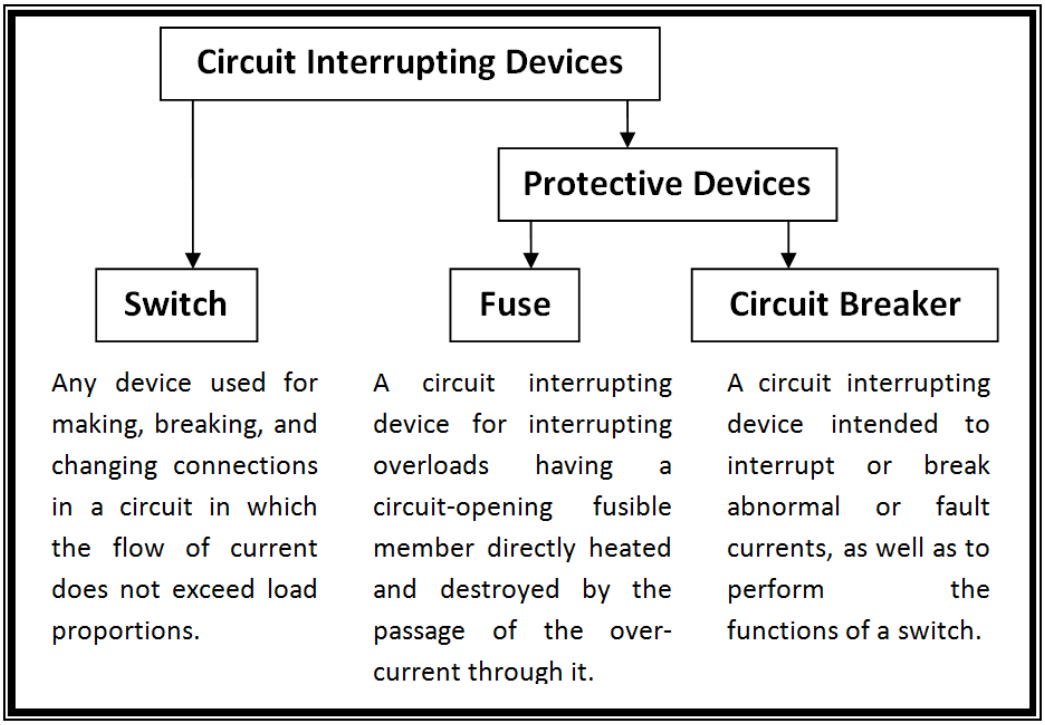

Figure 1.9: Circuit interruption devices

Generally, a direct current arc is extinguished by elongating the arc to such an extent that it can not be sustained by system voltage. The current then reduces to a zero value and the arc is extinguished. In an alternating current arc, this is not the case as the circuit interruption occurs at a point where there is a sudden transition of the arc space at a moment of zero current when the arc space from a conducting state becomes an insulating state.

The provisions used for describing circuit interrupting devices are, in general, descriptive of their operating characteristics. A general breakdown of the terminology may be illustrated as in the diagram as shown in figure 1.9 [Pansini and Smalling, 1994].

1.2.8 Current Interruption

Since the discovery of electric current there has existed a need to control its flow. Historically, the most common method of current interruption involved the separation of contacts in order to create an open gap using a 'mercury switch'; a set of conducting rods positioned within a pool of mercury.

The 'mercury switch' was subsequently replaced by the 'knife blade switch', though the latter is still used for some low-voltage, low-power applications [Garzon, 2002]. Flurscheim [Flurscheim, 1965] documents that such switches were "without any formal arc control other than that provided by the switch attendant who, armed with an insulated hatchet, was invited to chop the arc in two".

Current interrupters, more commonly known as circuit breakers, quickly became increasingly robust in order to cope with the escalating need for electric power.

Because of the absence of natural current zeroes in the Direct Current (DC) it is difficult to interrupt it compared to interrupting an Alternating Current (AC).

According to [Garzon, 2002], in order to achieve a successful DC interruption, it must be forced by increasing arc voltage to a level equal to or higher than the system voltage, using one of the following methods:

1) Elongating the arc column.

2) Decreasing the arc diameter, thereby increasing the arc voltage.

3) Developing a series of short arcs by positioning a number of metallic blades along the arc axis.

The method of Elongation, the arc column was tested by [Shpanin, 2006]. It was concluded that arc quenching in air at atmospheric pressure using the proposed interrupter produced similar results to quenching in SF_6. The second method of decreasing the arc diameter, to increase the arc voltage, commonly involves discharging a capacitor across the arc and, according to [Garzon, 2002], is intended for high-voltage systems, with Method three employed for low voltage applications.

1.2.9 Polymers Effects

PTFE belongs to a large family of chemicals known as Fluoropolymers; and they themselves are a part of a larger group of polymeric materials. Their complex formation is derived from compounds used in refrigerators over a period of 70 years. During the 1930's, safety concerns saw attempts to develop non-toxic, inert, environmentally-friendly liquid refrigerants with low boiling points. The unexpected discovery of PTFE by Plunkett in 1938 in the laboratories of the E. I. du Pont de Nemours & Company during the search for a suitable refrigerant added to material science an excellent insulator with a very strong dielectric and high melting point [Plunkett, 1941], which proved very stable when subject to

oxidation or high temperature.

PTFE is white in colour and possesses a pliability which makes it easy to manufacture. It is one of the most intensively studied and widely-used polymers to date. Its applications include electrical, automotive, chemical, and electronic industries, for communication, construction, medical devices, special packaging, and protective garments. PTFE has a configuration of a twisting helix comprising 13 CF_2 groups every 180^o turns; this configuration makes it thermodynamically favourable because of the mutual repulsion of the adjacent fluorine atoms [Drobny, 2001]. The twisting helix forms an almost perfect cylinder comprising an outer sheath of fluorine atoms enveloping a carbon-based core [Harrison, 2005].

The dielectric constant of PTFE is about 2.1, although it varies slightly depending upon the product. This value remains constant, with a slight increase after exposure at 300^oC for 9 months. The dissipation factor of PTFE was recorded to be about 0.0001 [Molyneaux et al., 2003]. Usually the dielectric constant of PTFE remains constant in the temperature range -40^oC to 250^oC; the dielectric constant remained the same for 2 to 3 years after measurements were taken [Gangal, 1989]. However, the dissipation factor can be affected by frequency, temperature, crystallinity, and void content of the fabricated structure [Drobny, 2001]. The surface arc-resistance of PTFE resin is high and is unaffected by heat aging. They neither track, nor form a carbonised path, when subjected to a surface arc in air [Gangal, 1989].

Some workers modelled an auto-expansion circuit breaker [Yan et al., 2004] using a commercial computational fluid dynamics (CFD) computer package (PHOENIX). [Looe et al., 2008], demonstrated the ratio of the distribution temperature of pure SF_6 gas to pure PTFE vapour through simulation results, before current-zero, as $2:3$; indicating that the arc-cooling capability of the latter is two thirds that of

the former.

Lee and Kim [Lee and Kim, 2007] have demonstrated that the net emission coefficient of the vapour of SF_6-PTFE mixture is similar to that of pure SF_6. The net emission coefficient represents the radiation per unit volume emitted by the plasma from a given position, including the radiation absorbed at the same position, from all other regions of the arc [Liebermann and Lowke, 1975]. A good approximation for calculating the temperature of the central arc was realised by deployment of the net emission coefficient [Liebermann and Lowke, 1975]; in other words, the effect of the vapor mixture of SF_6-PTFE on the temperature of the central arc is similar to that of pure SF_6. This further supports the consideration of PTFE as a possible replacement for SF_6.

1.3 Contribution

The present contribution aims to extend the scope of previously reported work through tests performed with different helical blade arrangements and various radial sizes and at different current levels. Technical improvements in high speed cameras have also enabled photographs to be used for extracting data to calculate the arc's velocity as it moves from the centre of the device to edge of the helical blades.

This work is mainly concerned with improving the DC current interruption principle. It is hypothesized that the arc control behaviour may be quantified so that further insight may be gained as to how the arc can be utilized for current interruption to better protect the network. This aspect of arc control may have wider industrial applications [Naidu and Kamaraju, 1996].

1.4 Structure of the thesis

The structure of the thesis is as follows.

Chapter 2 gives the general explanation about the experimental setup. It describes the different apparatus used in the experiments and how they function in general. Also states the detailed description of the individual parts used in the experiments.

Chapter 3 gives a detailed description of the experimental procedure used in the work described in this thesis. It presents the information regarding the features incorporated in different individual components and how they are arranged to perform the experiments.

Chapter 4 reports the helical arc experimental results. Different arrangements and sizes of blades were used in the experiments for current interruption and the performance and results obtained are presented. Also, results with and without the plunger in the arrangement of the blades are given.

Chapter 5 gives the detailed analyses of the results set out in chapter 5. In this chapter the relation between the high speed camera images and the graphical results is also derived.

Chapter 6 describes the modelling of helical arcs. In this chapter different forces associated with helical arcs have been studied and investigated. Also, a model has been developed explaining the expansion of the arc.

Chapter 7 discusses the analyses of experimental work (chapter 5) and the modeling work (chapter 6) and additional possibilities for improving the current interruption techniques are suggested.

Chapter 8 presents conclusions and also recommends future work that may be additionally useful.

1.5 Summary

This work is therefore concerned with investigating the advantages of using a helical arc principle for efficient current interruption (without needing a discharging capacitor across the arc) by combining methods 1-3 (section 1.2.8), together with the use of polymer material as a replacement for SF_6 gas (1.2.9). This is investigated through designing a DC interruption device, incorporating compact diameter helical blades made of PTFE/PE (plus a copper blade), which is capable of handling medium to high voltages (i.e. $>$ 3kV).

Chapter 2 details and explains the design options and setup conditions for this experimental helical arc device.

Chapter 2

Experimental Apparatus and Setup

2.1 Helical Arc Assembly

The helical assemblies used in these experiments are shown in figure 2.1a and figure 2.1b with the helical arc assembly mounted vertically. The construction consists of a tufnol core rod, termed a former, which is threaded, to allow the helical blades to be securely fixed to the core as shown in figure 2.1. Different diameters of helical blades (small, medium, large) and material composition blades were used to confine the arc between each blade. The arc behavior was experimentally investigated for a number of different arrangements. The arc is initiated by the vaporisation of a length of nickel alloy fuse wire, 0.193mm in diameter. This is wounded between the helical blades, over the surface of the core. The ends of fuse wire are then clamped to aluminium rings fitted tightly over the core, which also act as current connections. The core is made of tufnol, having a 38mm outer and 25mm inner diameter. Radial holes are drilled, equally-spaced,

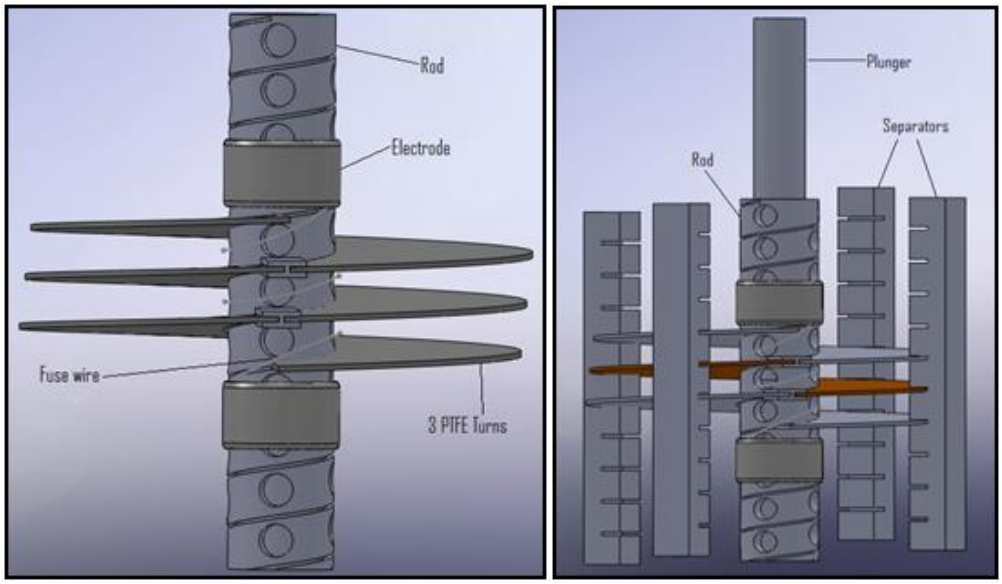

(a) (b)

Figure 2.1: Schematic of the helical arc

through the core, and these are effectively opened or closed by removing or inserting a rod called a plunger, shown on the right-hand diagram (figure 2.1b). The core, therefore, is effectively a solid (with the plunger inserted), or a hollow (with the plunger removed). The former, providing a helical pitch of 18mm, was used, and the size and the number of radial holes per helical turn were adjusted to suit the helical pitch. For an 18mm-pitch core, 4 holes of 12mm diameter were provided. Lastly, four Perspex 'separators' were arranged around the outside of the helix to prevent the blades from drooping at the edges.

2.1.1 Blade Sizes Arrangement

Three diameters were used for the blades. These are described as small (180mm diameter), medium (360mm diameter) and large (500mm diameter).

These blades were made from PTFE, PE and Copper. The use of copper discs was to provide additional arc rooting positions for the arc. It is expected that

if the arc does root on to the copper discs then the current would flow through the copper discs and therefore one helical turn of the arc would be lost. But the potential advantage of this is that the current flowing through the copper disc may set up a magnetic field which could couple with the arc providing additional movement. If no arc root is formed on the copper disc then the additional conductive losses from the arc to the copper disc may aid in arc control and interruption. Figure 2.1a shows 3 small blades employed in the helical arc system.

Seven small PTFE discs and three copper discs were available to be secured onto a tufnol former in any order. All the blades are 180mm in diameter. The use of PTFE blades was to keep separated the individual "turns" of arc to prevent them from short circuiting between turns.

For the medium sized blades the diameter of the blades was increased to 360mm. For this particular size of blade a number of options were available. 5 PTFE blades could be used together in any numerical combination. 5 PE blades could also be used and again these could be used in any numerical combination.

Also, available are 3 copper blades. These can be used in combination with either the PTFE or PE blades in order to assess the potential influence and benefits for arc movement and interruption. Moreover, 5 PTFE, 5 PE and 3 Copper blades were available for the arrangement. Different assemblies were arranged in different configurations of PTFE, PE and/or Copper blades for testing.

The largest size of blade used was 500mm in diameter. Available for the test were 3 PTFE and 3 PE. No copper blades were available in this size.

2.2 Synthetic Power Supply

Figures 2.2 to 2.4 show the high current synthetic power supply used for providing different short-circuit currents for the helical device. The power supply used for the experiments consisted of a capacitor bank, switching ignitrons, series resistor, resistive dump mechanism and a central control unit. The capacitor bank consists of 192 elements with each having a capacity of $185\mu F$ contributing to a total capacitance of $33mF$ with a maximum charging voltage rated at 6.3kV giving a total maximum stored energy of 695kJ. To produce a sinusoidal current of approximately 50Hz, a high current coil with an inductance of approximately $184\mu H$ is used to provide a tuned resonant circuit. Resistive losses and losses in the arc discharge damp the natural amplitude of successive oscillations. The capacitor bank was initially charged and triggered by a series ignitron allowing current to flow into the fuse wire of the test device with timing control for the firing of the ignitrons performed by a control unit. Voltage and current were monitored on a digital oscilloscope via a 1000:1 probe and $1m\Omega$ shunt respectively.

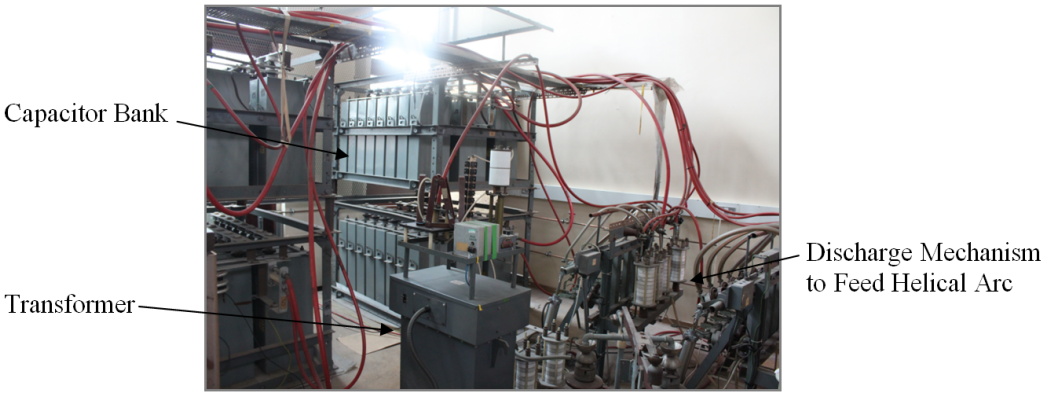

Figure 2.2: Photograph of capacitor bank and associated circuitry

Figure 2.2 shows some of the individual capacitors in racks constituting the capacitor bank. The charging transformer and discharge mechanism can also be seen, along with connecting cables.

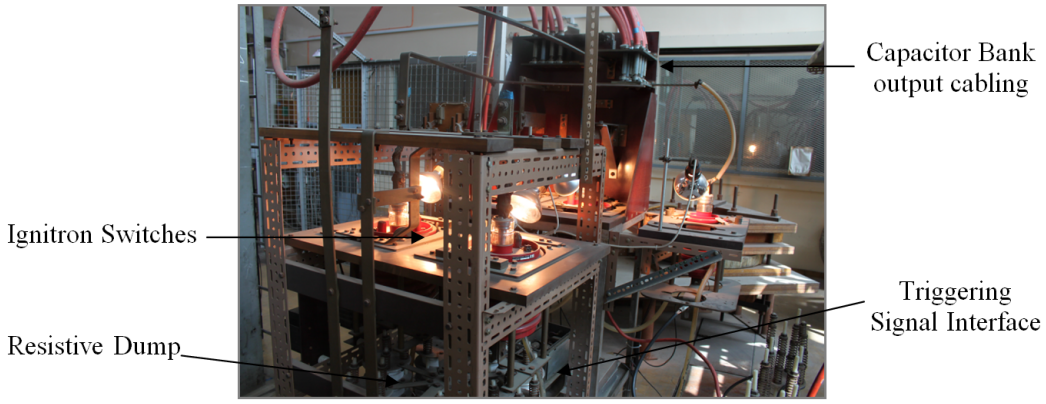

Figure 2.3: Photograph of ignitrons and control signal interface

Figure 2.3 shows a series of ignitron switches and the triggering signal interface. Also, outer cabling of the capacitor bank can be seen.

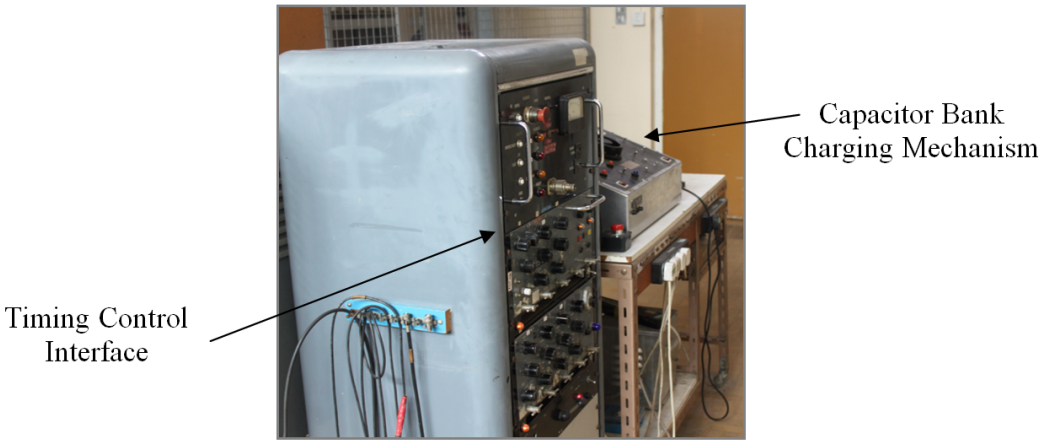

Figure 2.4: Photograph of the central control unit

Figure 2.4 shows the central control unit interface where both time and configuration can be controlled.

2.3 High Speed Camera Measurement

A high speed camera was used to view the expansion profile of the arc under different operating conditions. High speed photographs were also used to view

the arc formation and any eventual shorting between arc turns as it reached the outer circumference of the disc. At first a Nac 500 framing camera was used and this operated at 500 frames per second which gives 2ms between the frames with an exposure time 20μs. Later a photon SA-1 colour (figure 2.5) was used to gain better and clear images of the arc. This was operated at 20,000 frames per second which gave 50μs between the frames with an exposure time 20μs. Due to the sensitivity of the camera neutral density filters were used to reduce the intensity of the light entering the camera. The distance between the camera and the helical arc system was maintained at 3 metres in all the experiments.

Figure 2.5: High speed camera

Figure 2.6: Triggering box

The high speed camera was controlled by an external trigger unit (figure 2.6) which required a trigger waveform as shown in figure 2.7. An initiation trigger is sent from the control unit (figure 2.4) to this external unit in order to generate the 5 volt pulse required by the camera from the 32 volt peak-peak supplied by the control unit.

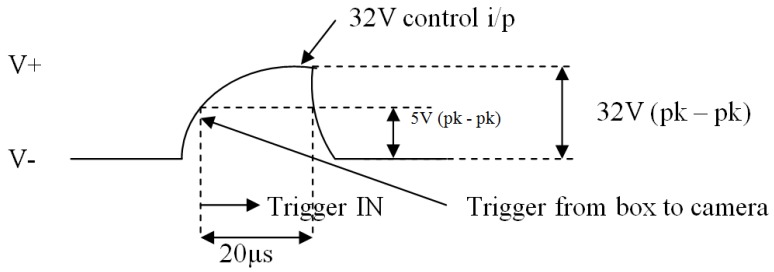

Figure 2.7: Trigger waveform

2.3.1 Arc Position

For monitoring the position and appearance of an arc, several techniques are available. One of them is high speed photography which is frequently used but this requires post processing and does take much time [Langeac and Barrault, 1987]. Another example is Optical fibres which are also widely used, either to view the arc directly, or to pass an image back to a second detector [Minoo et al., 1995] [Desaulniers-Soucy and Meunier, 1999], [Tekletsadik and Campbell, 1995].

The present investigation uses both the camera and fibre optic techniques. However, there are other advantages with fibre optics. These are:

a) The advantage of optical fibres is that they can be moved into positions which are not easily accessible by the camera.

b) They can also be placed very close to the arc if they are adequately protected, without introducing any electrical and magnetic disturbances.

c) In addition to this optical fibres can transmit light signals even if the environment is electrically noisy.

d) Lastly, the information from the fibres can be immediately converted to electrical signals and displayed along with current and voltage data, this reduces the time taken to perform a series of experiments and improves the accuracy of the information since all of the oscilloscopes can be synchronised to a common time-base.

There are, however, disadvantages due to the terminations of fibre optics, in terms of the numerical operation which lets light in over a broad range of angles thus reducing the positional accuracy. To overcome this, the fibres therefore must have their viewing angle restricted using collimating tubes. This restricts the viewing angle and therefore more fibres are required for the same viewing area.

2.4 Collimated Tube Design

The design for the collimated tube for the optical fibres is shown in figure 2.8a and figure 2.8b. The collimated tube consists of several elements. The rod, or the core, of the device is threaded to allow the SMA connectors at the end of the fibre optic to be screwed onto it from one end (figure 2.8a) while the other end (figure 2.8b) restricts the viewing angle. The result is that one fibre can only provide information about a small area. Two nuts are used to secure the arrangement into the mounting brackets. This holder is made of aluminium to protect the fibre optic from contact with the arc. Lastly, another holder was built to hold and prevent the fibre optics from becoming loose and then potentially coming in contact with the arc.

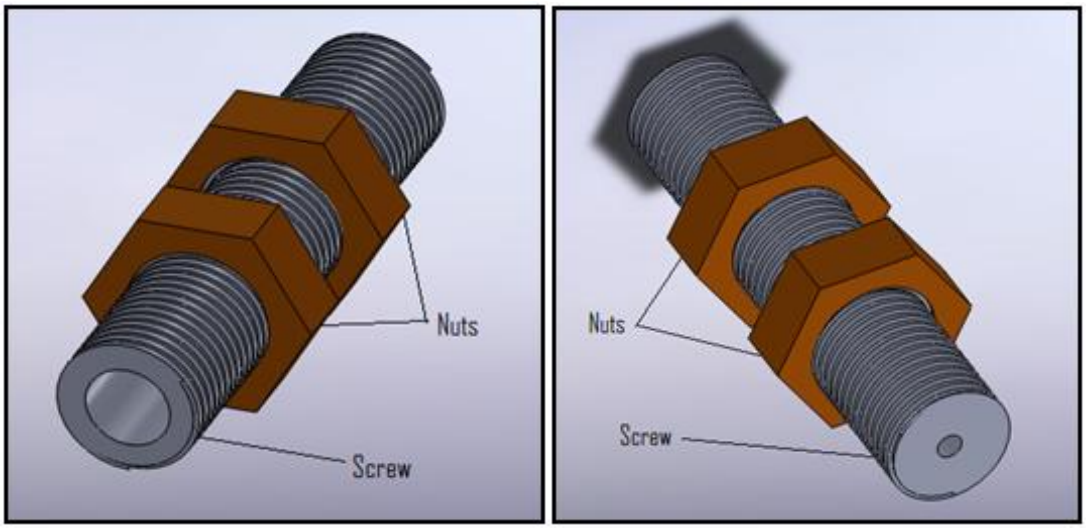

(a) back view (b) front view

Figure 2.8: Schematic of collimated tube

The design of the collimating tubes is shown in figure 2.9. An extension is added to the fibre. This is position to achieve the right level of viewing area.

A schematic of the collimating tube is shown in figure 2.9.

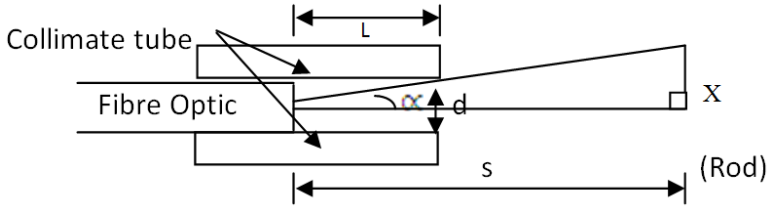

Figure 2.9: Collimating tube

The design considerations for the collimating tube are:

d=1mm (view point diameter of collimating tube)

L=32mm (from tip of the fibre optic to the outer edge of the collimating tube)

S=220mm (distance between tip of fibre optic inside collimating tube and Rod)

Where 2X is the fibre optic field of view in figure 2.9, X can be calculated as follows.

Since

$$\frac{\frac{d}{2}}{L} = tan \propto$$

therefore

$$\frac{x}{s} = tan \propto$$

so

$$\frac{\frac{1}{2}}{32} = tan \propto$$

x = 220 (tan(0.86))

= 3.3mm.

2.5 Fibre Optics Holder Design

Figure 2.10 shows the layout of the fibre optics holder that has been designed and fabricated.

The fibre optics holder is designed to prevent the collimating tube from getting loose. Two nuts have been inserted into the collimating tube inwards to hold it very tight (figure 2.8) for more accurate results. The holder is made of tufnol material to protect the fibre optic from having any contact with the arc.

The holder has a 190mm and 7mm wide slot in the middle allowing the collimating tube to be positioned along this slot. The size of the slot (190mm) for the small blades is slightly larger than the size of the blades. For medium size blades the size of the slot was chosen as 370mm.

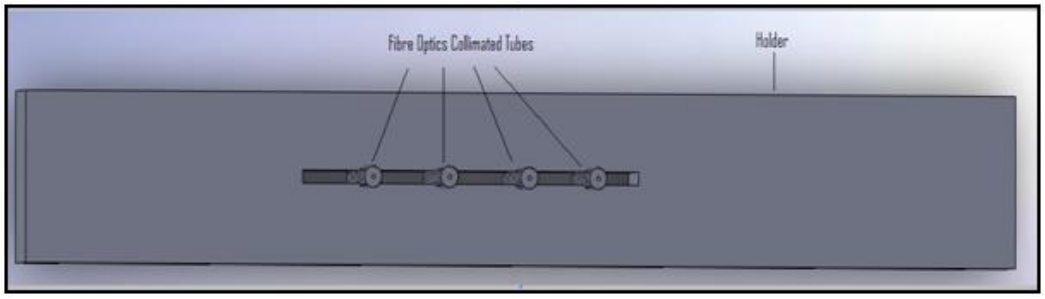

Figure 2.10: Schematic of the fibre optics holder design

2.6 Current and Voltage Measurement

A number of current and voltage measurements were recorded in the course of the work: arc current, I, arc voltage, V and spark breakdown voltage V_{bd}.

The high current shunt used (to measure I) is of the low inductance type with a rise time of tens of nanoseconds. The earth terminals of the shunts, on which the BNC coaxial connectors are mounted, are connected directly to the experimental earth, while the input connection is attached to the breaker terminals. Two 1000:1 high voltage probes were used to measure the arc and spark gap voltages, as seen from figure 2.11.

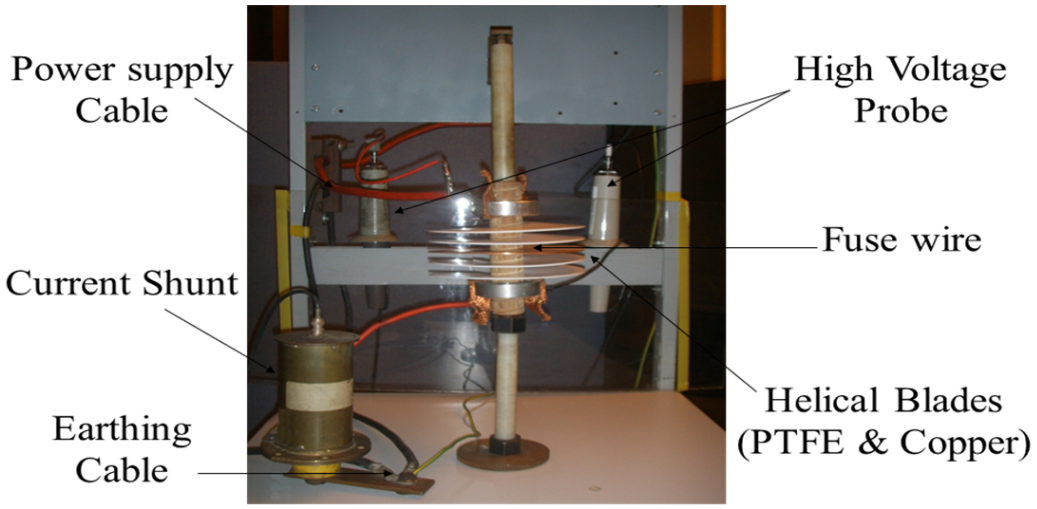

Figure 2.11: Experimental system setup

In both cases, the voltage measurements were taken from the aluminium rings, which are attached to the helical structure; the arc voltage is then really the voltage across the terminals of the helical arc, and therefore includes any voltage drops across bolted joints as well as the actual arc voltage.

2.7 Summary

This Chapter describes and explains the components of the experimental setup used for the work reported here. Different types of arrangements (3, 4, 5 and 7 blades), with different size blades (180mm, 360mm and 500mm) and various materials (PTFE, PE and copper) were used to monitor the behaviour of the arc. Different optical techniques used (high-speed camera and fibre optics) to obtain the results from the helical arc system are also outlined and compared in this Chapter.

Chapter 3

Experimental Procedure

3.1 Introduction

A number of experimental tests were conducted during the course of the helical arc investigations mentioned in the thesis. This chapter describes the experimental procedures that were implemented for the work. The intention of the helical arc experiment was to capture information about the aspects of the behaviour of the helical arcs. The test associated with helical arc experiments required synchronisation between the synthetic power source and the instrumentation and this complexity is reflected in the test procedures.

Varying the charging voltage on the capacitor bank allowed the maximum prospective arc current to be varied. Also the numbers of the helical blades were kept to three during the experiment for the first stage, so as to compare it with previous work by Ennis work [Ennis et al., 1995], and by Afanasiev [Afanasiev et al., 1981].

Later in the test sequence, the number of helical blades was increased up to 7 blades; and copper blades were introduced to examine the effect on arc

performance. The diameter of the insulation and copper blades was changed from 180 to 360 and 500mm. Two different types of polymer (PTFE, PE) were used for the insulation blades in order to determine the effect on the arc behavior and interruption performance.

3.2 Exponentially-Decaying Arc Current

The arc currents for the experimental test were supplied by the circuit shown in figure 3.1. This synthetic power supply system (section 2.2) produces the quasi- DC main currents via an over damped RLC (resistive-inductive-capacitive) circuit. The capacitor bank is formed from 192 capacitors arranged in series and parallel giving an overall capacitance of 33mF. A 184μH inductor is in series with the capacitor, and a 4.5Ω resistor is inserted between the capacitor bank and inductor.

The control unit (CU) has a number of functions. The main feature is the use of interlocks to provide safe operation of the capacitor bank and dumping of any excess energy that may remain in the capacitors at the end of the test. Another function of the CU is to charge the capacitor bank safely up to the required voltage. The CU also control's the timing for the firing sequence and triggers to the switching ignitrons, initiation of contact separation etc.

The current through the test device, I, and the arc voltage, V_{cb}, generated were measured using the 1mΩ shunt and 1000:1 divider respectively, described in section 2.6. An experimental earth provides the earthing between the synthetic power supply system and the test device during the experimental test investigation and reference point for all the measurement.

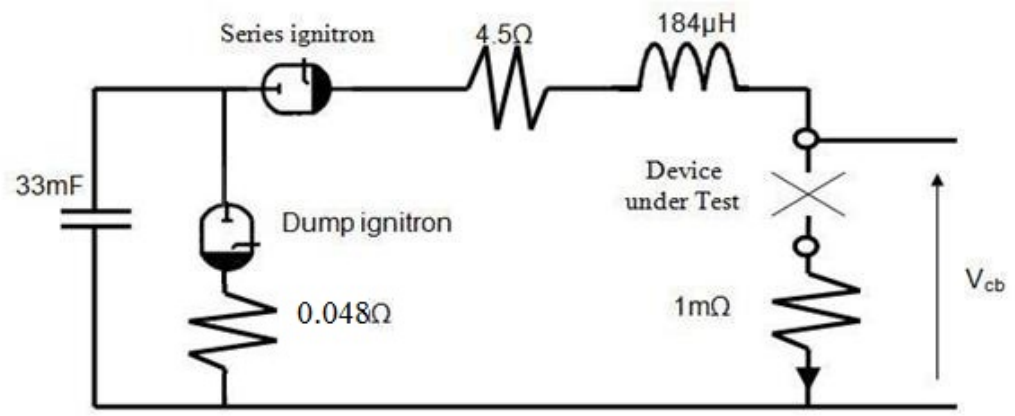

Figure 3.1: Power supply circuit for exponentially-decaying currents

3.3 Arrangement of Diagnostic Connection

Care was taken in connecting the equipment to a common experimental earth. Earth loops were removed when detected.

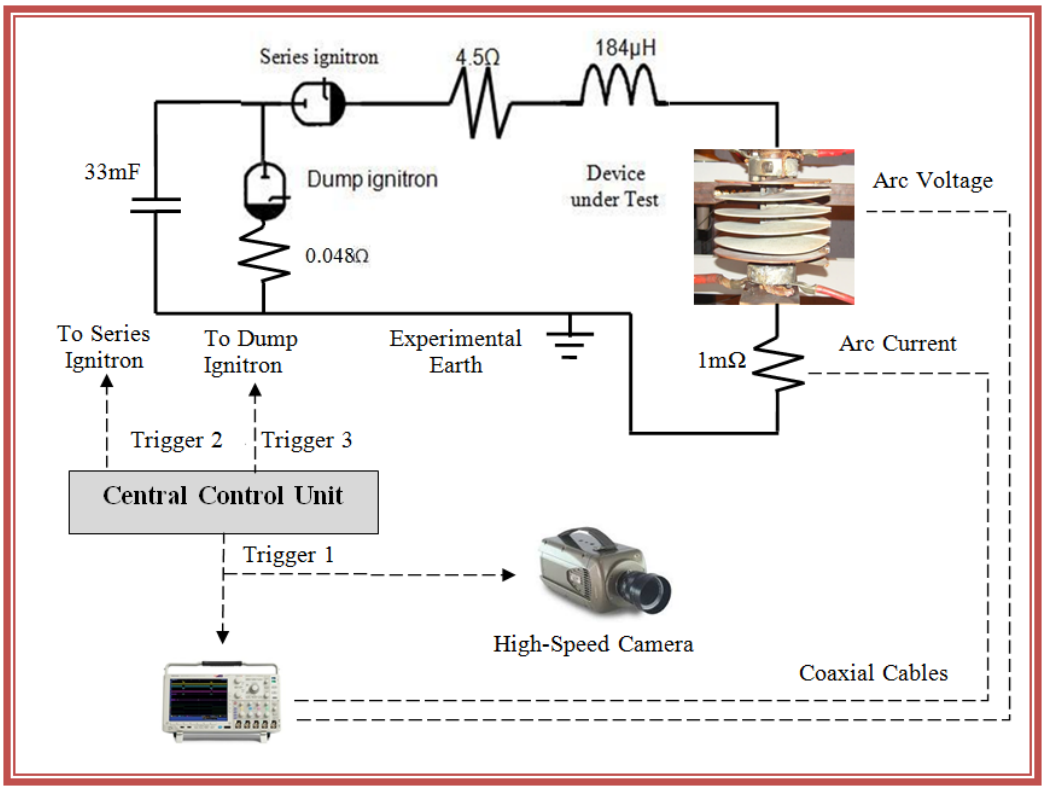

Figure 3.2: Layout of diagnostic equipment

The experimental earth point for the experiment was the earth side of the 1mΩ shunt shown in figure 3.2. All the oscilloscopes were connected to this ground only, with their main power supply isolated from the mains by 1:1 isolating transformers. The same system used for controlling the firing times of the ignitrons was also used to trigger the oscilloscopes. Trigger signals from the control unit passed through a pulse transformer. This again was to reduce the risk at earth loops. Figure 3.2 shows the location of each diagnostic connection on a schematic diagram of the test head.

3.4 Control and Timing Sequence

The CU is used to control the operation of the experimental test facility and coordinate the acquisition of measurements.

For the experimental test the electrical and optical equipment for monitoring the experimental device needed to be synchronised to operation of the capacitor bank. The timing diagram shown in figure 3.3 shows the sequence required for successful operation.

The recording equipment is triggered before triggering the Ignitrons in the synthetic power circuit. After 10ms, Trigger 1 opens the shutter of the high-speed camera and starts the oscilloscope recording. A further 10ms after Trigger 1, Trigger 2 activates Ignitron 1. Once triggered the over damped current flows into the external network and the device under test. This mode of operation is used for the quasi-dc arcing testing. This means that the discharge current starts flowing through the experimental device producing the electrical arc between the electrodes and decays over a period of time. The camera and oscilloscope are fully ready to record the event just prior to the current being initiated. The

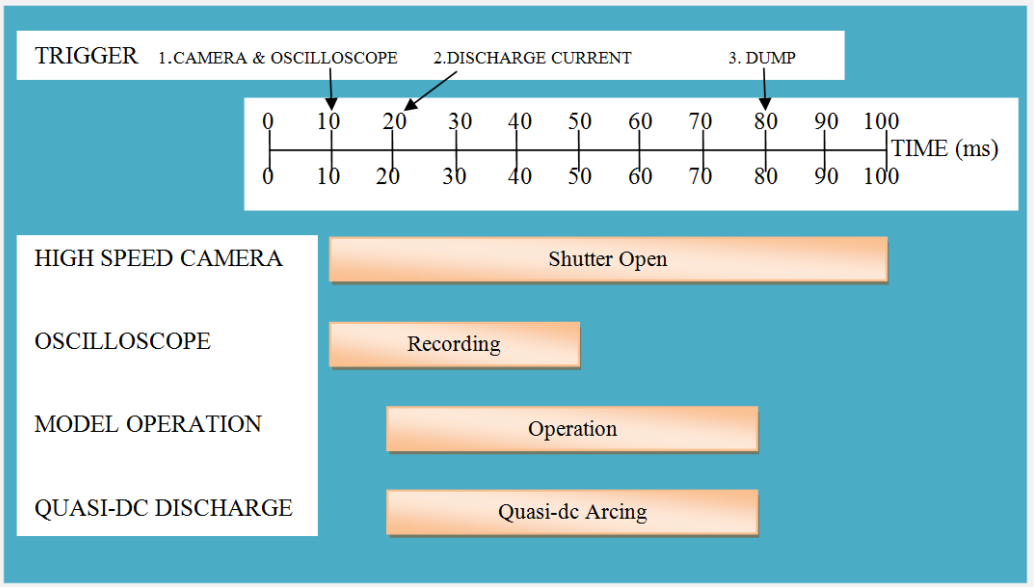

Figure 3.3: Experiments time sequence

high speed camera operates for 90ms and the oscilloscope recording time used in the tests is 40ms, and after about 80ms, the dump is operated (Trigger 3) and capacitor bank is fully discharged.

3.5 Experimental Earth and Isolation

For any high current and voltage test circuit a single local earth point is important. This is known as an experimental earth. Usually it is connected to a copper rod located in the foundations of the building. The earth connection was situated close to the test system and had a short cable with low impedance capable of carrying a current of several tens of kilo-amperes (kA). Electronic equipment connected to the test circuit operates from the normal 240V mains supply. This equipment is isolated from the main earth by 1:1 isolation transformers. This avoids the unintentional creation of duplicate earths, which could lead to earth loop currents leading to measurement errors etc. These transformers also provide

protection from the equipment in case of any fault development.

3.6 Return Path

The return path for the arc discharge current is through a return cable. This cable is firmly connected to the experimental earth and by doing so the equipment and source are tied down to the same relative level.

3.7 Optical Fibre Monitoring

Four optical fibres positioned in four collimating tubes were placed into a fibre optic holder as shown in figure 3.4. It was made from aluminium, and the distance between the adjacent fibre optics was 40mm. The zero position is calculated from the centre of the rod up to the edge of the blades. Arc velocity could also be determined.

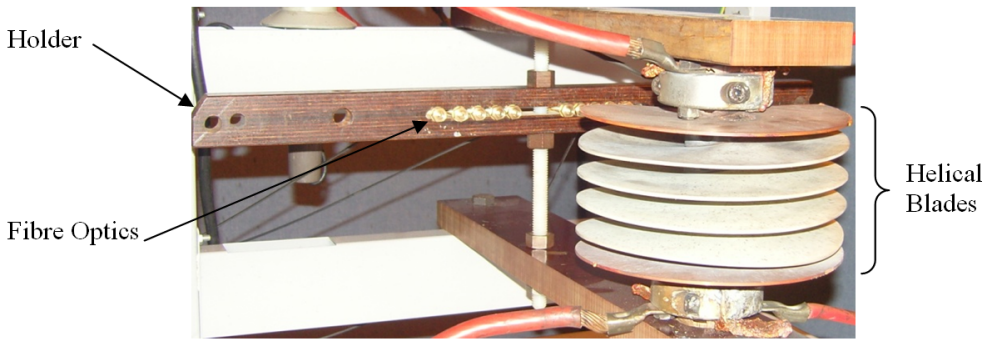

Figure 3.4: Fibre optic assembly

An advantage of being able to screw the fibres into this holder was all the fibres are aligned. The positions of the optical fibres were also changed to accommodate other experimental arrangements.

The signals from the optical fibres were detected by optoelectronic diodes with

a broad optical bandwidth. Each fibre was connected to its own photodiode. Each photodiode stage has an amplifier circuit with manually selectable gains. A schematic diagram of the optical fibre recorder system is shown in figure 3.5.

The electrical signal from the optoelectronic sensor box is recorded on an oscilloscope which is triggered from the central control unit. The data from the oscilloscope is analysed by a PC.

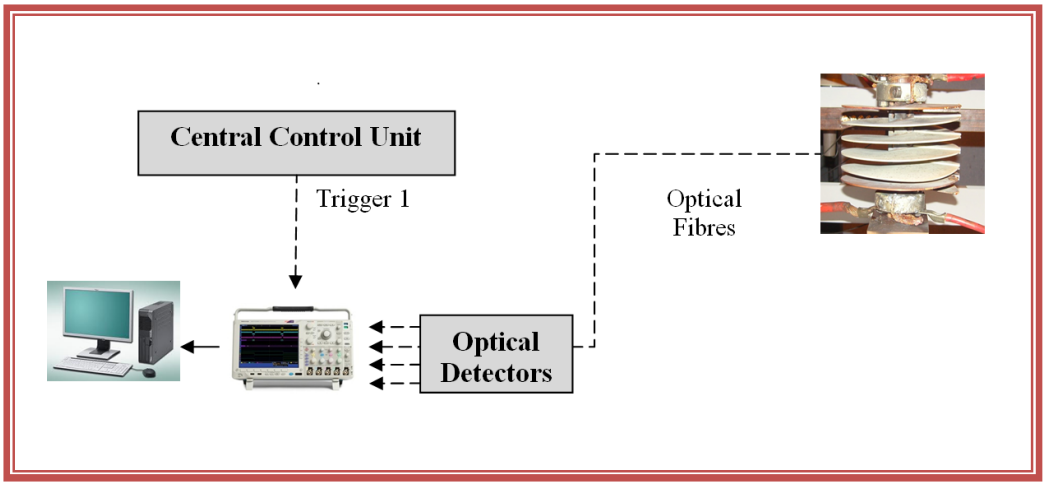

Figure 3.5: Layout of the optical fibre recorder system

3.8 Oscilloscope Recording Unit

A digitizing oscilloscope "DPO3034 Digital Phosphor Oscilloscope" was used in different parts of the investigation for this project. Current and voltage measurement taken during the arcing duration are accurately recorded on the oscilloscope. It has 4 analogue channels with a bandwidth of 300MHz and a high-resolution sample rate of 2.5 gigasamples/s. The input impedance of the oscilloscope was 1MΩ, the input capacitance was 11.5pF, and it uses internal memory for saving the waveform traces. USB port in both front and back panels made for quick and easy data copying, printing, and connecting other USB enabled devices.

3.9 Summary

This chapter describes the experimental equipment used in the helical arc tests. These include the helical arc chamber, and associated diagnostic equipment such as the optical fibre monitor, probe and high speed camera. It also explains how the measurements were taken for each test series.

Chapter 4

Experiment Results

In the current limiting device, the amplitude of the current flowing through the arc will vary from shot to shot. However, more important is the prospective fault current that would flow without an arc discharge and this is more predictable for a given charging voltage on the capacitor bank. The actual current compared to the prospective current is indicative of the efficiency of the helical arrangement to limit the current. Due to this shot to shot variation a comparison between results for exact current conditions is not possible but comparisons are made for similar currents.

The capacitor bank charging voltage and the series resistor determines the value of prospective current. Since the series resistance was kept constant throughout the investigation, the bank charging voltage effectively determined the fault current. For the experimental tests the capacitor bank voltage was altered in order to change the prospective fault current.

This chapter contains three main parts which shows the effect of using different arrangement of the helical blades, blades made from different polymers and the effect of different combinations of blades on the ability of the device to current

limit.

4.1 Experimental Tests

This section describes the test strategy used for each experiment involved in the experimental investigations. The motivation to perform each test along with the test results is reported (section 4.2).

4.1.1 Preliminary Test Using the High Voltage Bank

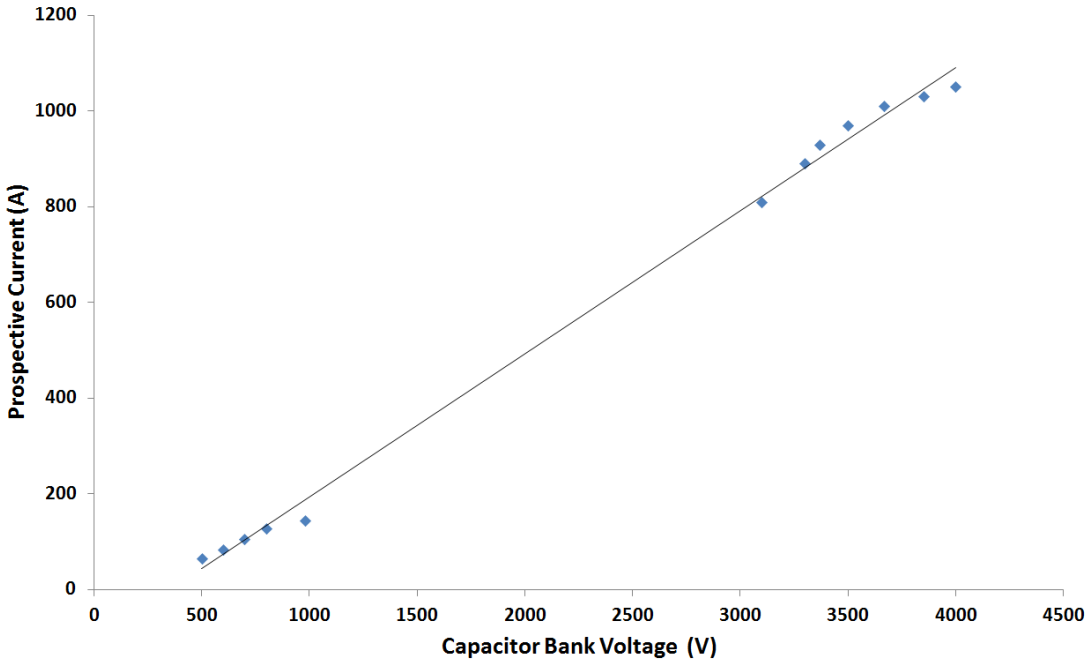

Figure 4.1: Prospective Current Obtained from Charging of the Capacitor Bank

Figure 4.1 shows the relationship between prospective current that flows in the circuit when a shorting strap is placed across the test rig versus capacitor bank voltage. It can be seen from the figure that as bank voltage increases, the value of prospective current increases. This result helps to set the charging voltage to give a set current for each test. The dependence of the current on the voltage

between 3.3 and 4.2kV is almost linear and to a first approximation it can be treated as such. The actual current will depend upon a number of factors such as energy loss during arcing.

4.1.2 Arc Control Test

In this section a description of the experimental tests relevant to arc control model (section 2.1) is introduced. The reported electrical parameter tests and optical test investigations (high-speed and video photographs) provides experimental information about the arc in air at atmospheric pressure for a range of experimental conditions.

Electrical Parameter Experiments

For the results presented in this chapter, the current and voltage were obtained as described in chapter 3 section 3.2. A quasi steady DC current was used throughout the test sequence.

Optical Test

Optical observation of the quasi-DC arc during the arcing period was made to provide a visual record of arc behaviour. A high speed camera provided sufficient temporal resolution to permit these observations. For examining the DC-arc discharging period a frame speed 20000 frames per second with an exposure time 20μs was used.

4.1.3 General Features of Helical Arc

From the number of test completed, it was possible to deduce a set of general features which were common to all of the tests conducted.

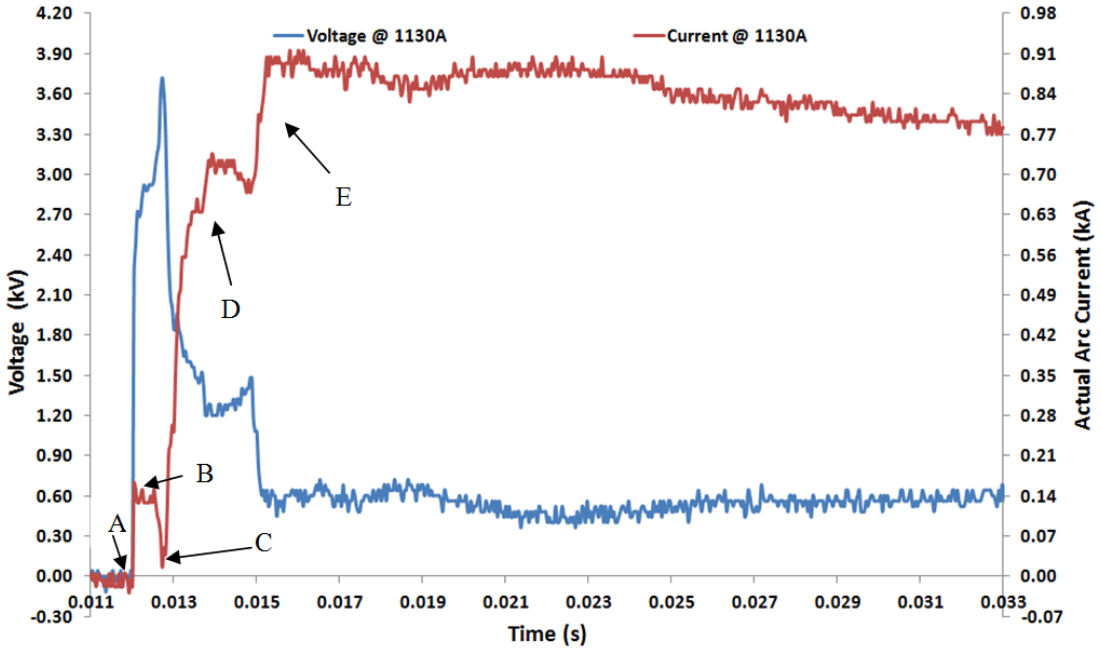

Figure 4.2: Current and Voltage characteristic for 2PTFE, 1Copper, 2PTFE

A typical result is shown in figure 4.2 which highlights features that were observable in many of the tests.

The current starts to flow at point (A) and the initial current hump (B) as shown in figure 4.2 was due to the fuse wire ignition [Shimomura et al., 1995], rather than any intrinsic arc behaviour, and this was confirmed from the high-speed photographs. The photographs show the ignition of the wire entirely up to a point where the segments are linked by short arcs; each short arc then extends until the fusing of the wire is complete and a helical arc is formed. If the current is extinguished during this ignition phase the current ceases to flow and no arc is established. If the arc is not extinguished then the current continues to flow until the arc leaves the blades when the automatic dumps are activated.

The typical sequence of results after current initiation is:

- There is a rapid increase in current through and voltage across the fuse wire (A).

- The fuse wire vapourise (B) and an arc is establish (C).

- The arc limits the prospective fault current during the period (D).

- Arc containment is lost when the arc moves outside the blades arrangement. When this happens there is an increase in arc current and a reduction in arc voltage (E).

- The current continues to flow until the energy is dumped from the capacitor bank with an auxiliary circuit on the arc extinguishes. In these tests there was no arc extinction while the arc was confined within the blades.

As the capacitor bank voltage is increased with the associated rise in prospective current, the expansion in general appears to be more rapid evident by the shorter time period after the fuse wire has vaporised and the arc left the blade structure.

4.2 Small Blades Arrangements

The results presented in this section are for a helical coil with blade sizes (180mm diameter) as has been described in section 2.1.1. The tests were divided into two stages with different arrangements of blades. In the first stage the plunger was inserted which is presented in sections 4.2.1 to 4.2.3 and in the second stage of testing the plunger was removed, sections 4.2.4 to 4.2.5. The purpose of these stages was to investigate the effect of plunger (inserted or removed) on the arc expansion and current limitation.

4.2.1 4PTFE Turns

4.2.1.1 Arc Current and Voltage

The time variation of the helical arc radius, as determined from the high-speed photographs, is shown in Figure 4.3, along with the time variation of current and voltage. It shows the arc voltage and current respectively as a function of time after fault-current initiation.

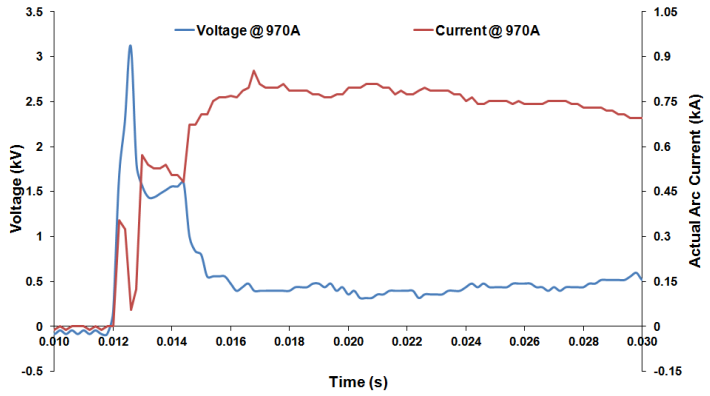

(a)

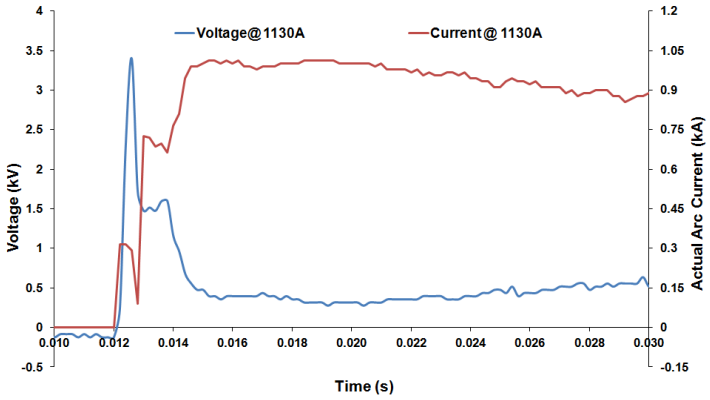

(b)

Figure 4.3: Time variation of arc Current and Voltage

Increasing the capacitor charging voltage produced a steeper initial di/dt value. Arc initiation occurred at progressively higher instantaneous currents and shorter time scales as the di/dt increased consistent with the energy in-

put required for fusing the inter electrode wire. Following arc initiation, the fault current reduces and is finally interrupted on arc extinction. When changing prospective fault current from 970A to 1130A (figures 5.3a and 5.3b respectively), it may be seen that the time at which interruption occurs is brought forward from 14.5ms to 14ms, indicating that the arc moves more quickly and reaches the edge of the blade faster with 1130A.

4.2.1.2 High Speed Photographs and Arc Shape

Figure 4.4a shows several frames of the arc expansion for helical arc device. The interval between each frame is 2ms, with an exposure time 20μs. In the first frame, the fuse wire is partly vaporized, and this was follow by 2 frames in which the fuse wire has completely vaporized. The period for the fuse wire vaporizes was used to synchronize the current and voltage waveforms with the high speed film record. Once the arc has fully formed its expansion continues until it leaves the confines of the helical blades. An enlarged frame is shown at figure 4.4b, where the separator is perspex comb which helps to keep the helical blades apart.

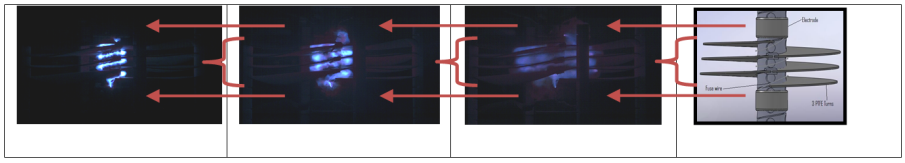

(a) High speed photographs taken during the system test

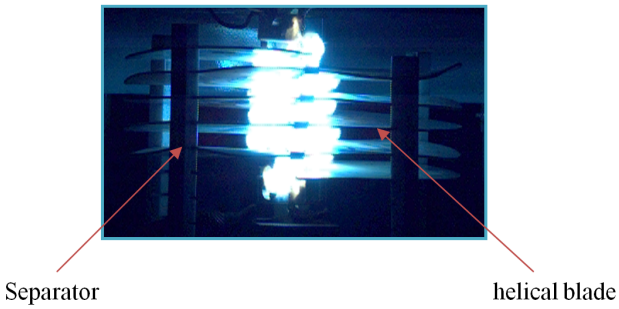

(b) Enlarged frame

Figure 4.4: High speed photographs

4.2.2 2PTFE + 1Copper + 2PTFE Turns

Figure 4.5 shows typical current and voltage results during the formation of the helical arc for a 2PTFE, 1Copper and 2PTFE blade arrangement. It is particularly interesting to note that the prospective fault current is forced to near zero towards the end of fuse wire vaporization and there is a subsequent rise in voltage to 3.6kV. As with other cases for a helical arc a relatively long discharge is produced in a relatively small volume. The subsequent rise in current (E) is a result of the arc moving outside of the helical blades. The sequence of events is that the current starts to flow through the fuse wire at point (A). During the period marked (B) the fuse wire completely vaporises and an arc is established (C). The arc then expands outwards during period (D) for approximately 2ms until it reaches the outer edge of the blades where inter turn short circuits occurs (E).

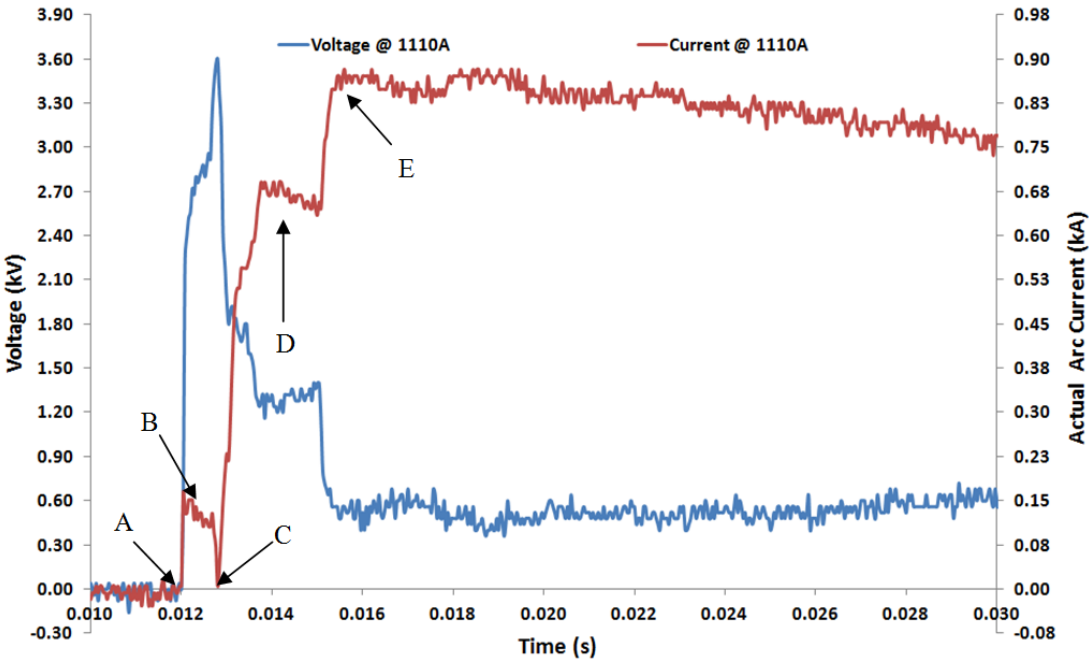

Figure 4.5: Current and Voltage characteristic for 2PTFE, 1Copper, 2PTFE blade arrangement

Figure 4.6 shows a more complete time sequence of typical frames during the expansion of the helical arc for the 18mm-pitch, solid-cored device where the expansion velocity is typically 40m/s. The high speed camera photon SA-1 colour was used where interval between each frame shown is 50μs, with an exposure of 20μs. The fault current was controlled to 530A whilst inside the blades and that developed an arc voltage of 1.55kV. The arc remained in the blade area for 2ms.

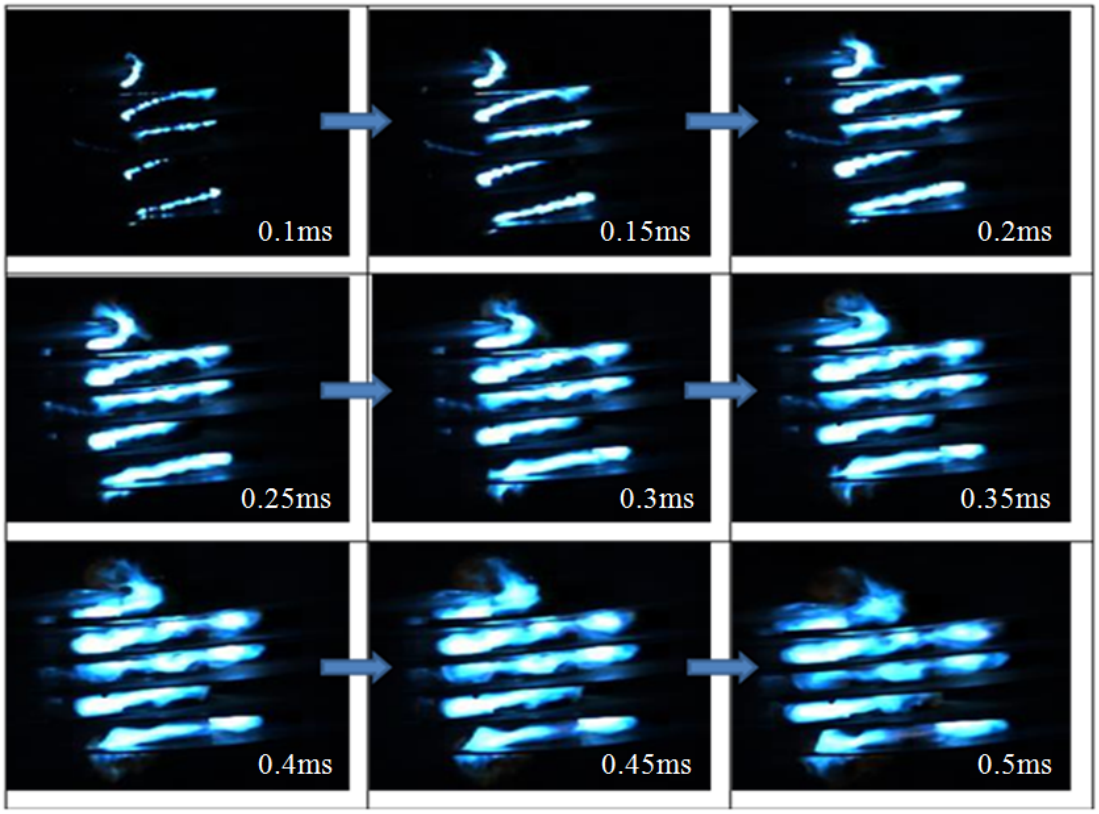

Figure 4.6: High speed photographs

Figure 4.7 shows the output recorded by the optical fibres with their positions as described in section 3.8.1. Light emitted by the arc is recorded by the fibres as it reaches their viewing area. These fibres still record a low level of light emission from the plasma before and after the arc front has passed, seen as a noise level on Figure 4.7, due to the convoluted helical shape of the arc. The signal recorded by F1 occurs before that on F3, confirming that the arc is expanding outwards.

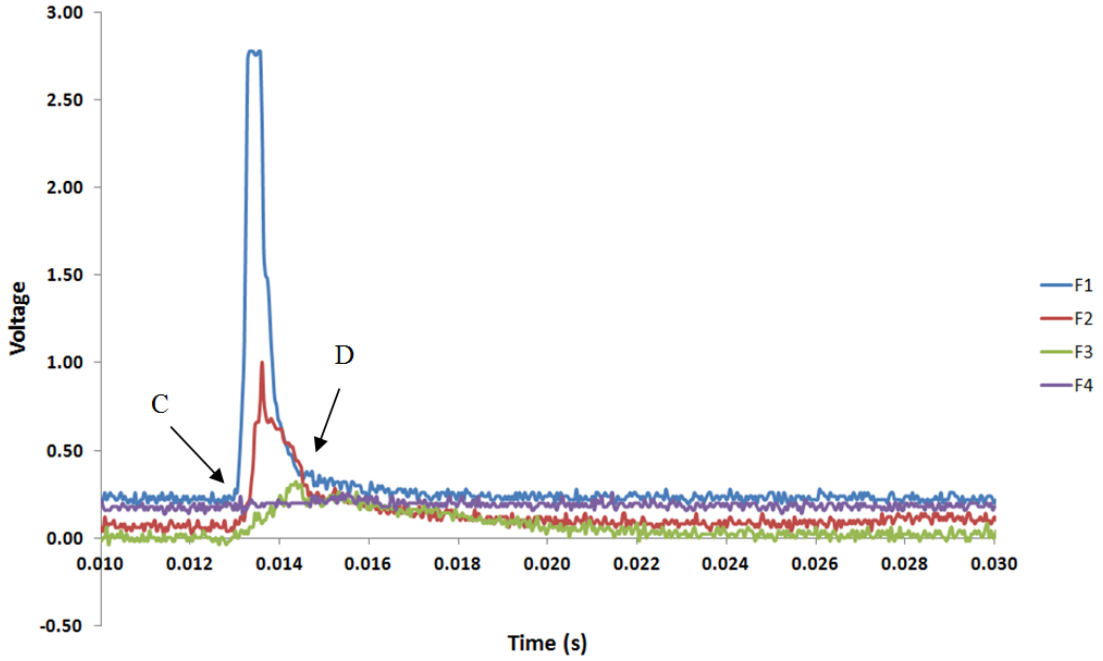

Figure 4.7: Optical fibre output for 2PTFE, 1Copper, 2PTFE

Through the arcing period the amplitude of the optical fibre signals varies as the arc moves outwards and after leaving the confinement of the blades the signal reduces to a low value. There is no signal recorded on F4 this is due to the arc not reaching the chosen fibre viewing point which is located outside the limit of the blades. The results for F1 to F3 confirm that the arc continues to expand.

The front edge of each pulse is used for the timing purposes. The time interval between pulses from one fibre to its neighbour represents the time taken for the arc to expand the incremental radial distance between one fibre viewing location and its neighbour. Moreover for each pulse on, say, F1, there is a corresponding pulse on F2 and F3, leading to three different values for the time taken by the arc travelling between these locations.

4.2.3 1Copper + 2PTFE + 1Copper + 2PTFE + 1Copper Turns

Figure 4.8 shows typical current and voltage results during the formation of the helical arc in a 1Copper, 2PTFE, 1Copper, 2PTFE, 1Copper arrangement. It is particularly interesting to note as before that the fault current is forced to near zero and high voltage is developed across the arc at 3.8kV (C). Note that this is due to the transition between the vaporisation of the fuse wire and the establishing of an arc. The maximum controlled fault current is approximately 530A with a mean voltage of 1.55kV (D). The arc was confined within the blades for 2.4ms.

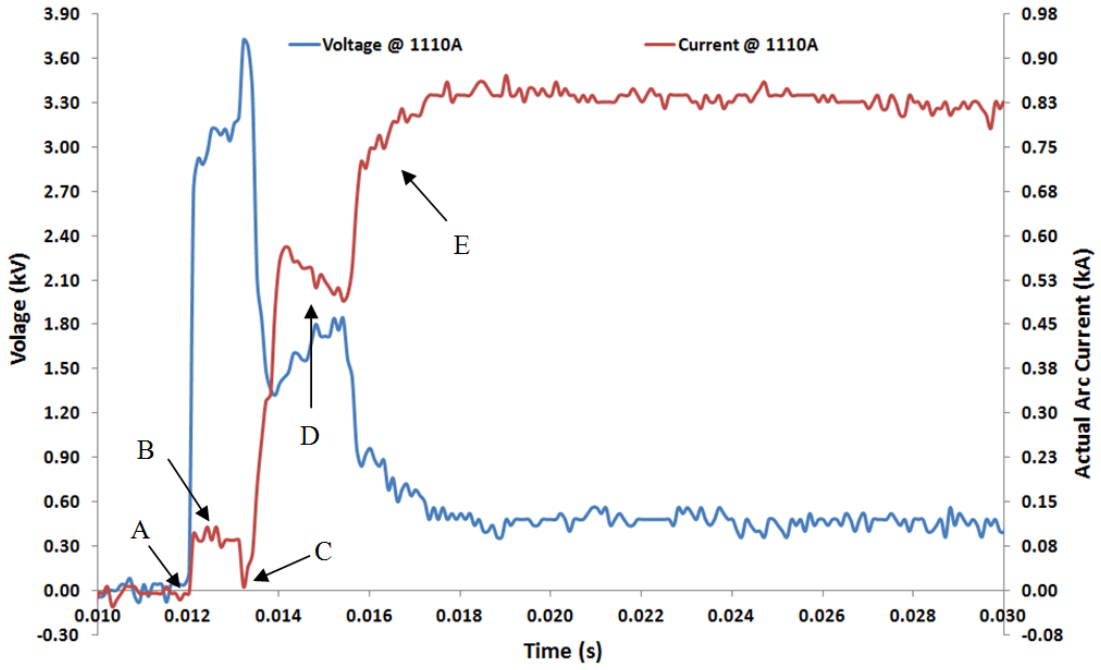

Figure 4.8: Current and Voltage characteristic for 1Copper, 2PTFE, 1Copper, 2PTFE, 1Copper

Figure 4.9 shows some typical frames during the expansion of the helical arc by using the high speed camera for 1copper, 2PTFE, 1Copper, 2PTFE, 1Copper.

These frames were taken with a high speed camera photon SA-1 colour was

used. The frame separation is 50μs with an exposure of 20μs. In the first frame, the fuse wire was partly vaporized, and this was followed by number of frames in which the fuse wire has completely vaporized by frame 20. After frame 20, subsequent frames show the influence of the middle copper blade in that it acts as an additional electrode by simply acting as a point to which arc roots attach and the current flows through the copper blade. Essentially, there are two arc discharges in series separated by this conducting blade (arc 1 and arc 2 on Figure 4.9).

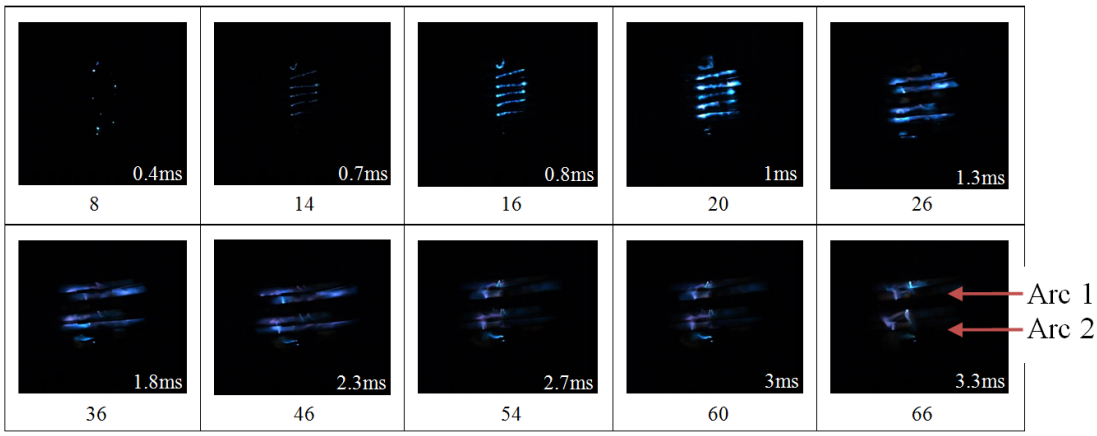

Figure 4.9: High speed photographs

4.2.4 1Copper + 4PTFE + 1Copper Turns

Figure 4.10 shows typical current and voltage results during the formation of the helical arc for 1copper, 4PTFE, 1Copper with the inner core unblocked.

During the controlling period the arc current was limited to 600A, about half of the prospective current, and the arc voltage was 1.55kV. The arc remained in the blades for 2.5ms.

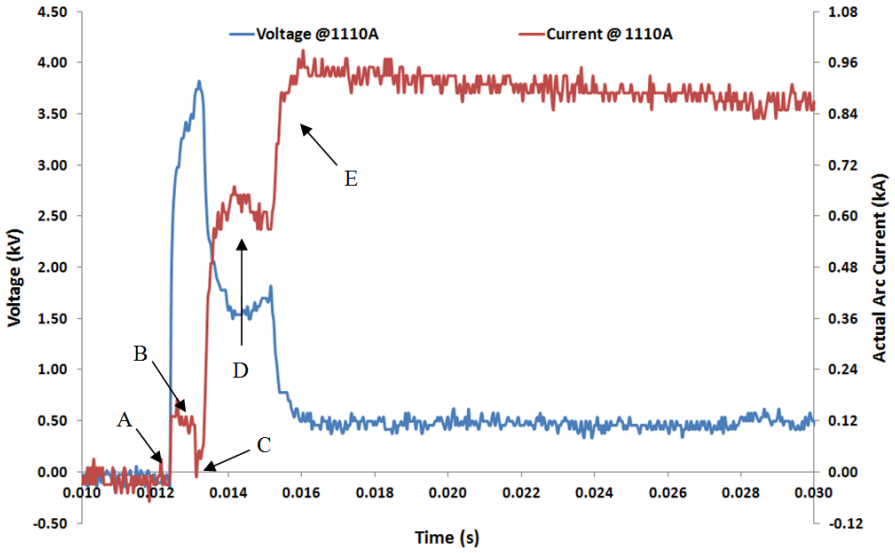

Figure 4.10: Current and Voltage characteristic for 1Copper, 4PTFE, 1Copper

4.2.5 1Copper + 5PTFE + 1Copper Turns

Figure 4.11 shows typical current and voltage results during the formation of the helical arc for 1copper, 5PTFE, 1Copper with the inner core unblocked.

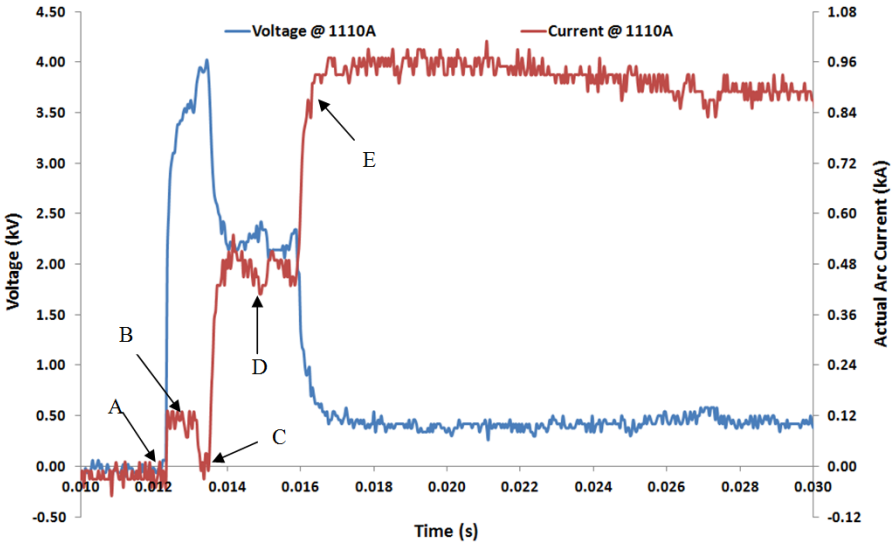

Figure 4.11: Current and Voltage characteristic for 1Copper, 5PTFE, 1Copper

The controlled fault current is 470A, less than half of the prospective current, and the associated arc is confined within the blades for 2.5ms.

4.3 Medium Blades Arrangements

The sizes of the blades were increased to 360mm diameter, twice the original size (180mm diameter), to investigate the ability of controlling the arc and limiting current over a large period of time. The tests were divided into two parts. In the first part the PTFE with copper turns were tested and in the second part of testing the PE with copper inwards were tested. This was to investigate the affect of different material on the arc movement. Using the high speed camera, the rate of arc expansion could be determined. A new plunger made of PTFE material instead of tufnol material was used in this type of tests. This new plunger was used to determine its influence on the behaviour of the arc expansion. The same plunger is used for test with large blades presented later (section 5.4).

4.3.1 PTFE and Copper Turns

4.3.1.1 2PTFE + 1Copper + 2PTFE

Figure 4.12 shows the test results of current and voltage characteristic for 2PTFE, 1Copper, 2PTFE blades. This shows the flow of the current through the fuse wire (A) then the arc start to establish after the fuse wire is completely vaporized (B). Thereafter, the prospective fault current is forced to near zero and a very high voltage is produced at 3.75kV(C). In this result, the arc voltage is ∼1.6kV and the fault current is limited to an average of 650A (D) with the prospective fault current being 1050A. The expansion time is 10ms before the arc leaves the confines of the blades (E). The average expansion velocity is 16m/s. The time to reach to the outer limit of the blades kept increasing and this indicates that PTFE does have a low amount of ablation since its melting point is high (330-372^{0}C) [Lide, 2004] which means the arc keeps expanding within the limit of the blades for

some period and is controlled.

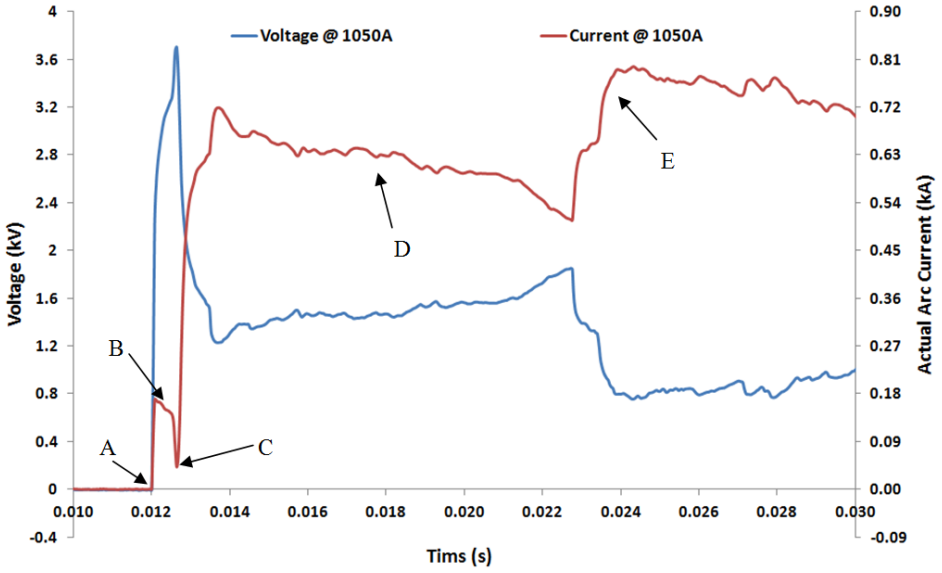

Figure 4.12: Current and Voltage characteristic for 2PTFE, 1Copper, 2PTFE

The high speed camera results give an indication of the arc behaviour for this type (Figure 4.13). The time between frames is 50μs with an exposure time of 20μs of the arc under these conditions. As may be seen in frames 5 to 8, the arc has established roots to the copper disc and current flow is through that. Effectively, there are now 2 arcs in series with the copper disc acting as an electrode. This confirms the behaviour observed for small blades as seen in Figure 4.9.

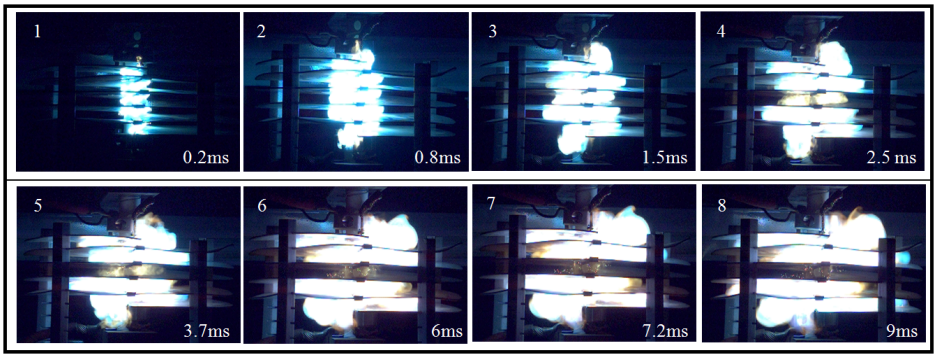

Figure 4.13: High speed photographs

4.3.1.2 2PTFE + 2Copper + 2PTFE

In Figure 4.14, the voltage rises quickly to a peak of 3.75kV after initiation forcing the arc current to a low value. The actual arc current rises sharply to approximately 700A, and then it starts to fall as the arc expands; while on other hand the voltage decreases for 1ms and starts to rise again. The actual arc current continues to fall steadily downwards for 6ms until it reaches 430A. Afterwards, the actual arc current rises gently before a rapid increase after 1.5ms. This is due to the arc leaving the confinement of the blades and in turn short circuits. For this result the 2 blades of copper in the middle of the arrangement allows the voltage to rise more rapidly for 6ms than the previous results for one copper blade. The prospective current of 1050A has been limited to an average of 540A i.e. to approximately 50%. It is lower than the previous arrangement.

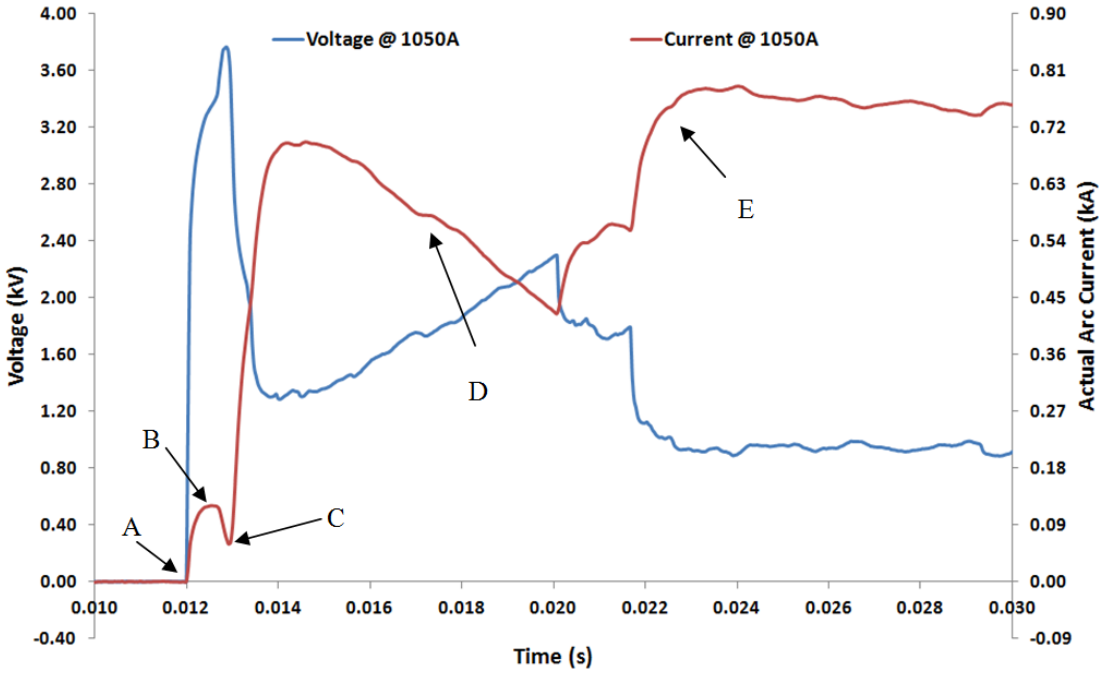

Figure 4.14: Current and Voltage characteristic for 2PTFE, 2Copper, 2PTFE

4.3.1.3 1Copper + 4PTFE + 1Copper

Figure 4.15 shows the arc current and voltage trace waveforms for 4PTFE and 2copper blades. 4PTFE blades are placed together with the copper blades on either ends of the arrangement i.e. top and bottom. Having copper blades in that position extends the existing anode and cathode electrodes.

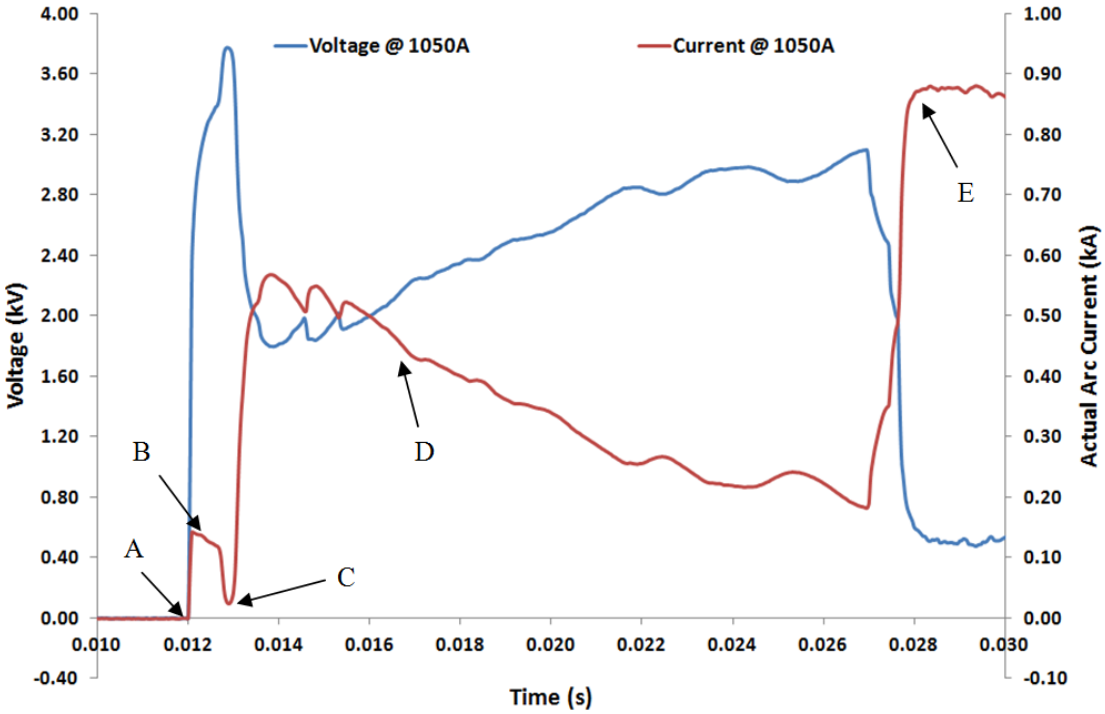

Figure 4.15: Current and Voltage characteristic for 1Copper, 4PTFE, 1Copper

The voltage waveform starts with a sharp rise up to a peak of 3.85kV. This forces the fault arc current to almost 0A after 1ms arc ignition. The actual fault current rises to 550A. At the same time the voltage falls to 1.8kV before rising gradually to approximately 3.10kV after 13ms. The actual arc current then continues to decay slowly for the next 13ms until it reaches 180A followed by a rapid increase to almost 880A and the voltage drops to 0.55kV as the arc leaves the confines of the arc blades. The arc was confined in the blades for a total of 14ms. Having 4 blades of PTFE in the middle and 2copper blades one

at each end resulted in a greater arc confinement time and therefore possibly improved arc control, whereas for the 2PTFE, 2Copper, 2PTFE arrangement the arc was confined for no more than 9ms and 10ms for the 2PTFE, 1Copper, 2PTFE arrangement.

4.3.2 PE and Copper Turns

4.3.2.1 2PE + 1Copper + 2PE

Figure 4.16 shows the test results of current and voltage characteristic for 2PE, 1Copper, 2PE blades.

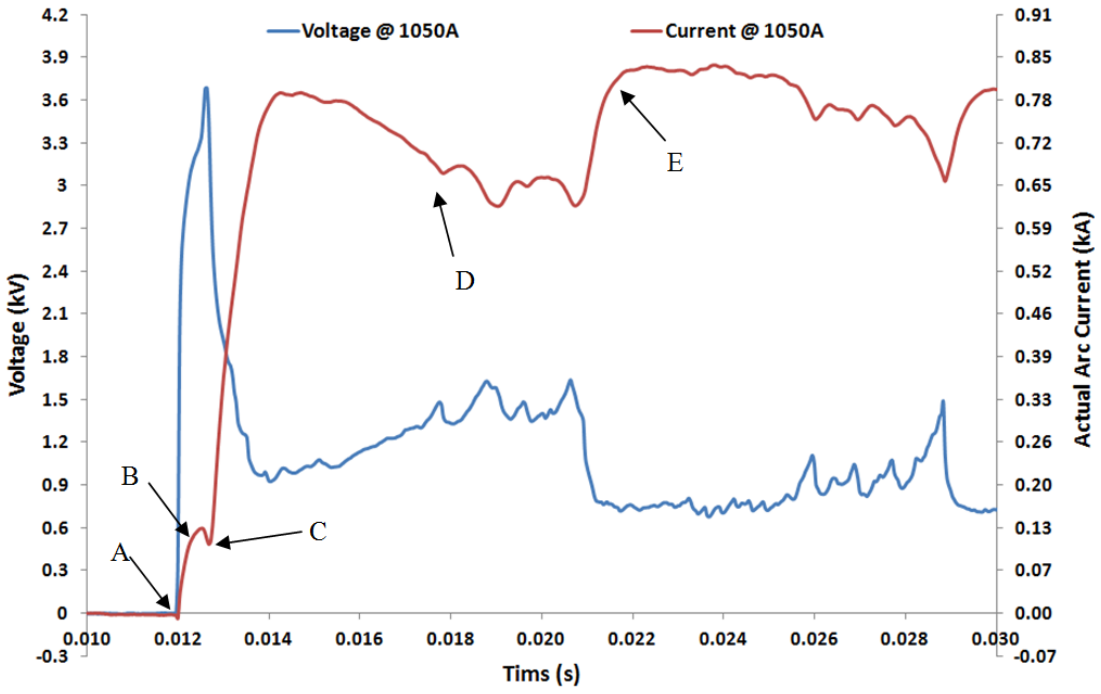

Figure 4.16: Current and Voltage characteristic for 2PE, 1Copper, 2PE

There is only a small reduction in arc current at (C) for this condition compared to the PTFE results. The current is limited to a mean value of 720A and the mean arc voltage was 1.2kV. The prospective fault current was 1050A. The arc remained in the blades for 8ms.

The high speed camera results give an indication of the arc behaviour for this different polymer. The time between frames is 50μs with an exposure time of 20μs allowed more detailed observation and better resolution. The frames shown in Figure 4.17 (PE) were taken at the same time periods from the arc initiation as those in Figure 4.13 (PTFE) which enables the images with the two polymers to be compared. The behaviours are very similar in general. The time to reach the outer limit of the medium PE (∼11.2ms) and PTFE (∼8.3ms) blades was longer in both cases than with small PTFE (∼4ms) blades.

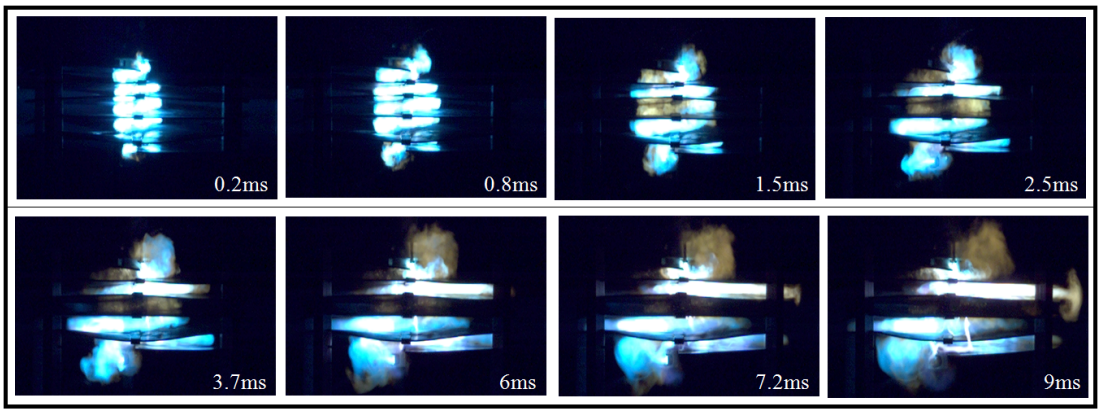

Figure 4.17: High speed photographs

4.3.2.2 2PE + 2Copper + 2PE

Figure 4.18 shows the current and voltage recorded for a 2PE, 2Copper, 2PE blade arrangement. As for the other results, after initiation of the arc the voltage raises quickly to a peak of 3.85kV forcing the arc current to reduce to a low value of (C). Once the arc is established the arc current rises rapidly to approximately 720A, and then it starts to fall; while on other hand the voltage initially decreases for 1ms and then starts to rise. The fault current continues to fall, for 7ms until it reaches 350A. As the discharge emerges from the blades the fault current rises gently for 1.5ms before a rapid increase. A similar profile was recorded for the

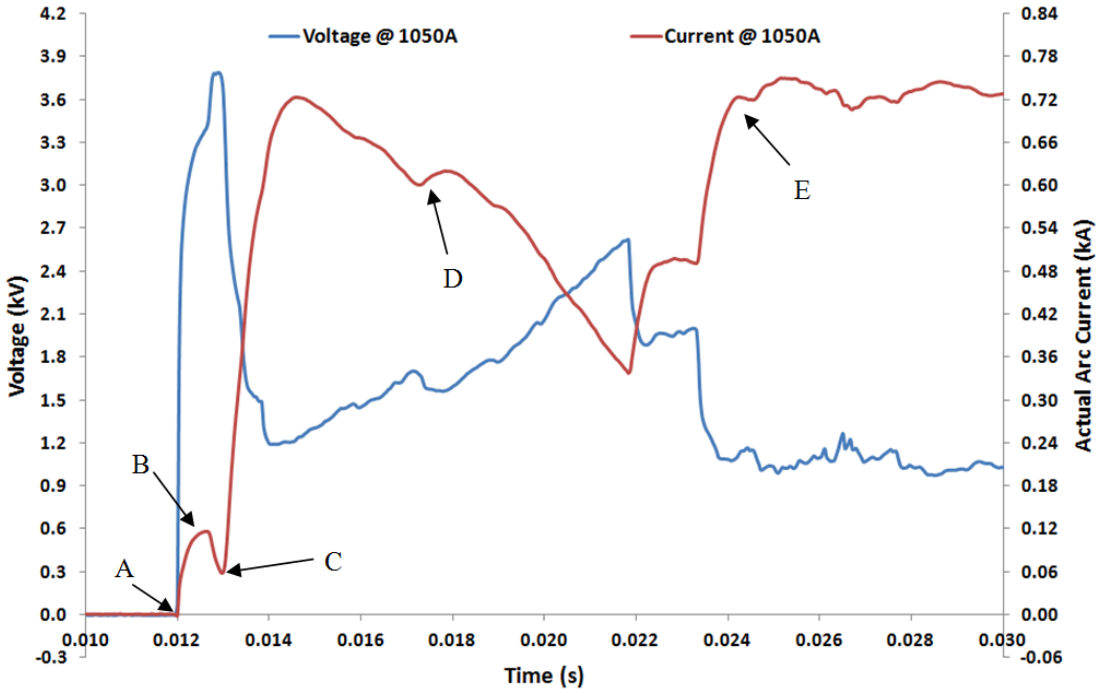

Figure 4.18: Current and Voltage characteristic for 2PE, 2Copper, 2PE

2PTFE, 2Copper, 2PTFE blade arrangement Figure 4.14. The prospective fault current of 1050A was limited to an average value of 550A.

4.3.2.3 1Copper + 4PE + 1Copper

A result for fault current limitation and arc voltage for a blade arrangement of 1Copper, 4PE, 1Copper blades is shown in Figure 4.19. The trends arc similar for the other test conditions. During the vaporisation of fuse wire the fault current reduce to 30A before it rises to 550A and reduces over time to zero. The arc voltage behaves differently reducing to 1.75kV after the fuse wire is vaporized and then build up again prior to current zero. The arc does not appear to have moved outside of the confines of the helical blades. This result shows a well controlled arc with a prospective fault current being reduced to approximately half its value (1050A to 550A), whereas for 2PE, 1Copper, 2PE arrangement the

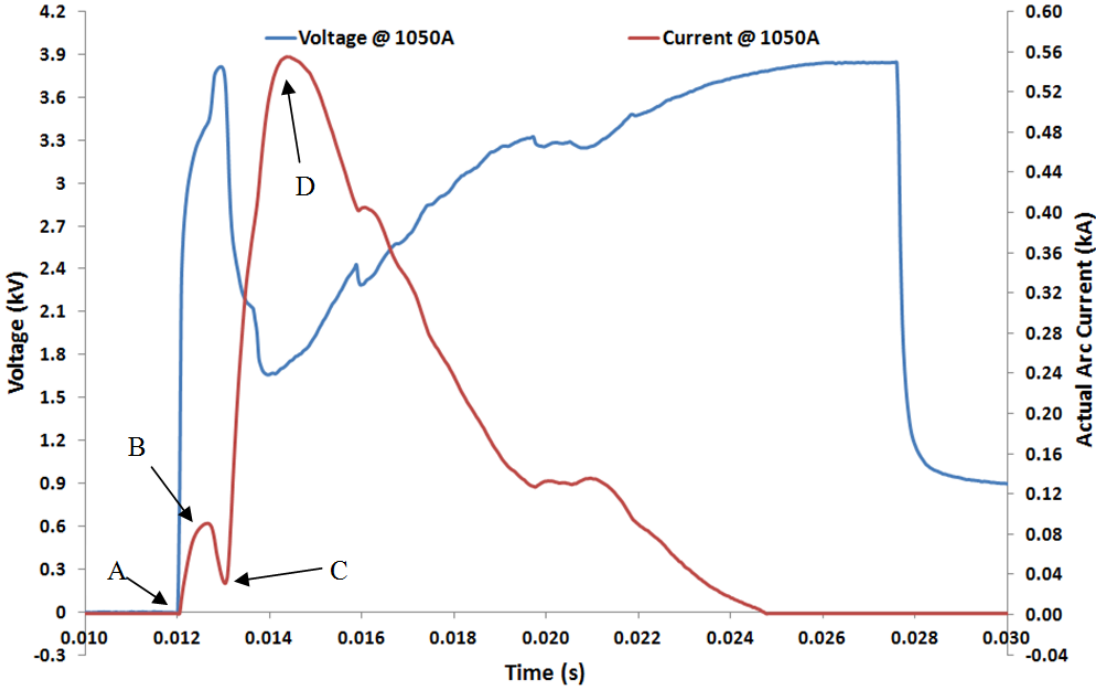

Figure 4.19: Current and Voltage characteristic for 1Copper, 4PE, 1Copper

arc left the blades structure.

4.4 Large Blades Arrangements

Large blades (500mm diameter) were inserted into the test rig and tested. Two blade arrangements were used; first test is a blade arrangement of 3PTFE turns. The second arrangement is 3PE blades these were selected to determine the effect that different material have on arc movement within the helical arrangement. High speed photographs can also provide information on the arc expansion.

4.4.1 3PTFE Result

As may be seen in Figure 4.20, vaporisation time is shorter here (∼0.5ms) than with the medium and small blades (∼1ms) but it is not considered to be a sig-

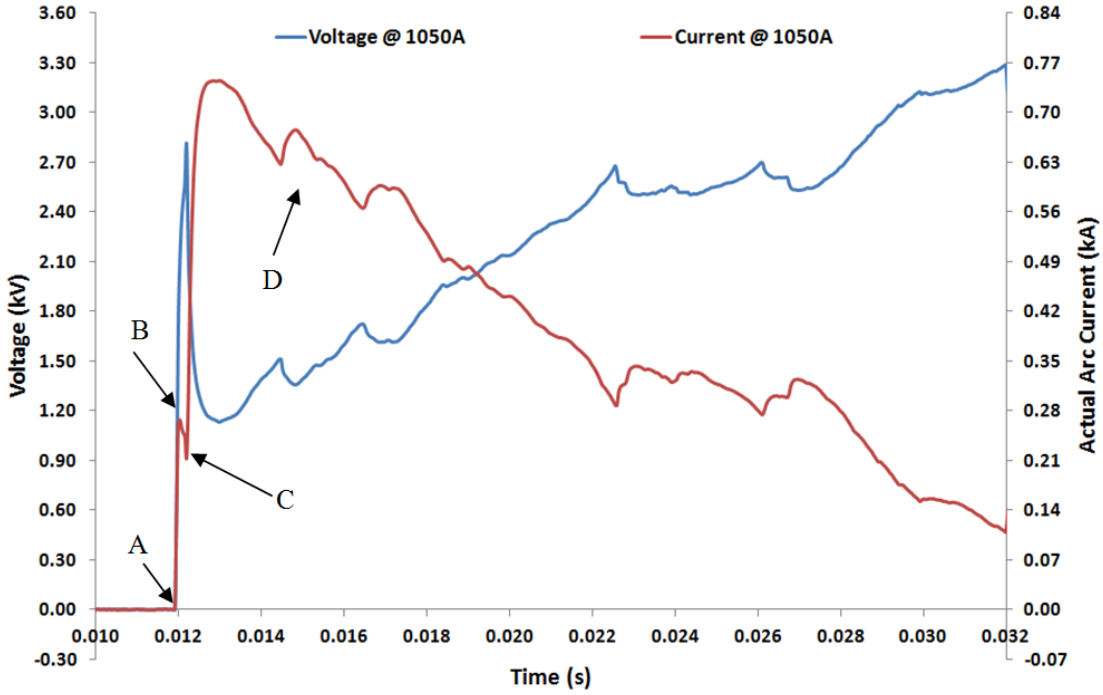

Figure 4.20: Current and Voltage characteristic for 3PTFE

nificant difference as it did not affect control of the arc by means of keeping it within the blade limits. (This applies also with the test shown on Figure 4.22).

The arc current and voltage waveforms for 3PTFE blades are shown in figure 4.20. The result for this arrangement is similar to those seen before, a rise in arc voltage during the forming of fuse wire and thus a sharp decline as the arc established; once the arc establishes then there is an increase in voltage as the arc expands outwards there are few small falls in voltage during the overall rise. The fault current was limited to an average of 470A with the prospective fault current being 1050A.

The arc current also shows the same trend as before. The high speed film images shown in Figure 4.21 are for a 3PTFE turns test with a selection of images during the arcing period.

The camera speed is 20000 frames per second, so that the exposure is 20μs

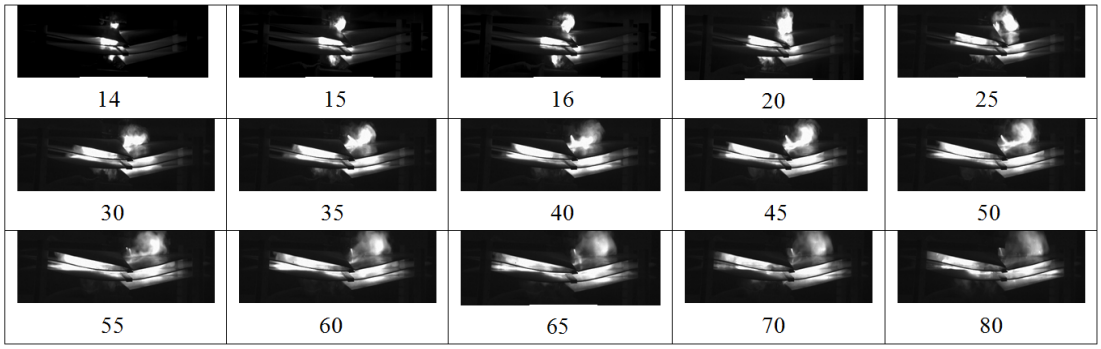

Figure 4.21: High speed photographs

with frame separation of 50μs. Frames 14, 15 and 16 shows the initiation of the arc and it is formation. In the frames which follow 20 to 60, the arc column is seen to expand outwards with the arc roots attached to the electrodes. The shaping of the fuse wire at the arc movement outwards pre-disposes the helical shape of the arc. In the last few frames 65, 70 and 80 these show that the arc remains within the limit of the blades.

4.4.2 3PE Result

Figure 4.22 shows arc current and voltage waveform for 3PE turns. With 3PE turns the fault current reduces to near zero within 14ms and the arc stays within the limit of the blades. The prospective arc current of 1050A has been successfully reduced and controlled. The fault current was limited to an average of 420A.

The high speed camera photographs shown in Figure 4.23 are for a 3PE blades test. The camera speed is 20000 frames per second, so that the exposure 20μs. In frames 20, 25, 30 and 35 the helical turn appear in a complete form. Frames 40, 45, 50 and 55 show that the arc remains within the limit of the blades. In the last few frames the helical turns do not persist for a long time but starts to collapse as the current reduces due to the arc limiting it. This decay of the arcs has been observed by [Spencer, 1987] and [Kolacinski et al., 1992]; for rotary arcs

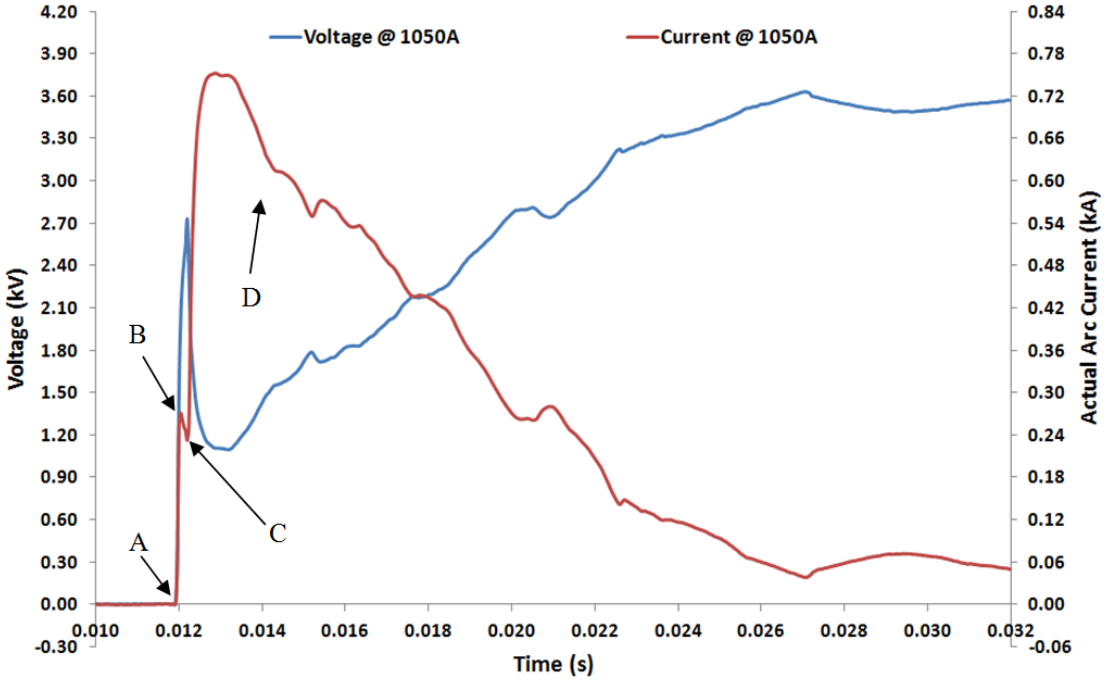

Figure 4.22: Current and Voltage characteristic for 3PE

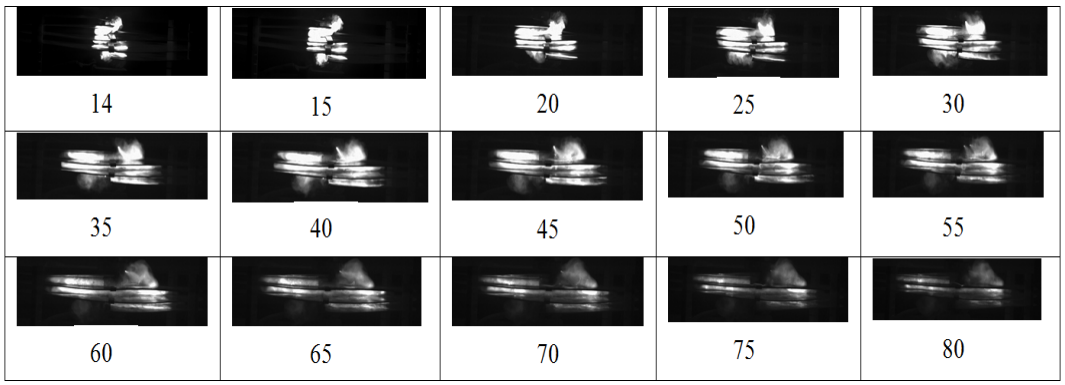

Figure 4.23: High speed photographs

and indicates the non-homegenesis in the cooling along the arc.

4.5 Summary

An arrangement for producing a helical arc has been experimentally investigated. Blades made from various materials have been used to keep the arc turns from

shorting. In addition, these blades also ablate and affect the arc's radial expansion. It is clear from the results that this arrangement can limit the arc current. Control of the arc is only maintained whilst it remains in the blades. When the arc emerges from the blades into turn shorting occurs and the arc is no longer able to limit the current as previously. Although a limit number of tests have been undertaken for different blade arrangements and despite shot-to-shot variations, it is possible to discern trends in the data but may contribute towards dc current limitation and interruption.

Table 4.1 shows, a summary results for the three blade sizes used and for all blade configurations tested, the average actual current during the current limitation phase (D) as a percentage of the fixed prospective current expected from the capacitor bank, and also the time instant (E) at which the arc leaves the confines of the blades.

Table 4.1: Summary Table

Test Size	Blade Arrangement	% of Current Limit	Time to Leaving Blades (ms)
180	4PTFE	33	15
	2PTFE + 1Copper + 2PTFE	50	15
	1Copper + 2PTFE + 1Copper + 2PTFE + 1Copper	52	15.4
	1Copper + 4PTFE + 1Copper	46	15.5
	1Copper + 5PTFE + 1Copper	58	16
360	2PTFE + 1Copper + 2PTFE	38	23
	2PTFE + 2Copper + 2PTFE	48	22
	1Copper + 4PTFE + 1Copper	66	27
	2PE + 1Copper + 2PE	31	21
	2PE + 2Copper + 2PE	47	23
	1Copper + 4PE + 1Copper	47	Did not reach
500	3PTFE	60	Did not reach
	3PE	65	Did not reach

As limiting the actual current and keeping the arc within blade confines is

useful, the utility of the blade sizes and configurations may be compared in the Table.

Chapter 5

Results Analysis

In this chapter the analysis of the results discussed in chapter 4 is presented. The analysis covers results obtained under a variety of different arcing condition including small blades (180mm diameter), medium blades (360mm diameter) and large blades (500mm diameter) arrangements in which different polymers (PE and PTFE) blades were also used.

5.1 Small Blades Turns (180mm diameter)

5.1.1 Helical Arc Radius (4PTFE Blades)

Using the high speed photographs it was possible to determine the average radius of the arc's within the four helical PTFE Blades. Figure 5.1 shows the helical arc expansion extent (diameter) with time for prospective fault currents of (890A - 1130A) which gave actual peak currents of (725A - 983A). Three frames were used to establish arc positions but two frames were available for arcs with currents of 970A and 1110A (prospective). Also shown is the limit of the size of the blades (diameter, dotted horizontal line). If the extent of the helical arc exceeds this

then the arc is outside of the helical blades (for example 1130A result). Note that the time shown on the horizontal axis is the time elapsed from just after the establishment of the arc. The results indicate that the helix expands throughout the arcing period, with the extent of the expansion influenced by the arcing current.

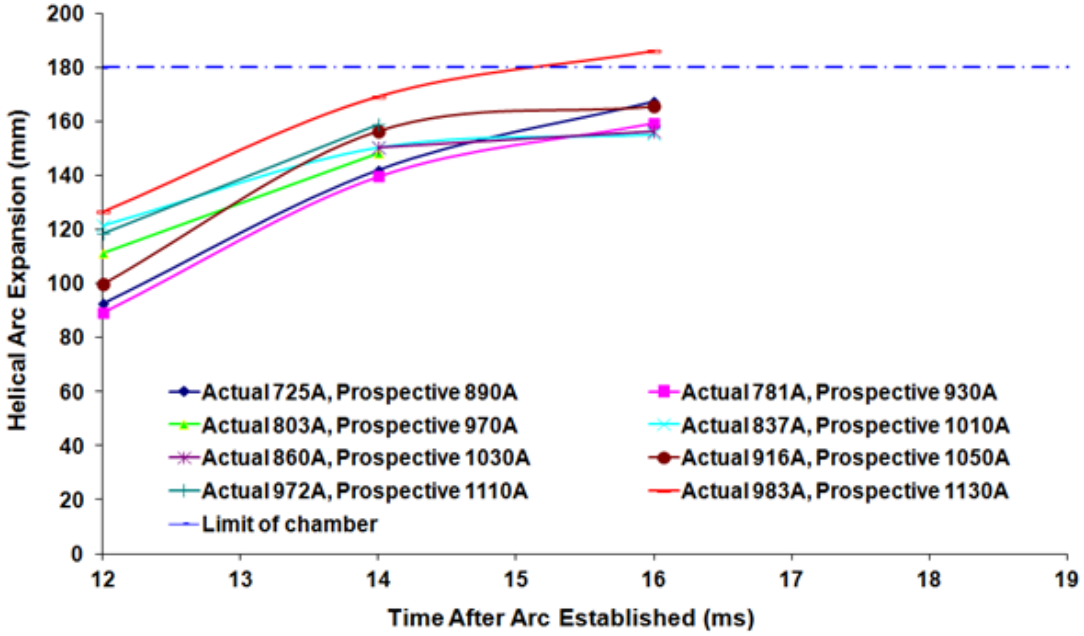

Figure 5.1: Radial expansion of the helix over the arcing period

Figure 5.1 implies that the expansion rate is not uniform over the entire period. Arc expansion rates (velocities) can be calculated from the time and radius data for the helical arc expansion (section 4.2.2). The average expansion velocity, V_c, is calculated according to equation 5.1, where $r_{(t)}$ is the arc radius at time t, and $r_{(0)}$ is the previous arc radius when the measurement was taken. $\triangle$t is the time difference between the two radial measurement times.

$$V_C = \frac{(r_{(t)} - r_{(0)})}{\triangle t} \tag{5.1}$$

It is worth reporting that all of the results show that the arc remained within

the confinement of the blades except for the prospective 1130A test result.

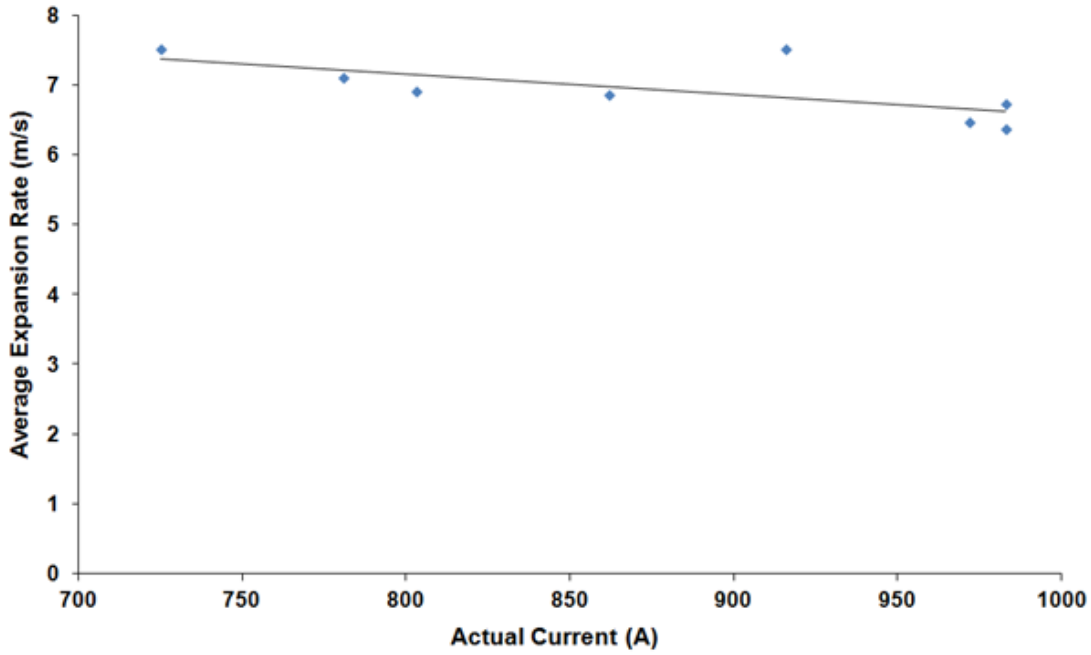

Figure 5.2: Expansion rate over actual current

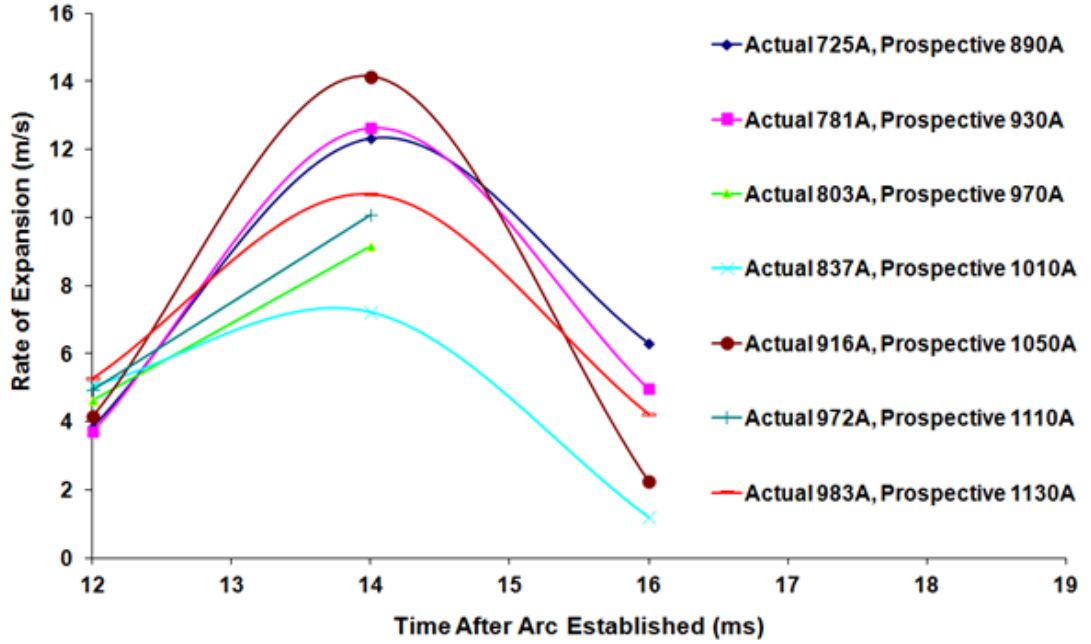

Figure 5.3: Expansion rate over elapsed time

Figure 5.2 shows the average expansion rate for the arcs generated at each

actual current. It indicates that the average rate of expansion tends to be almost constant at all actual currents (measured over the first 2-4 ms after arc establishment). Comparing Figures 5.1 and 5.2, the expansion rates are similar at all currents. But it may be noted on Figure 5.1 that the highest actual current arc (at 983A) at 12ms after arc established is already closer to the blade limits than the other arcs, which explains why it then exceeds the limits.

Figure 5.3 shows the rates of expansion for elapsed time after arc establishment. The figure shows an initial rapid rate of expansion which then slows.

5.1.2 Decay Time (4PTFE Blades)

A measure of the efficiency of arc control is the degree to which the arc current and voltage is affected. Ideally a rapid decrease in arc current with a corresponding rapid increase in arc voltage is required. This indicates that effective current limit mechanisms are in place.

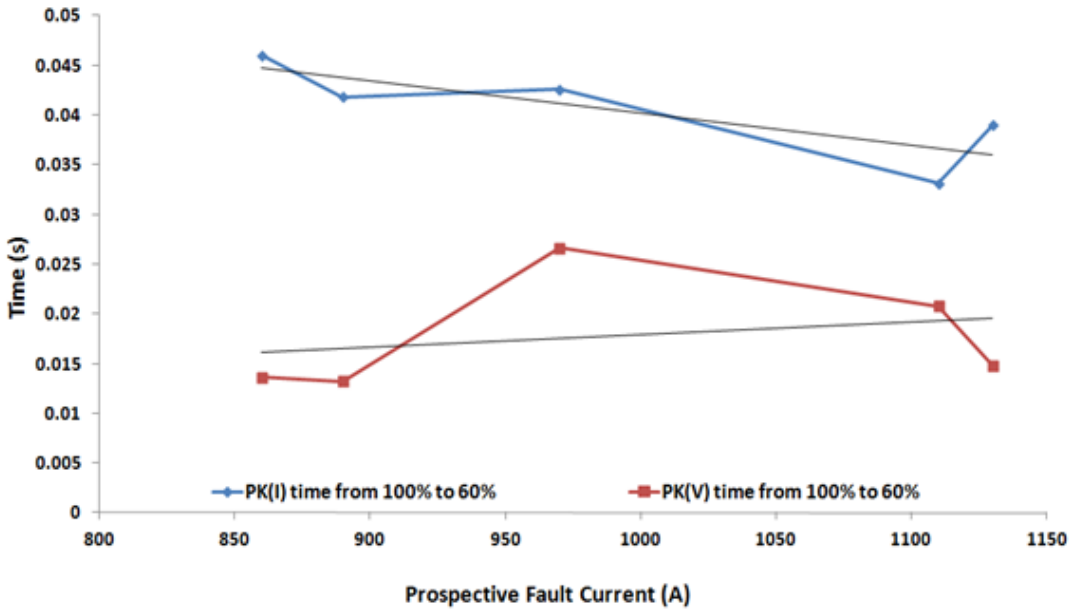

Figure 5.4: Decay time for the peak current and voltage from 100% to 60%

Figure 5.4 shows the decay time for the peak current to reduce to 60% of its peak value. The PK(I) value is for current. The trend shows that for higher fault currents the decay in current is quicker. The PK(V) value for arc voltage shows a corresponding rise as expected.

5.1.3 Arc Axial Velocity (Four PTFE)

Figure 5.5 shows the arc velocity, here in a downward direction (as opposed to arc radial expansion), for different fault currents measured from 3 frames of the high speed camera in each case (or 2, where only 2 are available). The trend line shows a gradual rise in the helical arc velocity as the fault current increases.

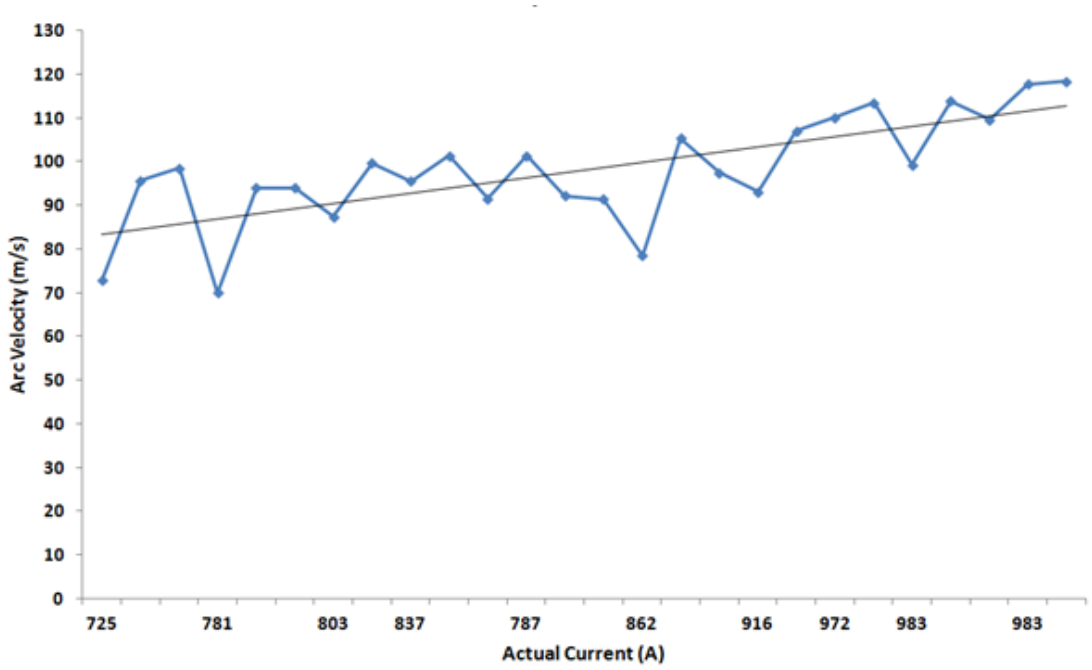

Figure 5.5: Arc velocity versus actual current

The arc velocity, V_a, is calculated according to equation 5.2, where l is the arc length and $\triangle$t is the time difference between the two measurement times (t_n-t_{n-1}).

$$V_a = \frac{l}{\triangle t} \tag{5.2}$$

Where

l = no.of turns x arc circumference

= no.of turns x π x arc radial expansion ($d_{(n)}$-$d_{(n-1)}$)

5.1.4 Radial Arc Expansion Velocity with 2PTFE + 1Copper + 2PTFE Turns

Radial arc expansion velocities for the configuration with 1 copper blade in the middle of the PTFE blades are shown on Figures 5.6 and 5.7 as a function of time and arc radius as calculated using equation 5.1.

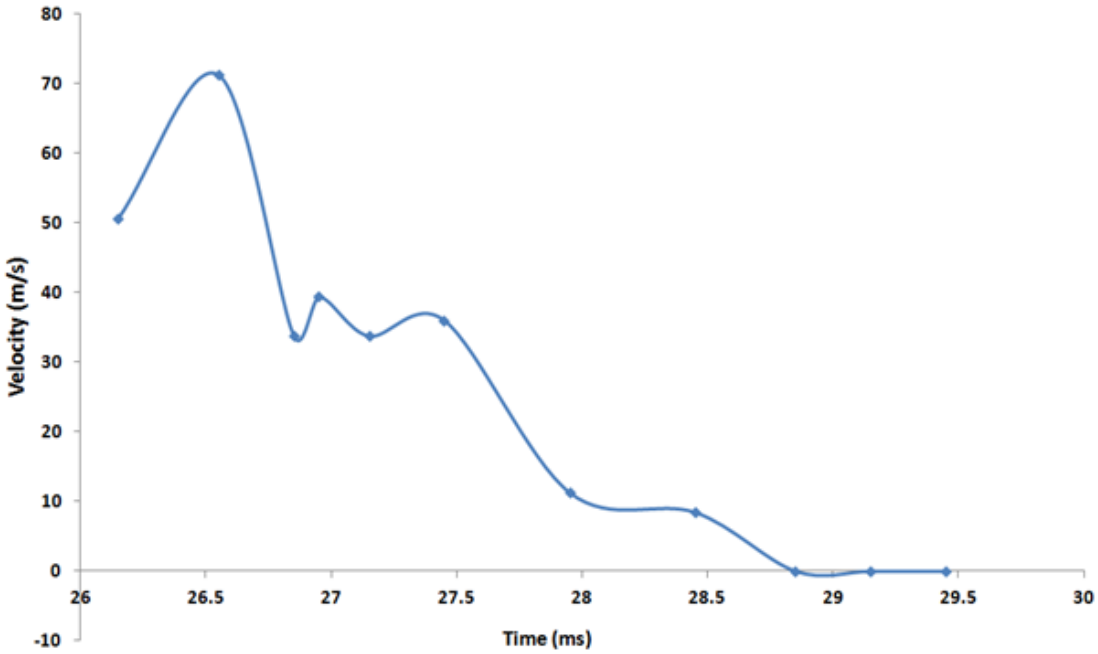

Figure 5.6: Arc expansion velocity as a function of time

The results in figures 5.6 and 5.7 show that for this test condition (where I_{pk} fault is 963A with a prospective fault level of 1110A), the arc leaves the device

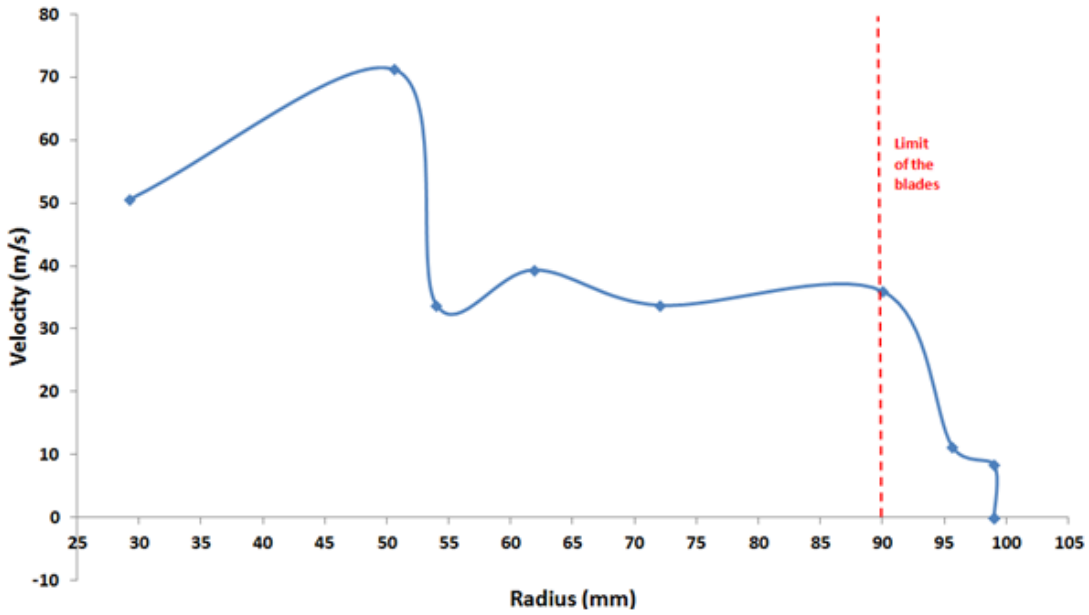

Figure 5.7: Arc expansion velocity as a function of arc radius

before the end of the arcing period ($\sim$ 28.5ms, Figure 5.6). The results also show that as the arc expands outwards its velocity decreases. This is also seen in Figure 5.3 where the expansion slows during the arcing period.

5.1.5 Relation between Actual Current And Prospective Current

Figure 5.8 shows the relationship between actual current and prospective current for 1Copper, 2PTFE, 1Copper, 2PTFE, 1Copper arrangement. A similar relationship holds for the other arrangements. It can be seen from the figure that prospective fault current is always higher than the measured actual current. The prospective fault currents were produced by placing a shorting strap across the electrodes and then charging the capacitor bank to some different levels of fault current. Actual currents were taken from the experimental tests with arcs for the same bank charging voltage. Figure 5.8 also illustrates that the actual current

achieved is linearly related to the prospective fault current.

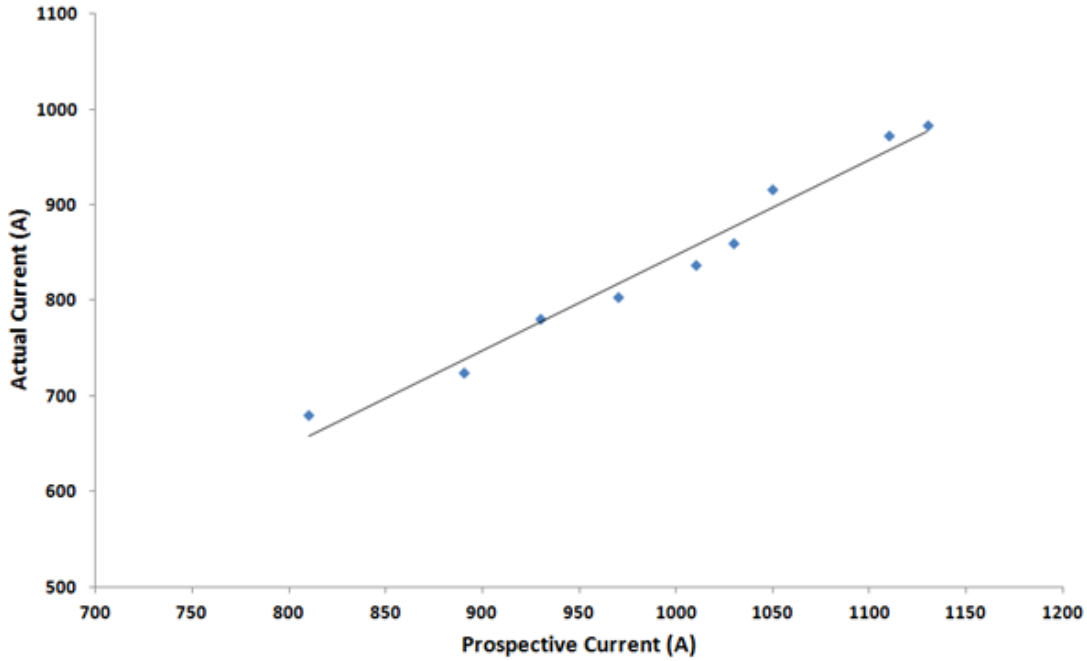

Figure 5.8: Plot between prospective current and actual current

5.1.6 Relation between the High Speed Camera Images and The Oscilloscope graph

Figure 5.9 shows results for 2PTFE, 1Copper, 2PTFE blades for a prospective fault current of 1110A the actual current is 963A. The results were obtained using high speed camera and are recorded in the form of a video during the experiment. Frames from the video were extracted to produce visual representation of features on the current and voltage records. The synchronization of the visual data with the current and voltage data was done through the same trigger signal triggering the camera and the oscilloscope. As may be seen from the graph, at 12ms the fuse wire starts to vaporize which leads to the arc expansion after the effects of fuse wire is finished at 12.8ms. The arc continues to expand until it reaches the

edge of the blades at 15ms where inter-turn shorting takes place. During this expansion period the arc does not appear at the central copper disk. It is likely that an arc root formed on the copper disk and current is passed via the copper disk to another arc root to the lower arc. It may be considered that there are 2 arcs in this arrangement.

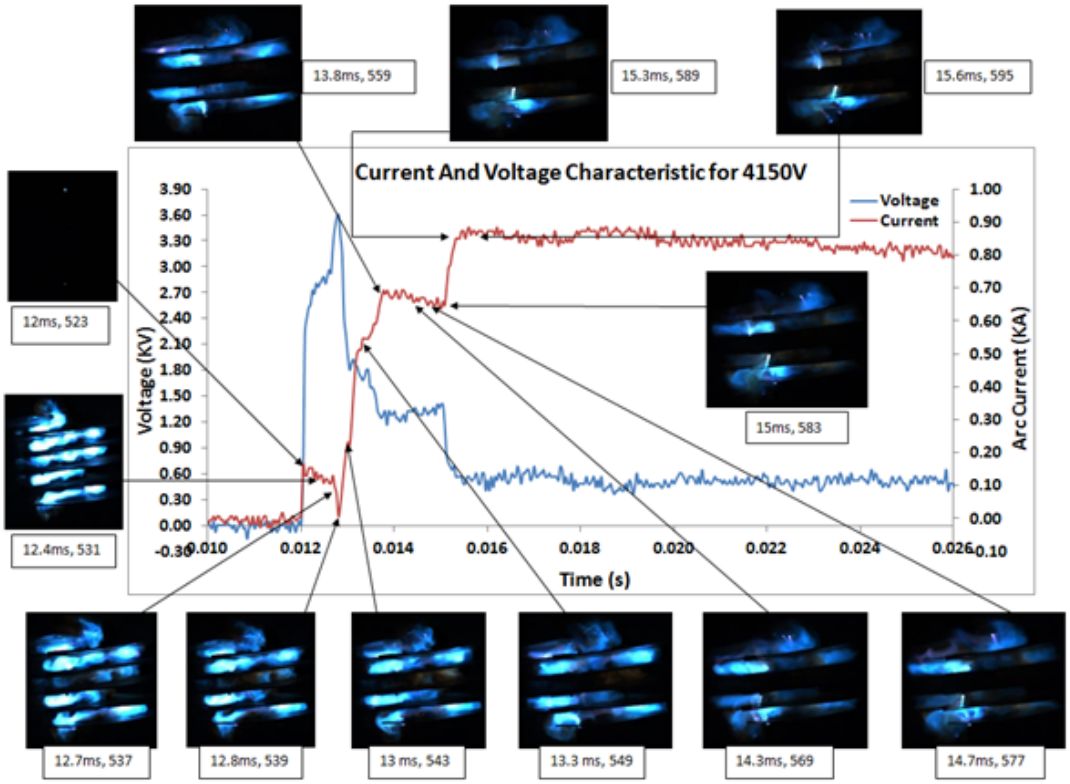

Figure 5.9: graph results of 2PTFE, 1Copper, 2PTFE with high speed camera images

5.1.7 Comparisons of Different Blade Combinations

Figure 5.10 shows a comparison of results for different arrangements of PTFE and copper blades for arc extinction. One arrangement has 4 PTFE and 1 copper blade (2PTFE, 1Copper, 2PTFE) and the other has 4 PTFE and 3 copper blades (1Copper, 2PTFE, 1Copper, 2PTFE, 1Copper). The arrangement with more

copper blades (3 copper, 12121) extinguished the arc more efficiently as is evident by no arcing being observed below a charging voltage on the capacitor bank of 4150V, whilst for the other arrangement arcing occurred at bank voltage of 3500V (Figure 5.10).

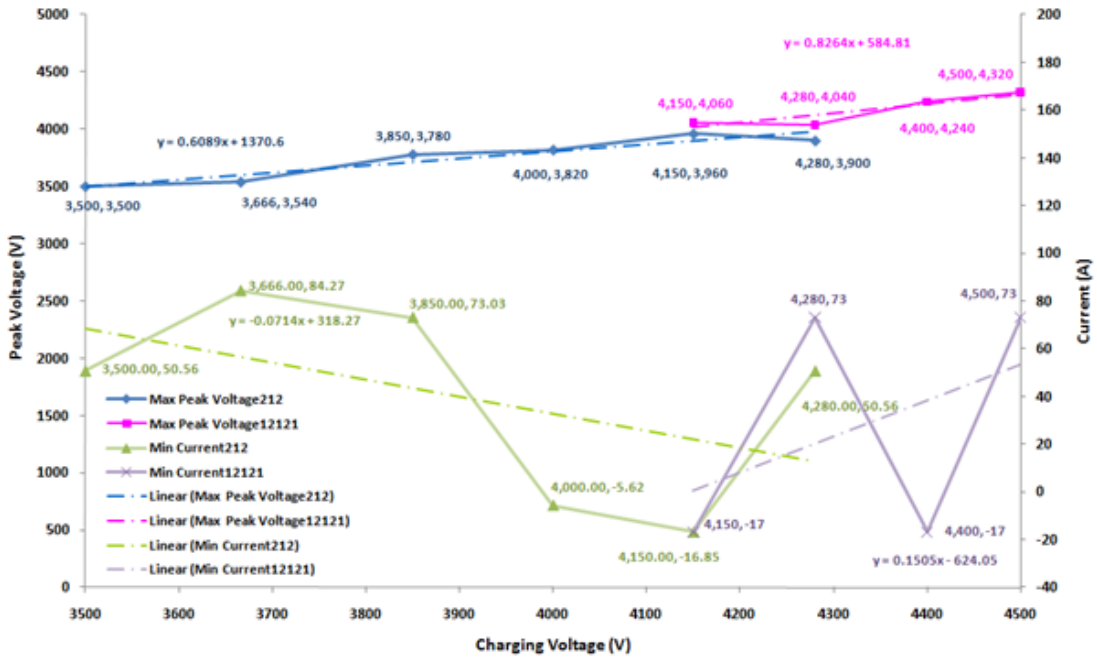

Figure 5.10: Comparison of Different blade Combinations

Figure 5.11 shows the limit current (period D, cf section 4.1.3, figure 4.2) against the actual current for three different types of geometries. The 3 sets of data which have been chosen are 4 PTFE and 1 Copper, 4 PTFE and 2 Copper, and 4 PTFE and 3 Copper. The latter set has 3 Copper blades configured as 1Copper, 2PTFE, 1Copper, 2PTFE, 1Copper. This last result shows that it is more effective in reducing the fault current from the same current e.g. current limitation ($\sim$ 520A) than the others ($\sim$ 650A current limitation) at the same actual current ($\sim$ 870A).

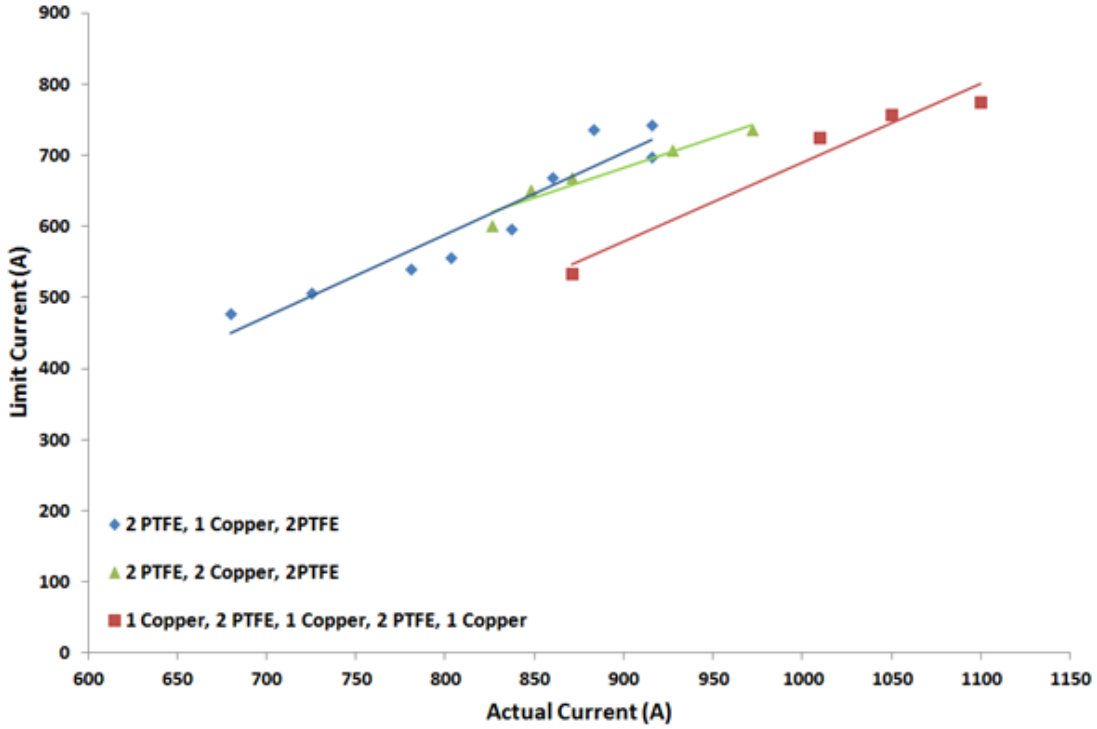

Figure 5.11: Comparison between actual current and limit current

5.2 Medium Blades Turns (360mm diameter)

5.2.1 Radial Expansion over the Arc Period (PTFE Blades)

Figure 5.12 (a-c) shows the expansion of the helical arc with the plunger inserted made of PTFE material (instead of tufnol material) throughout the arcing time period, where the extent of radial arc expansion is strongly influenced by the arcing current. With the exception of 930A (prospective, 3 turns), during the expansion time, the arc always stays within the limits of the blades indicating a stable arc which is under full control. Taking the exception case above, the graph closely follows the trend until the limits of the blades are exceeded, 35ms after the start of the experiment. The figure shows that the more turns that are added the less the arc moved to the external edge of the blade. With 5 blade arrangement this stopped approximately 40mm short of the edge.

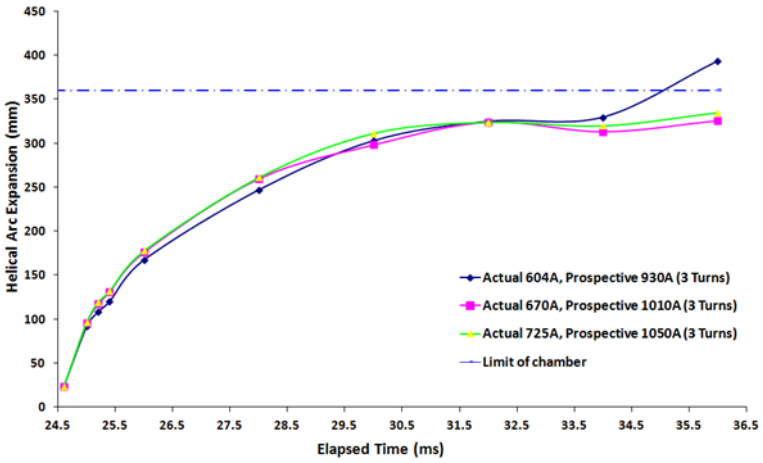

(a) 3 Turns

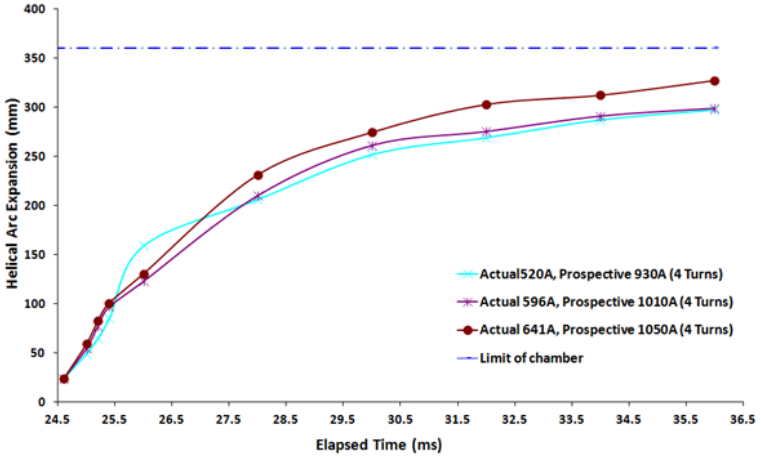

(b) 4 Turns

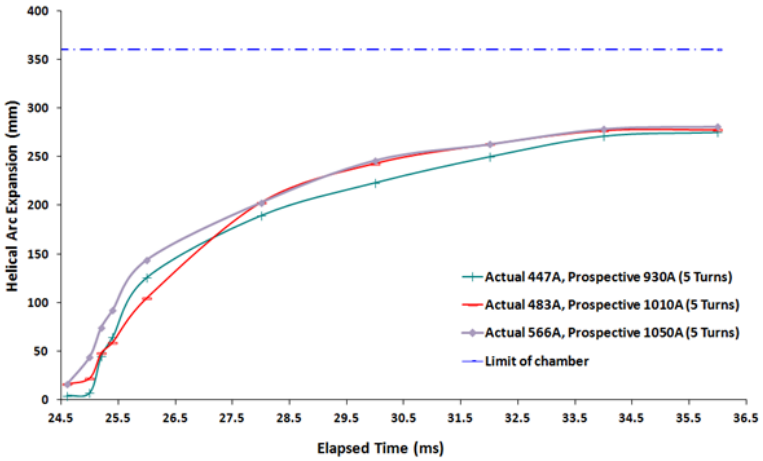

(c) 5 Turns

Figure 5.12: Radial expansion of the helix over the arcing period (plunger inserted)

Figure 5.13 shows the resultant plot for the average expansion rate against the actual current. There are three trend lines indicating 3, 4 and 5 turns each being represented by red, blue and orange lines respectively. The trends in expansion rates are constant with all currents for 3 and 4 turns but there is some shot to shot variation for the 5 turn results. Figure 5.2 (small blades) shows a similar trend with a more downward trend as the actual current increases. The average expansion rate is much greater here with medium blades than in Figure 5.2. One possible reason may be related to the availability of greater blade area to increase the driving force which is modelled in Chapter 6.

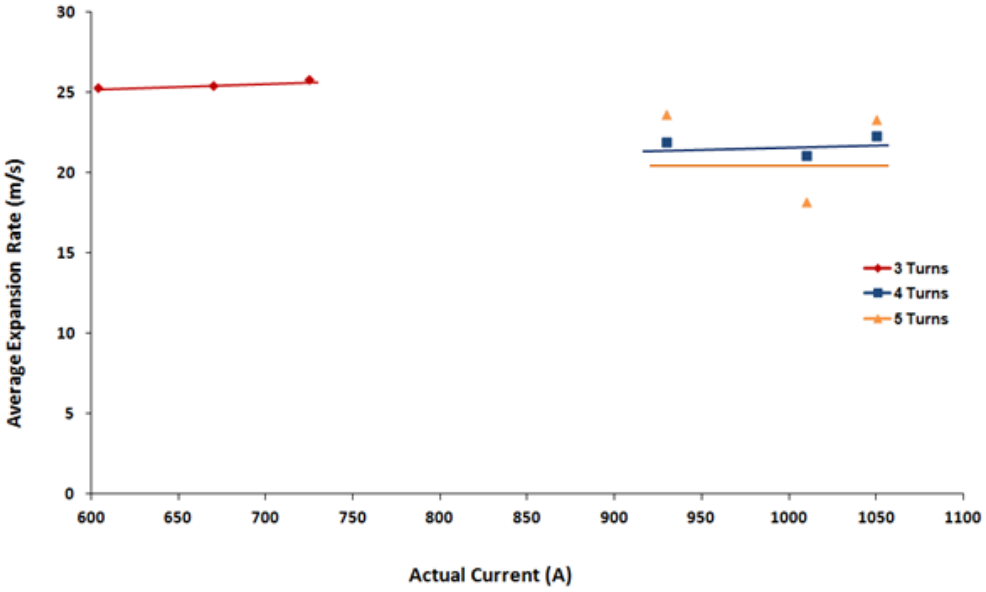

Figure 5.13: Expansion rate over actual current

Figure 5.14 (a-c)shows an initial rapid rate of expansion of arc radius which then slows over a relatively longer time period for all currents. For 3 and 4 turns, as the current increases this rate of expansion also increases based on the time after the arc is established, until it starts to decay. For 5 turns, at their peak (25ms), the rate of expansion also increased between 1010A and 1050A but the rate of expansion for 930A exceeded the rate of both 1010A and 1050A. To a first

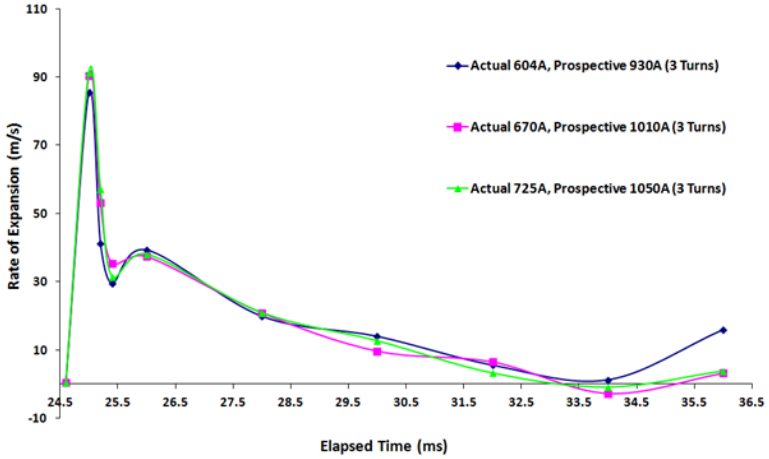

(a) 3 Turns

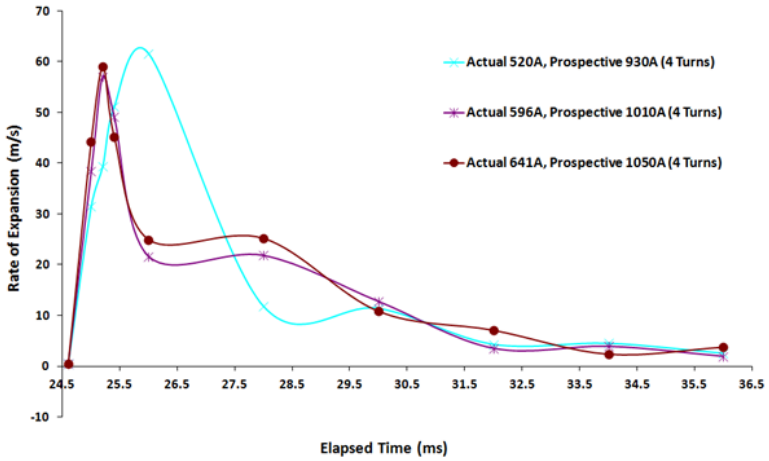

(b) 4 Turns

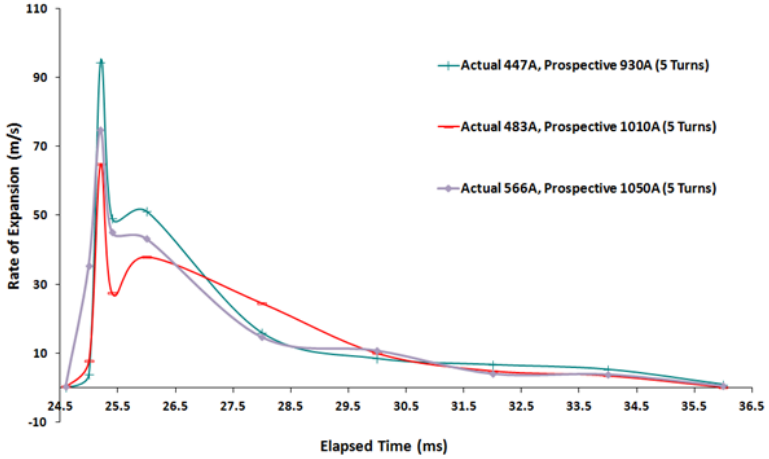

(c) 5 Turns

Figure 5.14: Radial arc expansion rate over elapsed time

approximation, the expansion rate for each of the three tests for the given blade arrangement is similar. For 5 blades (Figure 5.14 c) there is some variation in the peak expansion rate but it is not attributed to the actual fault current. It could indicate probabilistic behaviour of the arc.

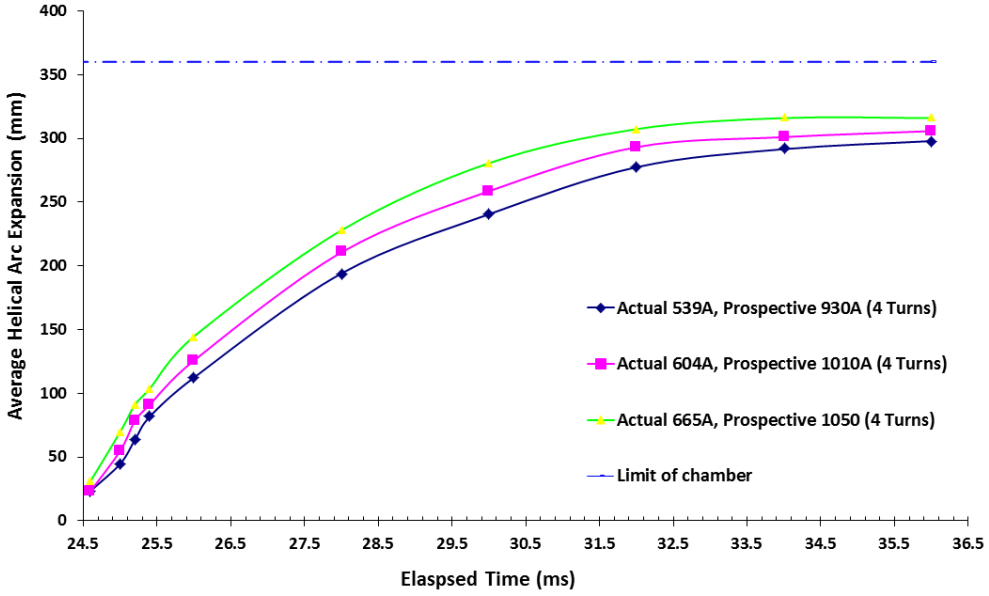

(a) 4 Turns

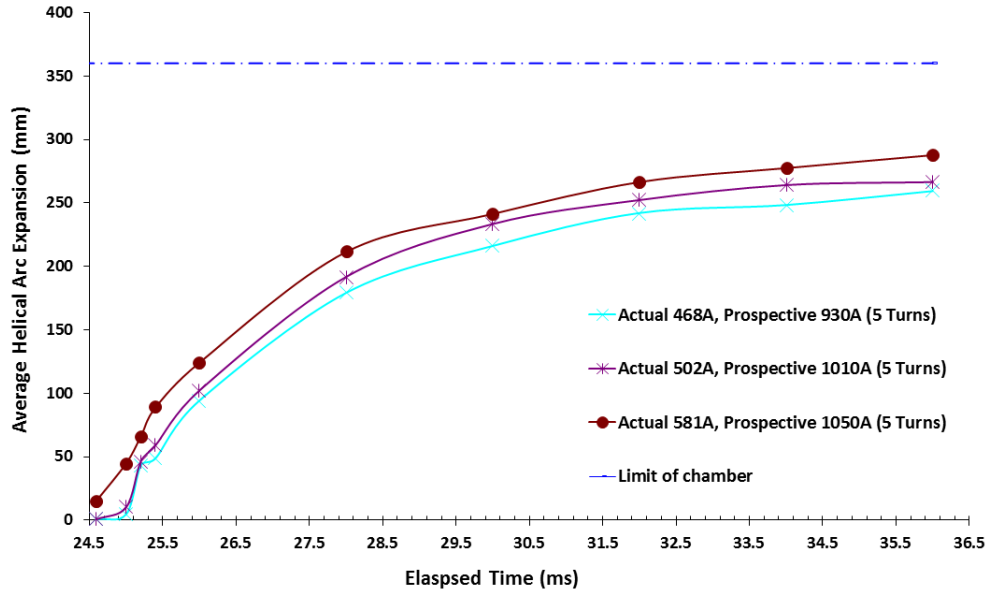

(b) 5 Turns

Figure 5.15: Radial expansion of the arc over the arcing period (plunger removed)

Figure 6.15 (a-b) shows the expansion of the helical arc with plunger removed throughout the arcing period time. The expansion is influenced by the arcing current whereas previously for this correlation was not as clear (Figure 5.12 b,c). During the expansion period the arc remains within the limit of the blades indicating that the arc remains under control. With the plunger removed gas can escape through the drilled holes in the rod (section 2.1). For the current range investigated, the arc expansion is marginally affected by the plunger with results for the plunger removed being lower than those with the plunger inserted. However the small difference implies that gas entering the core when the plunger is removed does not significantly affect the arc expansion. Chapter 6 explains more about the arc movement based on the different factors which affect the expansion speed and direction.

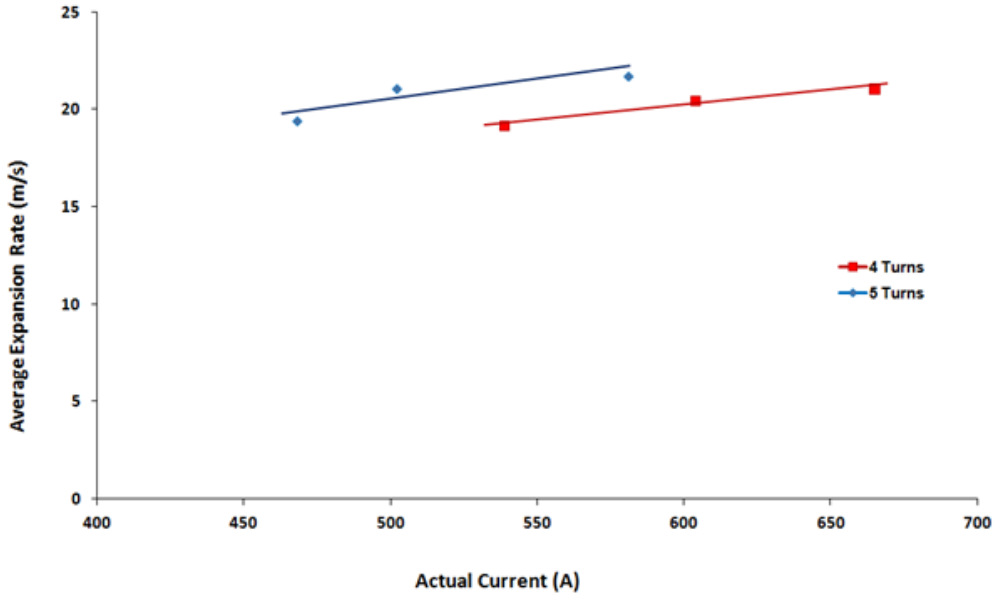

Figure 5.16: Expansion rate over actual current

Figure 5.16 shows the resultant plot for the average expansion rate against the actual current. There are two trend lines indicating 4 and 5 turns each being represented by red and blue lines respectively. The results show a slight increase

as the actual current increases. This is contrary to what was reported on figure 5.1, 5.2 and 5.13. The effect of removing the plunger is marginal from comparing figure 5.13 and 5.16.

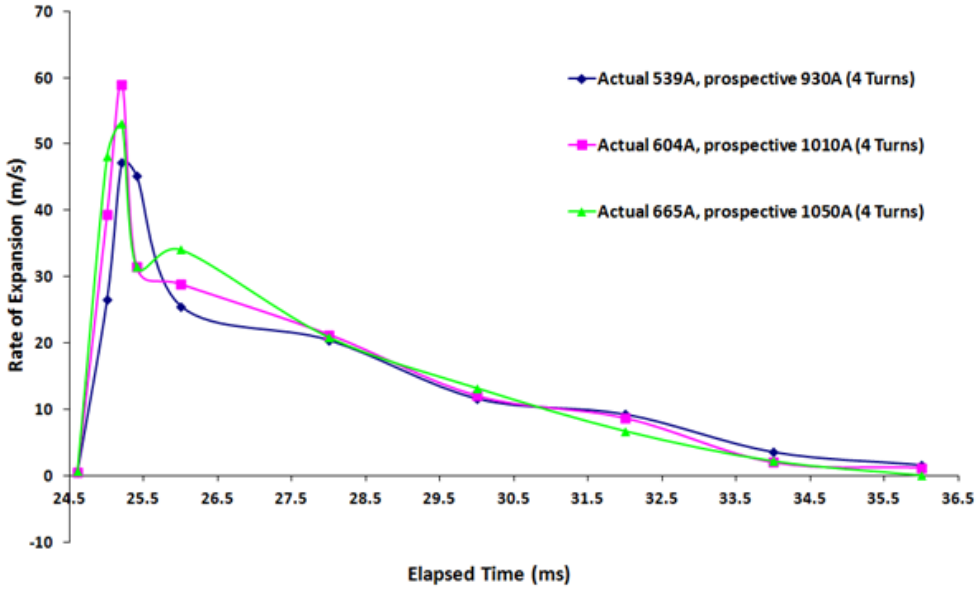

(a) 4 Turns

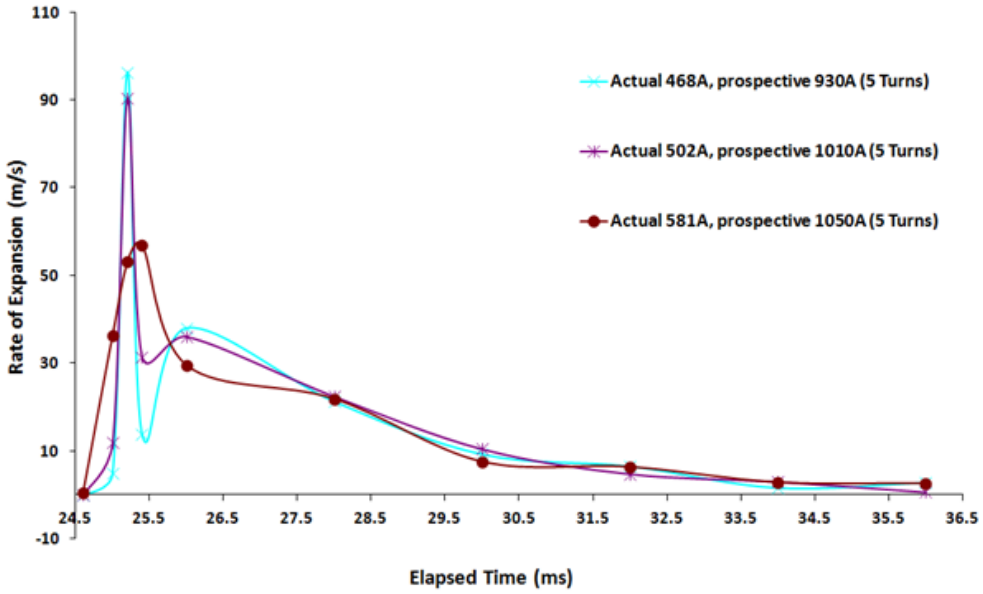

(b) 5 Turns

Figure 5.17: Expansion rate over elapsed time

Figure 5.17 (a-b) shows an initial rapid rate of expansion of arc radius which

then slows over a relatively longer time period for all currents similar to these results in Figure 5.14. In this case, with the plunger removed, there is little correlation with the peak rate of expansion (25ms) and current for the 4 turn case. At 5 turns the correlation is negative.

In summary, the expansion profiles for each of the tests without the plunger are similar to those with. Again, there is little correlation with current. This may be influenced by hot gas escaping via the holes in the rod.

5.2.2 Arc Axial Velocity (PTFE Blades)

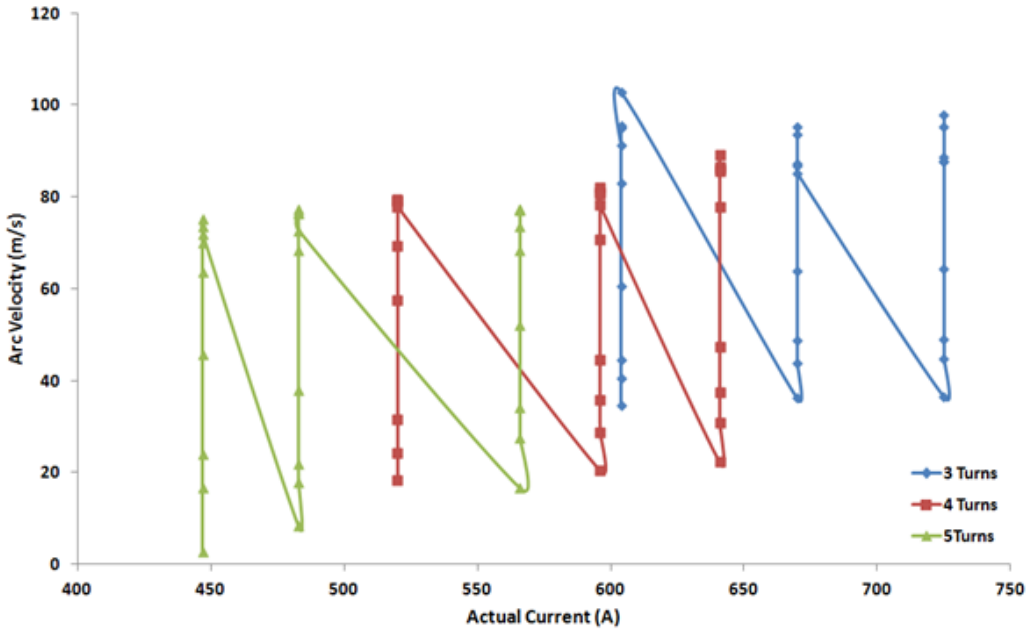

Figure 5.18: Arc velocity versus actual current for different blades set, plunger inserted

Figure 5.18 and Figure 5.19 shows the arc velocity in two different conditions, the first with the plunger inserted and the second with plunger removed. Figure 5.18 are results for 3, 4 and 5 PTFE blades, while Figure 5.19 is for 4 and 5 PTFE blades, for three different currents in each case. There does not appear to

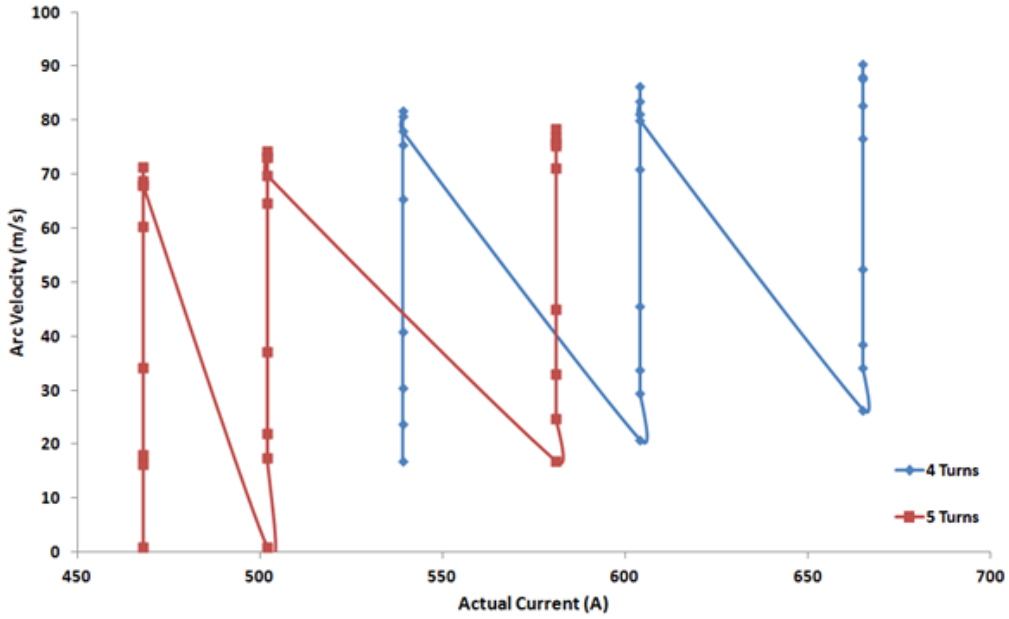

Figure 5.19: Arc velocity versus actual current for different blades set, plunger removed

be any large changes in maximum velocity as the current increases. For the first case it can also be seen that the average peak arc velocity is around 95m/s for 3 blades, reducing to approximately 80m/s for 4 blades and approximately 75m/s for 5 blades. Without the plunger the average peak velocities were similar. For the 4 blades this was 85m/s and 75m/s for the 5 blades. It is clear that an arc in a system with the central plunger moves about the same velocity. The inference is that gas escaping through the central core does not significantly lessen the outward expansion force in the arc. This type of expansion will be described in a more fundamental way in chapter 6, where different type of forces which affect the speed and direction of expansion are explained.

5.2.3 Time to Interrupt

From the analysis of the results (at medium blade size, 360mm), table 5.1 shows the comparison between PE and PTFE based on (i) time to reach the outer limit

Table 5.1: Comparison between PE and PTFE

Material	No. of Blades	Max Arc Current (A)	Max Arc Voltage (V)	Time to reach outer limit (ms) (i)	Time to Interrupt (ms) (ii)
PE	3	651	2350	9.7	22.7
		716	2450	9.9	23.0
		808	2570	14	27.2
	4	527	2810	Did not reach	28.0
		609	3100	Did not reach	29.4
		669	3080	Did not reach	29.5
	5	452	3090	Did not reach	29.1
		505	3260	Did not reach	28.5
		578	3480	Did not reach	33.2
PTFE	3	657	2510	11.9	25.0
		732	2520	7	19.9
		787	2670	6.1	19.3
	4	592	2990	Did not reach	29.0
		725	3210	Did not reach	25.2
		789	3420	8.6	22.7
	5	445	3080	Did not reach	32.5
		479	3380	Did not reach	26.2
		559	3540	Did not reach	31.1

of the blades (e.g. period A to E, Figure 4.2) and (ii) time to interrupt. If the outer limit of the blades is reached (e.g. point E, Figure 4.2), interruption occurs at that point by means of the arc shorting between the turns, so essentially (i) and (ii) occur at the same time (e.g. (ii) = $\sim$ (i) + 13ms). If the outer limit is not reached, then the system usually interrupts, at a time which may vary slightly. For this blade diameter the arc discharge did not reach the outer diameter of the blades with 4 and 5 turns except in one case for 4 PTFE blades at a peak current of 789A.

Polyethylene (PE) produces a sharp increase in the arc voltage which suggests that the energy loss from the discharge related to evaporation is greater than with other plastics [Ito et al., 2002]. As the melting point for PE lower than PTFE

the weight loss in the blade should be higher.

Figures 5.20 and 5.21 show maximum arc current against time to interrupt for 2 different polymers, PE and PTFE. The results in Figure 5.20 and 5.21 imply that there is no great advantage in using PTFE or PE blades to decrease the time to interruption. For 5 blades the interruption times are similar at around 0.03s. For 4 blades the limited set of the results suggest the PTFE is marginally better. However, this is experimental uncertainty.

These results and similarities are produced despite that PE has a melting point of 173-200^{o}C which is lower than PTFE 330-372^{o}C [Lide, 2004]. It should be noted that PE and PTFE, 4 turns reach higher peak arc currents than the 5 turns arrangements.

Referring to table 5.1, the arc did not reach the outer limit for 4 PTFE except for 789A which took 8.6ms and is shown in figure 5.20 as green square dot.

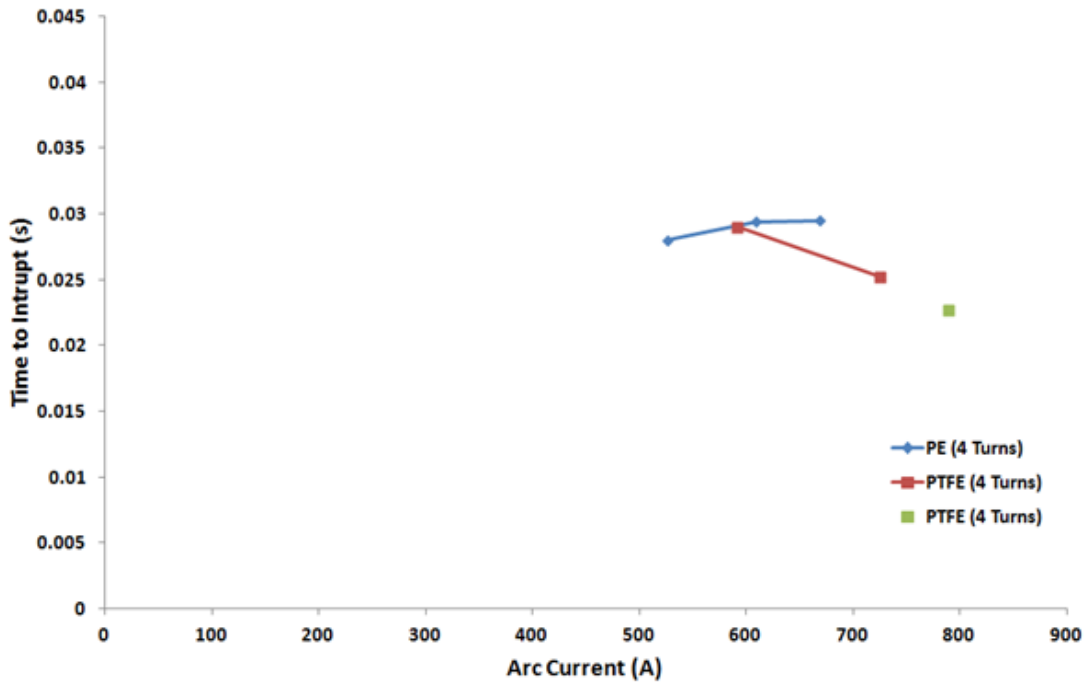

Figure 5.20: Time to interrupt over max arc current for PE and PTFE (4 Turns)

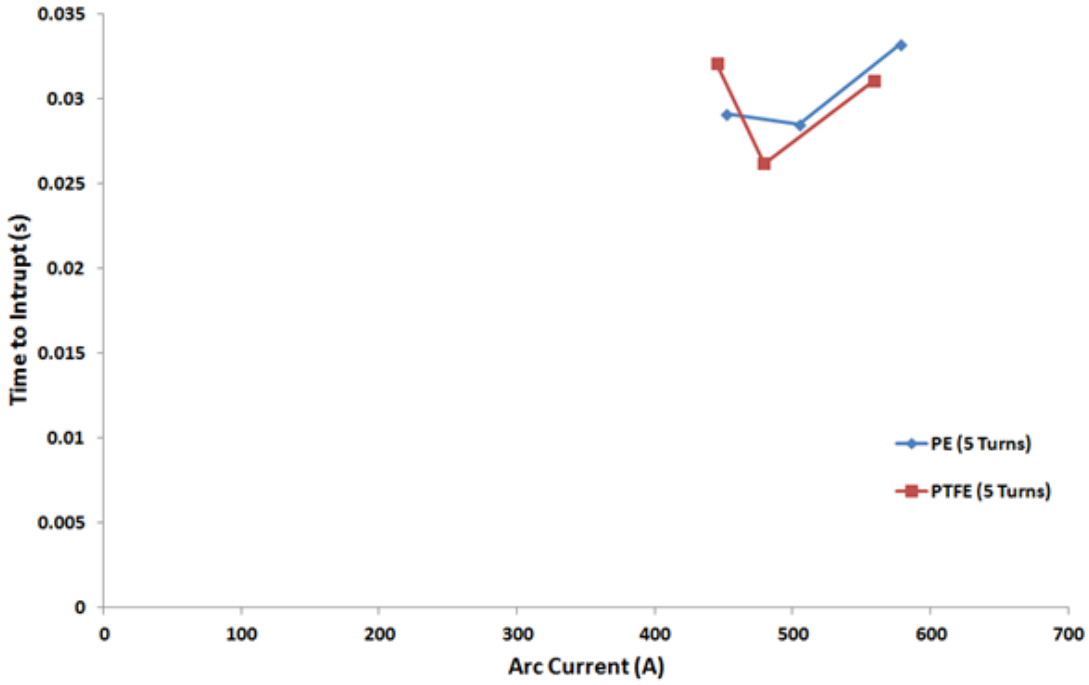

Figure 5.21: Time to interrupt over max arc current for PE and PTFE (5 Turns)

5.2.4 Radial Arc Expansion Velocity with 2PTFE + 1Copper + 2PTFE Turns

The helical arc data of subsection of 4.3.1 (2PTFE + 1Copper + 2PTFE) for this arrangement is shown in figure 5.22 and 5.23 as arc velocity as a function of time and radius respectively. The average arc speed or the expansion speed, V_c, is calculated according to equation 5.1.

Figure 5.22 and 5.23 show that as the arc expands radially it slows down. This is similar to the previous result(Figures 5.6 and 5.7). Both of these results (Figures 5.22 and 5.23) suggest that if the blades were made large enough the arc expansion would stall and the arc would be contained within the helical arc unit.

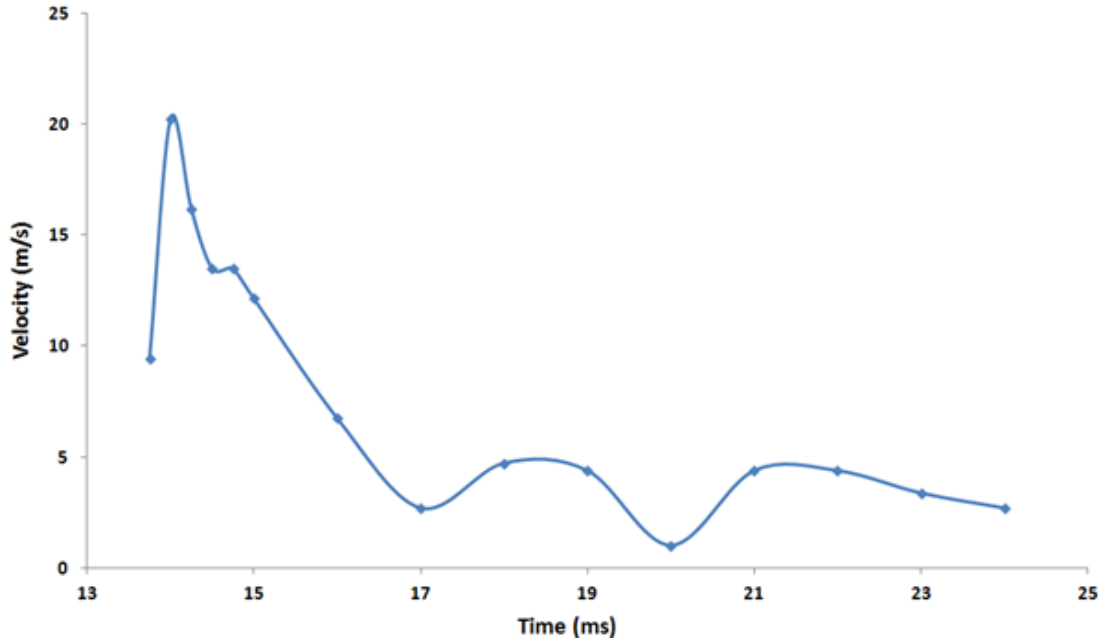

Figure 5.22: Arc expansion velocity as a function of time

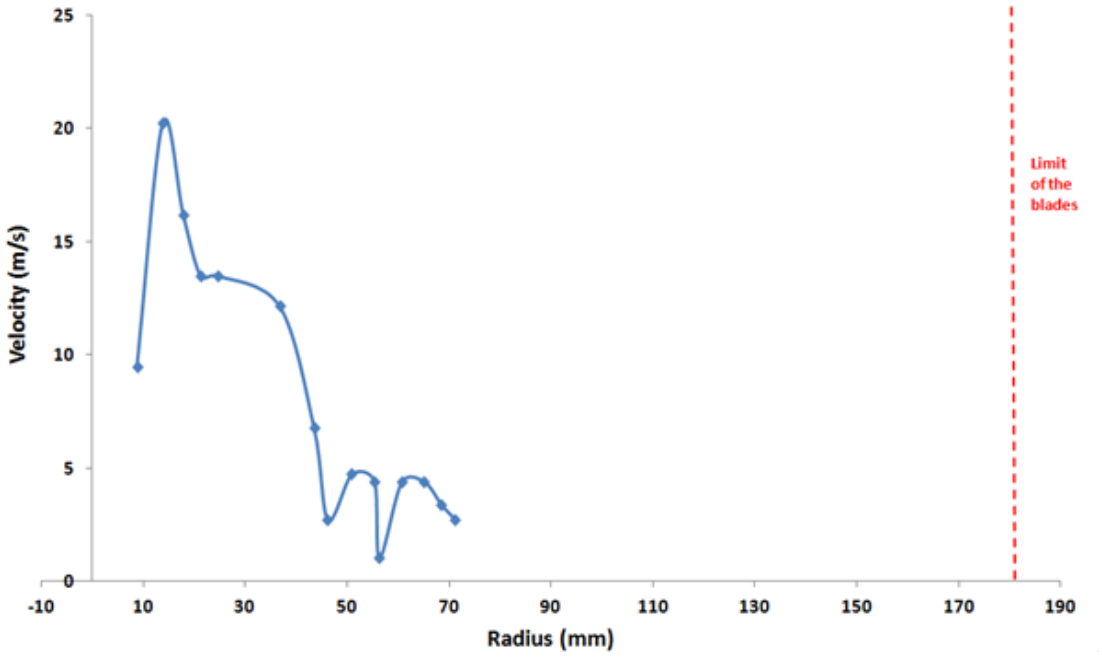

Figure 5.23: Arc expansion velocity and radius

5.2.5 PE Blades to Replace PTFE Current and Voltage

The PTFE blades were replaced with PE blades and the tests were repeated. This time the arc emerged from the confining blades and underwent in turn shorting

(Figure 5.24).

Figure 5.24 shows both the high speed images of the arc and when they were taken in relation to the current and voltage for 2PE, 1Copper, 2PE at a prospective arc current of 1050A but the actual was limited to 916A. The high speed camera was used during the experiment to record the movement of the arc. The images and the current and voltage waveforms were synchronized as indicated in section 3.3.

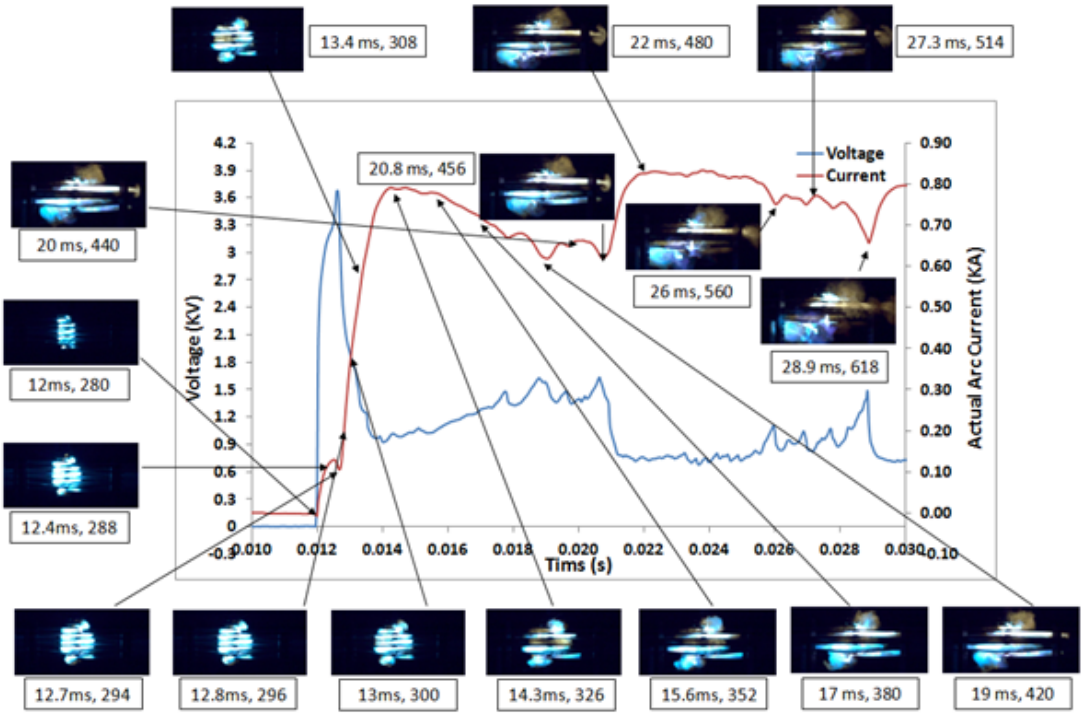

Figure 5.24: Graph results of 2PE, 1Copper, 2PE with high speed camera images

Similar to the case with PTFE the centre copper blade acted as an arc striking point the arc simply attaching and using the blade conducting. At 20.8ms the arc starts to leave the limit of the blades (internal shorting).

5.3 Large Blades (500mm diameter) with 3 Turns

The 3 medium sized blades of PTFE were replaced by a set of 3 larger PTFE blades of 500mm diameter. The axial arc velocity profile for changes in current is seen in Figure 5.25. The figure shows 3 results for different fault currents. Each shows the arc velocity rising to a maximum before reducing. All the peak velocities are similar and the overall velocity profiles are also similar.

The same procedure was performed with 3PE blades of 500mm replacing the 3PTFE blades. The results are shown on Figure 5.26 and the pattern and results are very similar to those of Figure 5.25, with a slight increase in PE's arc velocity with fault current as compared with no increase for PTFE.

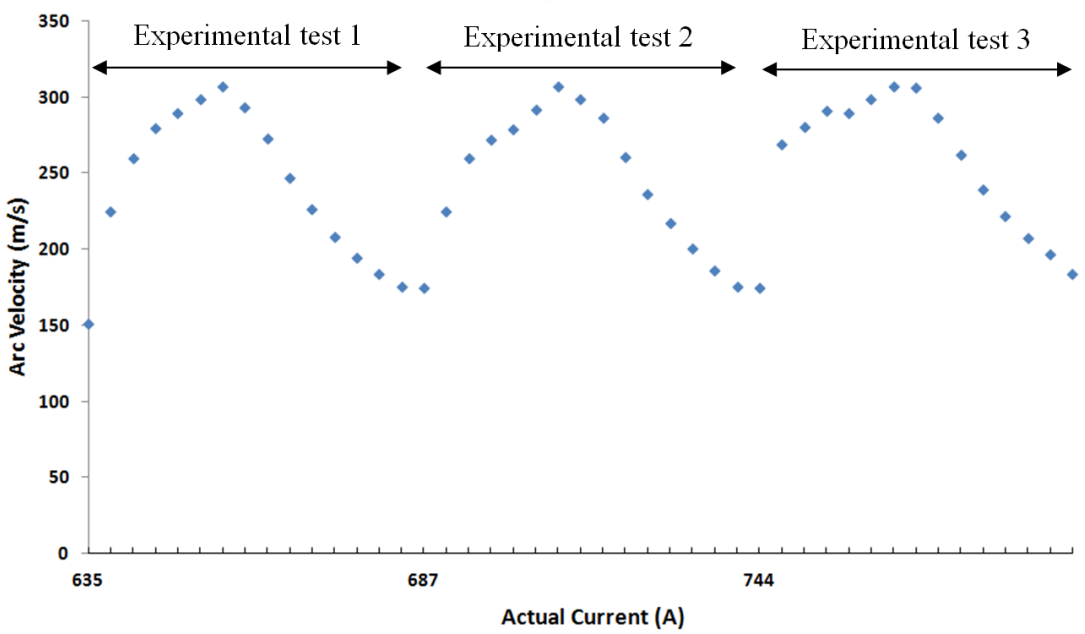

Figure 5.25: Arc velocity versus actual current (PTFE)

Table 5.2 shows the same information for the large blades (PTFE and PE) as table 5.1 for the medium blades. With the large blades, the arc voltages achieved were slightly higher and also the times to interrupt were considerably longer, as

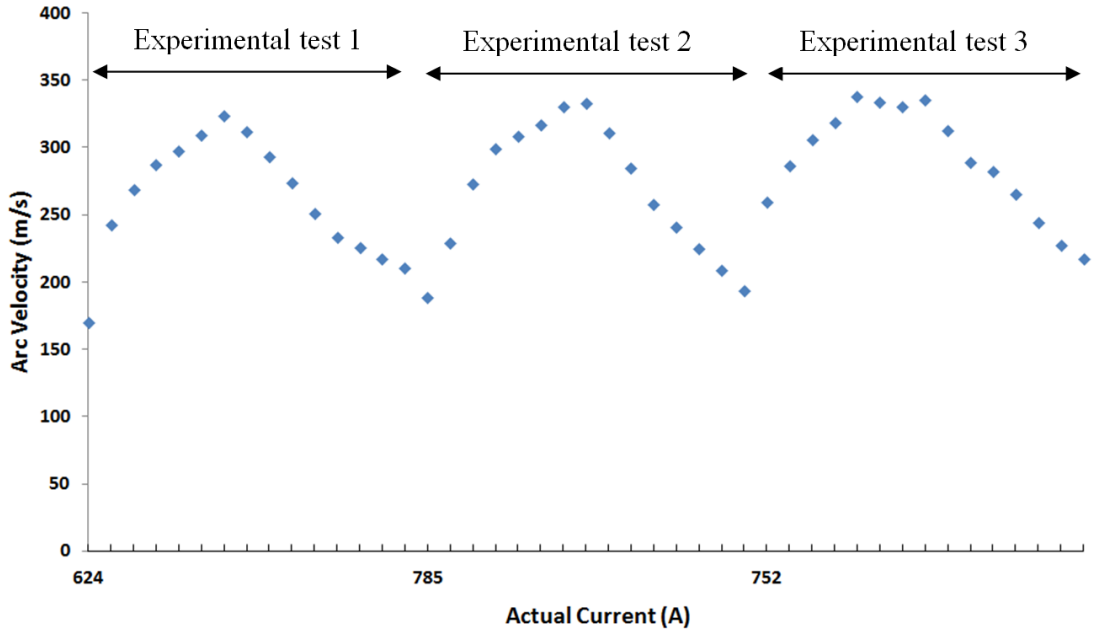

Figure 5.26: Arc velocity versus actual current (PE)

Table 5.2: Comparison between PE and PTFE

Material	No. of Blades	Max Arc Current (A)	Max Arc Voltage (V)	Time to reach outer limit (ms) (i)	Time to Interrupt (ms) (ii)
PTFE	3	635	2500	Did not reach	37
		687	2530	Did not reach	23.0
		744	2800	Did not reach	44
PE	3	624	2580	Did not reach	36
		672	2560	Did not reach	38
		752	2730	Did not reach	40

the arc was contained within the blade limits.

5.4 Summary

This chapter considers the results of chapter 4 in greater depth, by commenting on and analysing their significance. In summary, the analyses examined test results with:

- Small, medium and large blade sizes.

- Three, four and five blades (turns), mainly (plus the use of up to seven turns in total, 1copper, 2PTFE, 1copper, 2PFTE, 1copper).

- PTFE and PE material, alone and with copper.

- Charging currents 890A to 1130A.

and compared arc radii, time for the arc to reach the outer blade limit, radial arc expansion velocity, time to interrupt the arc and maximum arc current.

All tests were performed with the plunger inserted but one set of tests (3 and 4PTFE blades) was also performed with the plunger removed.

The analyses highlight the importance of certain aspects of the helical design and the materials used. These include blade size, blade material, number of turns, and their effects on time to interrupt and maximum arc current. These aspects are discussed in Chapter 7.

Chapter 6

Arc Modelling

6.1 Introduction

For several decades the principle of interruption utilizing an electromagnetically driven arc has been well known and widely used. For this investigation, when the arc is initiated by excessive current through fuse wire wound round the central rod axis, a magnetic field is produced from the flow of current through the turns of arc plasma which persists for the duration of the arcing event. The electromagnetic field forces the arc to rapidly expand outwards from the central rod. This movement is opposed by drag forces as the arc moves through cooler gas. However, there is an additional force that also could aid in the expansion produced by heated gas being trapped between the arc and the inner rod. The potential build up of pressure will act to drive the arc outwards. In summary, therefore, there are two driving forces and one retarding force. The effect of these will be explained in this chapter through a very simplified model.

6.2 Magnetic Force

6.2.1 Magnetic Field

First discovered by Oersted in 1819, a magnetic field is produced whenever there is current flow [Purcell, 2011] [Jiles, 1998] [Grant and Phillips, 1997].

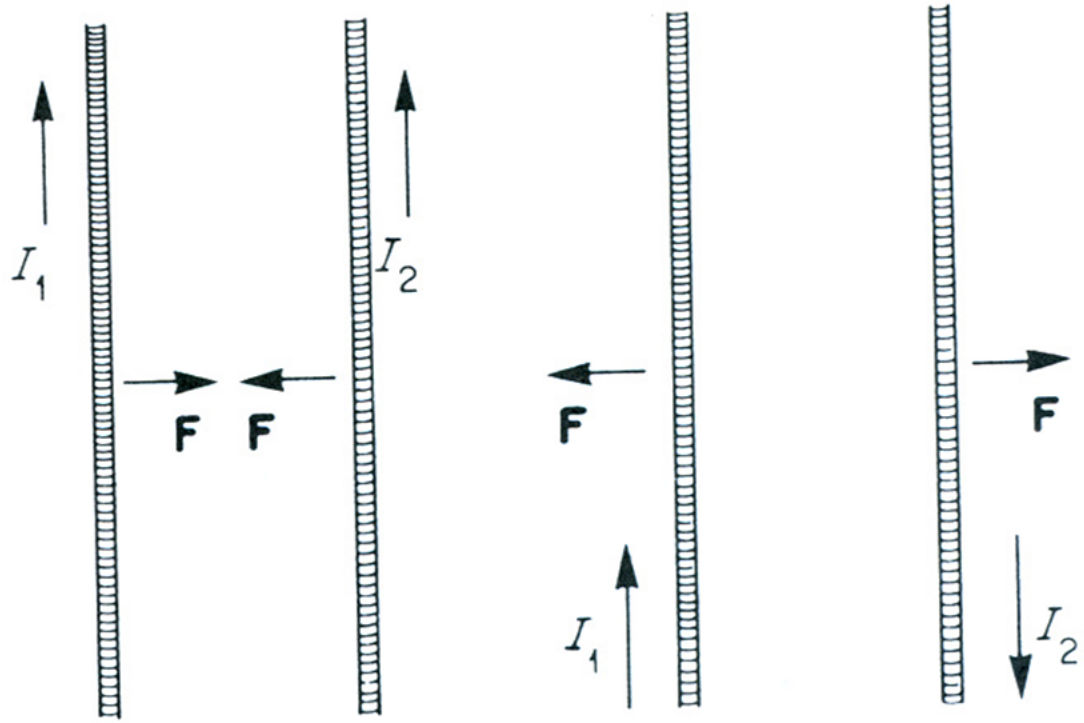

Figure 6.1: The forces between parallel wires carrying currents. Diagram taken from [Kraus, 1991]

For example, if two parallel metal wires are brought near to each other and steady currents flow through them, there is a force between the two wires as shown in Figure 6.1. If the currents are in same direction the force is attractive, and if the currents are in opposite direction the force is repulsive. An efficient way to produce magnetic fields is to loop the wire making turns; this forms a coil or solenoid. Each turn produces its own magnetic field which contributes to the neighbouring fields produced by the current flowing through a wire. In the

experimental arrangement here, the external magnetic field is produced by the arc due to the passage of current through it.

6.2.2 Calculation of the Magnetic Force F from the Centre of the Rod

This section describes the calculation of magnetic field forces acting on the arc, between the anode and the cathode.

Magnetic force F is the product of current (I) and magnetic flux density (B) as shown in equation 6.1

$$F = I \times B \tag{6.1}$$

where $B = \mu \times H$ and H is magnetic field intensity, and μ is relative permeability.

Therefore $|F| = \mu \times H \times I$

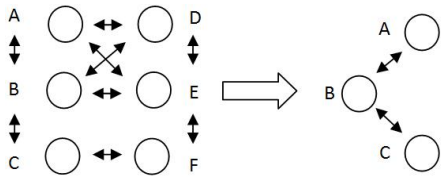

Figure 6.2: Interactions between the individual arc turns

There are a number of possible interactions between the individual arc turns. The diagram above (6.2) shows these possibilities for a limited number of arc loops. The first set of interactions to consider is between A, B, C, as the current is flowing in the direction of the arc and magnatic loops are generated from it. The same will be true for D, E, F. The advantage of this is that the arc is forced onto the surface of the PTFE or PE aiding further ablation. This is the possibility that one of the arc segments may advance further outwards than the others.

For example, B may move further out than either A or C (as shown in Figure 6.2). The force between AB and BC will act to keep the turns of the arc in line i.e. B will experience an attractive force from A,C which will tend to keep it aligned with the other turns. This promotes an even expansion of the arc loops outwards and the high speed experimentally photography shows this.

It is also interesting to note that as the arc is forced out the PTFE/PE blades energy is lost from it thus assisting in cooling the arc and lowering its conductance and its ability to limit the fault current. Through the consideration of the interaction of each loop Figure 6.2 shows the geometric arrangement of the arc turns.

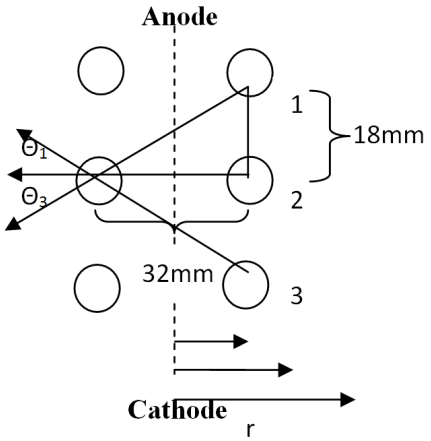

Figure 6.3: Magnatic force between anode and cathode

To calculate force (F_m) between points that are situated between an anode and a cathode, the formula becomes:

$$F_m = \frac{\mu I^2 L}{2\pi r} cos\theta \tag{6.2}$$

Where

L = length between Anode and Cathode (m)

r = radius of the arc expansion from the centre of the rod (m)

I = current (A)

$\mu = 4\ \pi\ 10^{-7}\ N/A^2$

and θ is the angle between points as illustrated in Figure 6.3.

Figure 6.3 shows 3 paths (m1, m2, m3) across the blades. The magnetic force for each is calculated as:

$$F_{m1} = \frac{\mu I^2 L}{2\pi r} cos\theta_1$$

$$F_{m2} = \frac{\mu I^2 L}{2\pi r}$$

$$F_{m3} = \frac{\mu I^2 L}{2\pi r} cos\theta_3$$

Where

$\theta = tan^{-1}\frac{18}{32}$ as depicted on Figure 6.3.

The other arrangement in the interaction is A-D, A-E, A-F and B-D, B-E, B-F and C-D, C-E, C-F. As the current is flowing in the opposite directions in A, B, C compared to D, E, F the forces will keep the arc loops away from each other (i.e. cause the arc to radially expand). These forces can be calculated. Careful examination of the forces as shown in Figure 6.3 Show that radial forces acting on B from D, E, F add while the vertical components of the force cancel.

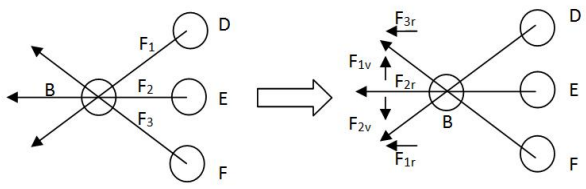

Figure 6.4: Geometric arrangement of the arc turns

In the diagram (Figure 6.4) F_{1v} and F_{2v} cancel but the F_{1r}, F_{3r} components add to the F_{2r} between B and E. If now we consider the interaction with loop A.

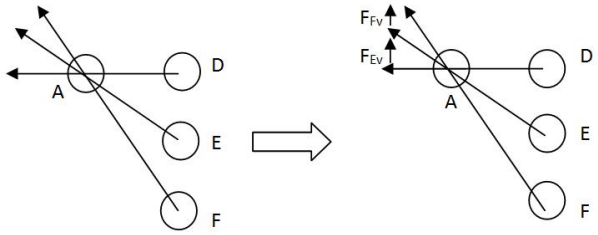

Figure 6.5: Geometric arrangement of the arc turns

The radial forces add as per the previous example but the vertical forces no longer cancel (Figure 6.5). $F_{AV} = F_{EV} + F_{FV} + F_{DV}$ indeed these add together.

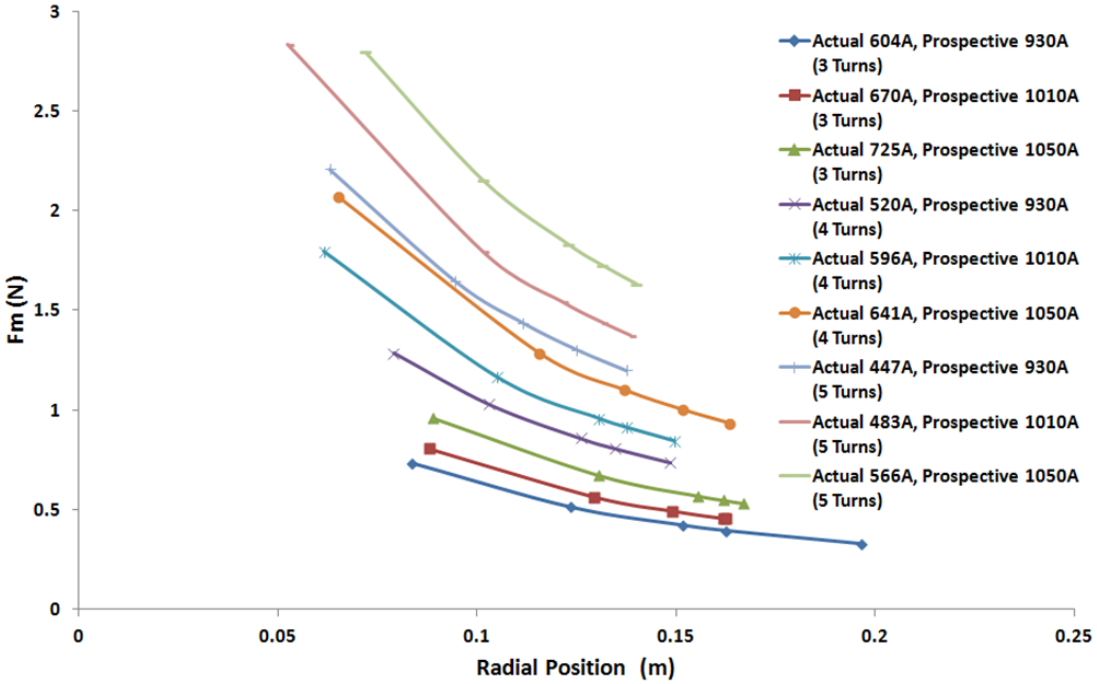

Figure 6.6: Variation of magnetic force F_m with radial position at different combinations of arc currents and blade turns: with plunger inserted (medium blade 360mm diameter)

Figure 6.6 shows calculated values of the force due to magnetic field at different radial positions for different combinations of currents and number of turns with plunger inserted. Three sets of prospective current were selected (930A, 1010A

and 1050A) for 3, 4 and 5 blade turns. As seen from the figure the radial force arising from the magnetic field increases with increase in current and number of turns of the blades. However, a decrease in magnetic force is observed with increase in radial position (distance from the centre of the arc).

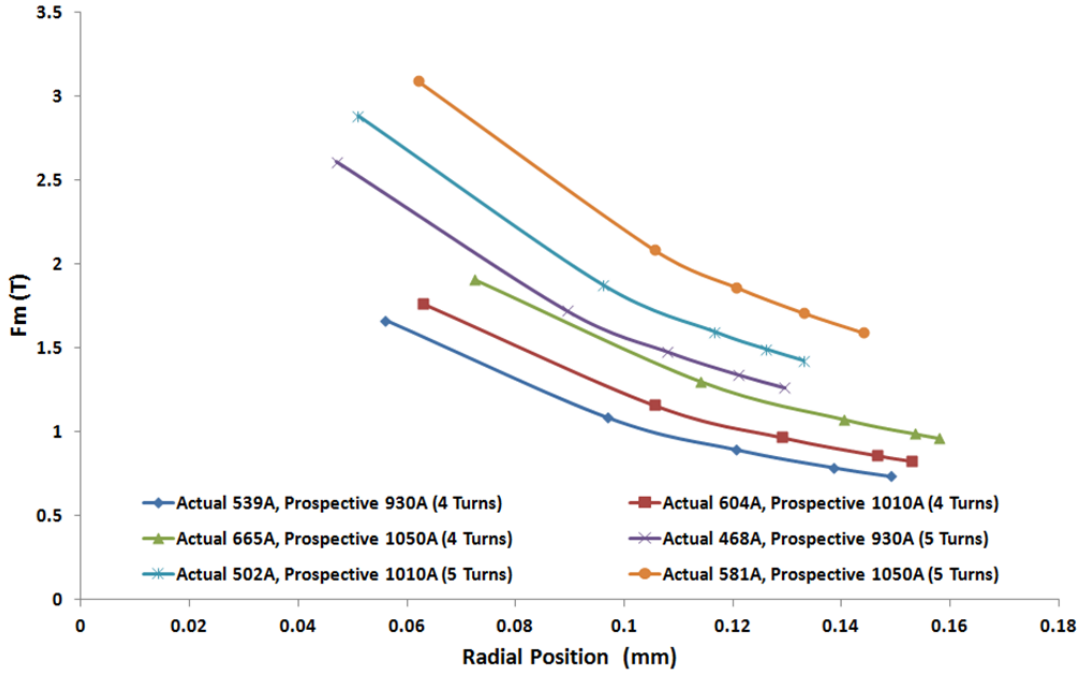

Figure 6.7: Variation of magnetic force F_m with radial position at different combinations of arc currents and blade turns: with plunger removed (medium blade 360mm diameter)

Figure 6.7 shows calculated values of the force due to magnetic field at different radial positions for different combinations of currents and number of turns with plunger removed. Three sets of prospective current were selected (930A, 1010A and 1050A) for 4 and 5 blade turns. As expected the forces are similar only being moderated by the actual fault current. The variation with number of turns and current is also similar. However, upon comparison of Figure 6.6 and 6.7 it should be noted that with plunger removed the magnetic force is higher compared with plunger on for same values of currents and number of turns.

6.3 Arc Volume

Alongside the forces between the arc turns (section 6.4), arc volume is one of the important modelling parameters in determining the behaviour of the arc. In this case the volume of the helical arc in small blades was calculated for two different scenarios: first for the entire expansion period, and secondly for the initiation period. Once the arc volume was calculated, pressure (P) per shot of the area (50mm radially from the rod wall, Figure 6.10) is also calculated [Uchii, 2011]. This area is selected because it is where the ablation of the blades take place (Figure 6.13).

From the ideal gas law (equation 6.3)

$$PV = nRT \tag{6.3}$$

Where

$R = 8.314JK^{-}1mol^{-}1$

T = 3,000K

n = number of moles (moles)

P = presure (Pa)

From the literature a number of researchers have estimated T= 3000K [Reynolds and Jones, 2010] [Tanaka, 2005]. This value however varies from experiment to experiment but for the purposes of this model, to a first approximation this temperature is used.

The chemical structure of PTFE is shown in Figure 6.8. Figure 6.9 shows how the molecules are affected by heat (ablation).

To find the atomic mass of PTFE:

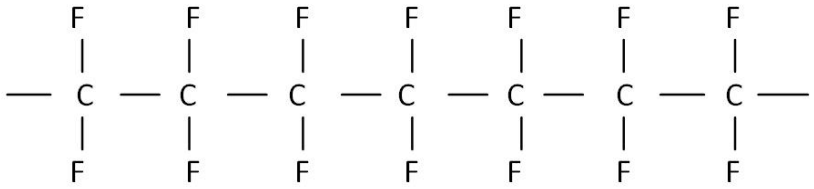

Figure 6.8: Solid PTFE polymer molecule

Effect of Ablated Gas on PTFE

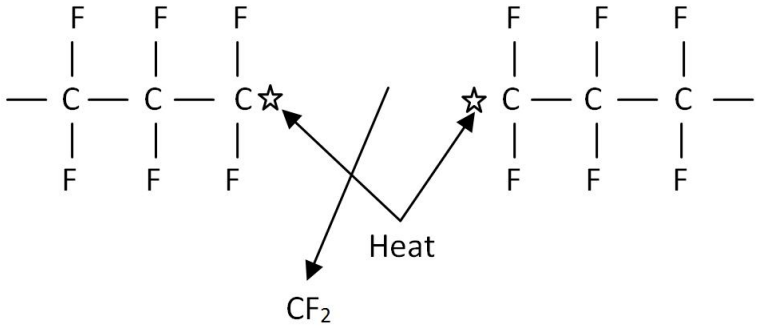

Figure 6.9: Gas molecule

At 3,000K, the dissociation products of PTFE are mainly CF_2 and F. For this simple model the concentration of F can be neglected and subsequent calculation are based on CF_2 (Zhang; 2002). The molecule mass of $CF_2 = 50$ (g/mol). The total number of moles can be calculated from the total mass loss from the PTFE blades on the assumption that all this material is converted to CF_2. This mole result is for the total arcing period where the duration was 0.09s. The calculation for mass loss from the blades is the difference between the weight of the new and used blades:

New Blade weight ——— 107.640g

Long use (200 shots) blade weight —– 102.040g

Mass = 107.640 - 102.040 = 5.6g polymer ablated so the number of moles is obtained as

$$n = number of moles = \frac{mass(g)}{atomic mass(\frac{g}{mol})} = \frac{5.6}{50} = 0.112 moles$$

6.3.1 Whole expansion volume

This calculation deals with the ablation being attributed from the whole losses of the blade. Assuming that all the ablated material is from the whole blades (i.e. between r_1 and r_2) then the effect of this ablation on the pressurisation behind the arc can be calculated. However this simplistic model and in reality the ablation takes place over a smaller area.

On the assumption that all the ablation takes place in the r_1 to r_2 region then a simple calculation can be made regarding the pressurisation.

The volume, V_{total}, (Figure 6.10) can be calculated as

Volume

$$V_{total} = L \times \pi \times (r_2^2 - r_1^2) \tag{6.4}$$

$$\begin{aligned} V_{total} &= 0.016 \times \pi \times (0.067^2 - 0.017^2) \\ &= 2.11 \times 10^{-4} m^3 \end{aligned}$$

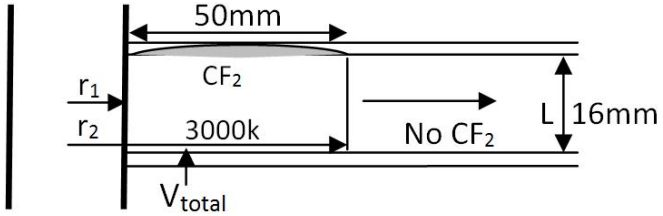

Figure 6.10: Ablation volume

Loss of PTFE is approximately 5.6g for 200 shot, so the loss of PTFE per shot = 5.6g/200 = 28mg.

Number of moles based on loss of PTFE per shot = 28mg/50 = 0.56m moles

From equation 6.3 pressure is :

$$\begin{aligned} P &= nRT/V_{total} \\ &= 0.56 \times 10^{-3} \times 8.314 \times \frac{3000}{0.000211} \\ &= 66.2kPa \end{aligned}$$

6.3.2 Initiation point for all the ablation

The assumption for this model is that all the ablation takes place where the arc is initially initiated. Again this is a broad simplification but it will provide a limit to the upper level of pressurisation.

The pressure for a situation where ablation has taken place where the arc has initially started can be calculated using the initial volume, V_i, (Figure 6.11), as

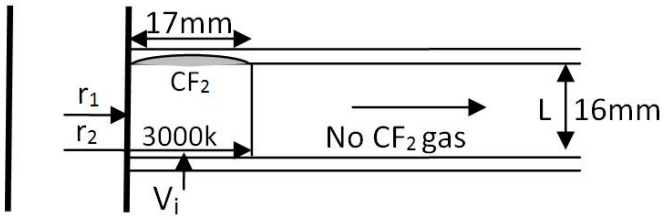

Figure 6.11: Ablated volume

$$V_i = L \times \pi \times (r_2^2 - r_1^2) \tag{6.5}$$

$$\begin{aligned} V_i &= 0.016 \times \pi \times (0.034^2 - 0.017^2) \\ &= 4.36 \times 10^{-5} m^3 \end{aligned}$$

The proportion of loss where the arc is initially started is (area where the arc is)/(area of the blade)=0.23 [Spencer, 2012]

Using the same number of moles of PTFE lost per shot 0.56m moles, than the total number of moles ablated to assist the initial arc movement is 1.3×10^{-4}

From equation 6.3 the pressure is

$$\begin{aligned} P_i &= nRT/V_i \\ &= 1.3 \times 10^{-4} \times 8.314 \times \frac{3000}{0.0000436} \\ &= 74.6kPa \end{aligned}$$

The pressure rise is relatively higher than the background pressure. This pressure is around 13% increase of the total pressure. These calculations show that a pressure rise from 66kPa to 75kPa.

6.3.3 Calculation of the volume lost from the weight of the blades lost

The volume of the material lost through ablation of PTFE can be calculated from knowing mass of material lost (Figure 6.12) as follows.

Density = $2200kg/m^3 = 2.2g/cm^3$ (solid PTFE)

Loss weight = 5.6g

$$Volume = \frac{mass(g)}{density\frac{g}{cm^3}} = \frac{5.6}{2.2} = 2.545cm^3$$

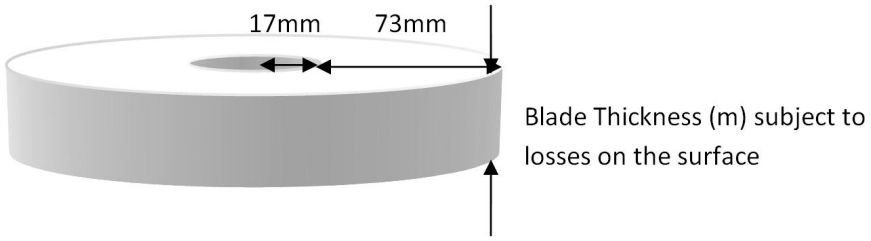

Figure 6.12: Blade thickness

The original blade volume is $\sim 50cm^3$ and the ablation volume lost is therefore $\sim 5\%$ for 200 shots. Figure 6.13 shows a profile of the loss of thickness of the blade from the inner edge (at 17mm from the centre of the blade), shown as 0 on the graph, to the outer edge of the blade shown as 73mm on the graph (i.e. at 90mm from the centre of the blade).

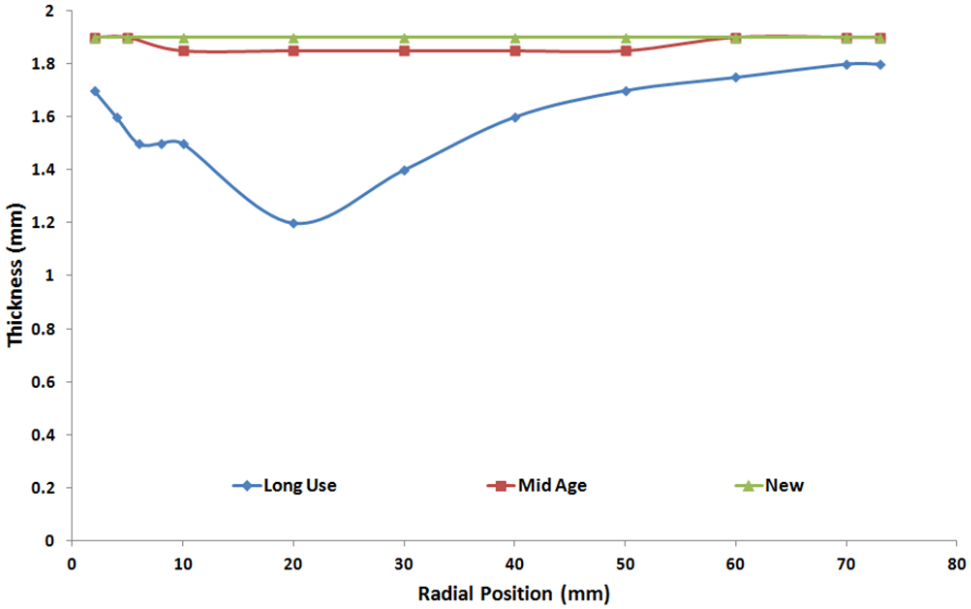

Figure 6.13: Loss of thickness of the blade from the inner edge

The graph shows that the greatest loss of material is at 20mm with significant wear between 2 and 55mm. This loss profile the model that best fits the experimental were profile is one which distributes this over the whole area of the blade. Consequentially, the expected pressure rise will be around 66kPa.

6.4 Forces on Arc

There are two types of driving forces acting on the helical arc, as shown in Figure 6.14. These are aerodynamic F_A and electromagnetic F_E. There are two main forces opposing arc movement. These are drag F_D and friction F_F.

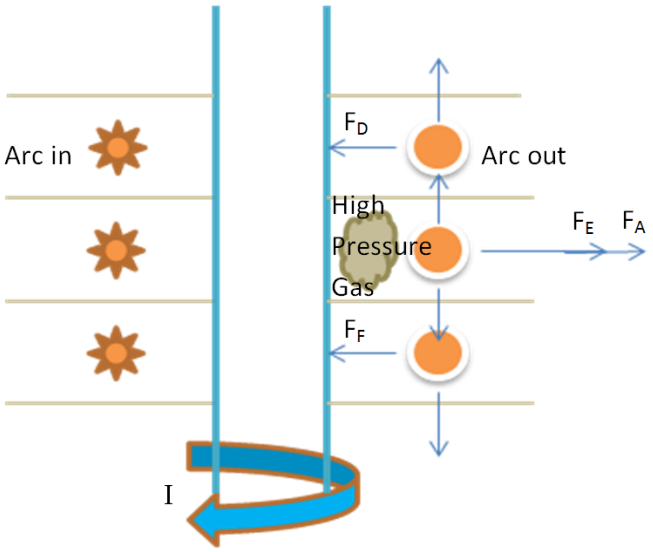

Figure 6.14: Sketch of the elements of the arc model

Both the aerodynamic and electromagnetic forces serve to drive the arc radially outwards. As the arc moves thus other forces resist its movement. Friction of the arc moving along the blade may not be significant and therefore to a first approximation this is neglected, while the drag force is the only opposing to the other forces (i.e. aerodynamic and electromagnetic).

The drag force is the action of air resistance on the arc, which has the effect

of slowing the arc expansion and limiting its radius.

Calculations are made for the small blades since they are representative of the process with medium and large blade sizes as well. Forces are calculated for the ablation occurring within a maximum radius of (17mm) and for entire blade (50mm)

6.4.1 Forces calculation for the entire blade

The aerodynamic force, the acceleration of the driving force, and the dragging force for the whole expansion period may be calculated as follows.

To calculate the aerodynamic force (equation 6.6):

$$F = PA \tag{6.6}$$

Where

The area A (Figure 6.15) is equal 2 $\pi r_{arc} \times d$ where d is the blade separator and r_{arc} is the arc radius where the pressure exerts itself on the rear side [Spencer, 2012].

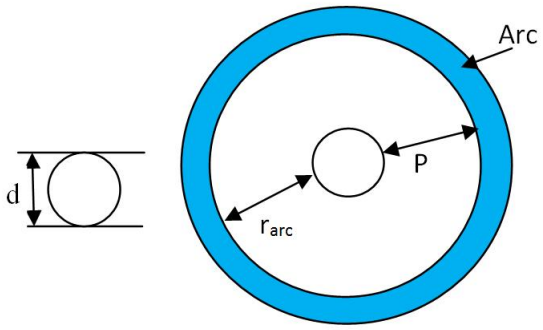

Figure 6.15: Pressure area

The pressure is that calculated before (section 6.3.1)

P = 66.2 $\times 10^3 Pa$

$A = 2\pi \times 5 \times 10^{-3} \times 16 \times 10^{-3} = 5 \times 10^{-4} m^2$

$F = 66.2 \times 10^3 \times 5 \times 10^{-4} = 33.3N$

To calculate the acceleration A_c of driving force(equation 6.7):

$$F = m_t \times A_c(SolidState) \tag{6.7}$$

Where m_t is the total mass which $= m_p + m_c$

m_p = mass of hot gas (g)

m_c = mass of cold gas (g)

The volume of V_{total}(Figure 6.16) at high pressure plasma has been calculated in 6.2.1 as $V_{total} = 0.000211m^3$

And the mass density at high pressure plasma, where T = 3,000K, is given by:

Density = $0.11464 \times 2 = 0.2293$ (kg/m^3) [Tanaka, 2004]

$$\begin{aligned} m_p &= V_{total} \times Density \\ &= 0.000211 \times 0.2293 \\ &= 4.838 \times 10^{-5} kg \end{aligned}$$

Now the cold gas volume of V_2 (Figure 6.16) can be calculated as

$$\begin{aligned} V_2 &= L \times \pi \times (r_3^2 - r_2^2) \\ &= 0.016 \times \pi \times (0.090^2 - 0.067^2) \\ &= 1.82 \times 10^{-4} m^3 \end{aligned}$$

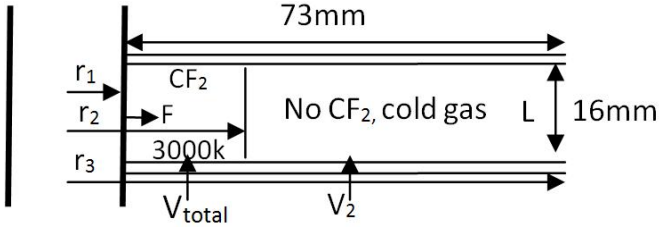

Figure 6.16: Arc volume

Density at 300K open air = 1.1738 (kg/m^3) [Tanaka, 2004]

$$\begin{aligned} m_c &= V_2 \times Density \\ &= 0.000182 \times 1.1738 \\ &= 2.136 \times 10^{-4} kg \end{aligned}$$

$m_t = 4.838 \times 10^{-5} + 2.136 \times 10^{-4} = 2.619 \times 10^{-4}$kg

Using the mass (m_t) of the whole area of the blades(hot and cold gas).

$$\begin{aligned} A_c &= F/m_t \\ &= 33.3/2.619 \times 10^{-4} \\ &= 127.19 \times 10^3 m/s^2 \end{aligned}$$

The acceleration of the driving force calculated using assumed/theoretical values in part with the small blades (180mm diameter) is therefore high.

The drag force may be modelled by that for a heated body. The assumption is that cold gas flows around the arc and is hot entrained in it. The drag force(equation 6.8) for a solid body is given by:

$$F_D = \frac{1}{2}\rho v^2 C_D A \tag{6.8}$$

Where

A is the area of the helical arc on blades(m^2)

ρ Arc density (kg/m^3) for cold gas

v Velocity of the arc (m/s)

C_D Drag coefficient

Acceleration (A_c) as calculated above and time (t) as measured

$$\begin{aligned} \rho &= 1.1738(kg/m^3) \\ v &= A_c \times t \\ &= 127.19 \times 10^3 \times 1 \times 10^{-3} \\ &= 127.19 m/s \end{aligned}$$

The velocity of the forces calculated using assumed/theoretical values in part with the small blades (180mm diameter) is also high.

The drag force may therefore be calculated as:

$$F_D = \frac{1}{2} \times 1.1738 \times (127.19)^2 \times 0.47 \times \pi \times (8 \times 10^{-3})^2 = 0.9N$$

Since the calculated driving force F is greater than the drag force F_D, it explains why the arc keeps expanding away from the centre rod.

6.4.2 Forces calculation for the initiation point

The aerodynamic force, the acceleration of the driving force, and the drag force for the initiation period may be calculated as follows.

To calculate the aerodynamic force (equation 6.6) on the arc:

Where

The area A (Figure 6.15) is equal 2 $\pi r_{arc} \times d$ where d is the blade separator and r_{arc} is the arc radius where the pressure exerts itself on the rear side. [Spencer, 2012]

The pressure is that calculated before (section 6.3.2)

$P_i = 74.6 \times 10^3 Pa$

$A = 2\pi \times 5 \times 10^{-3} \times 16 \times 10^{-3} = 5 \times 10^{-4} m^2$

$F = 74.6 \times 10^3 \times 5 \times 10^{-4} = 37.5N$

To calculate the acceleration A_c of driving force (equation 6.7):

The volume of V_i (Figure 6.17) at high pressure plasma has been calculated in section 7.3.2 as $V_i = 0.0000436 m^3$

And the mass density at high pressure plasma, where T = 3,000K, is given by:

Density = 0.11464 × 2 = 0.2293 (kg/m^3) [Tanaka, 2004]

$$\begin{aligned} m_p &= V_i \times Density \\ &= 0.0000436 \times 0.2293 \\ &= 9.997 \times 10^{-6} kg \end{aligned}$$

The volume of V_2 (Figure 6.17) can be calculated as

$$\begin{aligned} V_2 &= L \times \pi \times (r_3^2 - r_2^2) \\ &= 0.016 \times \pi \times (0.090^2 - 0.034^2) \\ &= 3.49 \times 10^{-4} m^3 \end{aligned}$$

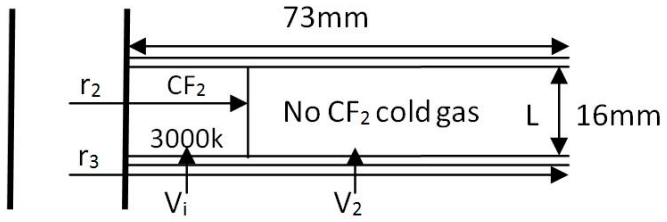

Figure 6.17: Arc volume

The mass of V_2 is calculated using its density and volume as:

Density at 300K open air = 1.1738 (kg/m^3) [Tanaka, 2004]

$$\begin{aligned} m_c &= V_2 \times Density \\ &= 0.000349 \times 1.1738 \\ &= 4.097 \times 10^{-4} kg \end{aligned}$$

$m_t = 9.997 \times 10^{-6} + 4.097 \times 10^{-4} = 4.197 \times 10^{-4}$kg

$$\begin{aligned} A_c &= F/m_t \\ &= 37.5/4.197 \times 10^{-4} \\ &= 8.939 \times 10^4 m/s^2 \end{aligned}$$

The acceleration of the driving force calculated using assumed/theoretical values in part with the small blades (180mm diameter) is therefore very high.

The drag force may be modelled by that for a heated body. The assumption is that cold gas flows around the arc and is hot entrained in it.

The drag force for a solid body is been described by equation 6.8

so

Acceleration (A_c) as calculated above and time (t) as measured

$$\begin{aligned} v &= A_c \times t \\ &= 8.939 \times 10^4 \times 1 \times 10^{-3} \\ &= 89.39 m/s \end{aligned}$$

The velocity of the forces calculated using assumed/theoretical values in part with the small blades (180mm diameter) is also high.

$$F_D = \frac{1}{2} \times 1.1738 \times (89.39)^2 \times 0.47 \times \pi \times (8 \times 10^{-3})^2 = 0.4N$$

Similarly for the initiation of the arc, since the calculated driving force is greater than the drag force, it explains why the arc keeps expanding away from the centre rod.

Table 6.1 summarises the calculations of the driving (F) and drag (F_D) forces for small and medium blade based on two different assumptions of temperatures reached and PTFE material correspondingly ablated into the principle gaseous compounds CF_4 and CF_2 in each temperature range.

Comparing the arc expansion velocities derived from high speed photography

Table 6.1: Comparison of different gases base on the temperature [Zhang et al., 2002]

Blade Size	Main Gas produced	Temperature (K)	Period	Pressure (bar)	F (N)	Velocity (m/s)	F_D (mN)
Small	CF_2	3000	Total	0.66	33.3	127.2	897
			Initial	0.75	37.5	89.4	443
	CF_4	2000	Total	0.25	12.6	42.4	99
			Initial	0.28	14.2	33.2	61
Medium	CF_2	3000	Total	0.12	5.9	8	3.5
			Initial	0.77	38.5	20.7	23.8
	CF_4	2000	Total	0.04	2.2	2.3	0.3
			Initial	0.29	14.5	7.8	3.3

with those calculated in table 6.1 for each assumed temperature range suggests, based on the initial period, that the actual gas temperatures would have been in the region of ∼3,000K for the small and medium blades. The calculation for the medium blade can be seen in appendix B (B.1 and B.2) since it is similar to the small blade calculation.

6.5 Summary

Modelling of different arc parameters and properties along with factors influencing arc behaviour - arc volume, arc temperature, blades effects (with and without plunger), and driving, drag and magnetic forces - are described in this chapter.

Arc volume for the initiation period and whole expansion period is calculated. The driving force on the arc was found to be greater than the drag force, which explains why the arc expands from the centre of the rod.

For the modelling of force arising from the magnetic field, the results indicate that the magnetic field is higher when the plunger is removed.

Chapter 7

Discussion

The interactions of the mechanisms involved with the DC interruption process in which an arc is generated and extinguished may be described on a flowchart (section 7.4). This flowchart is also useful for structuring the discussion of the results analysed in Chapter 5. The arc can be divided into three phases in its behaviour [Elzagzoug et al., 2012], 1, 2 and 3 (section 7.1) where:

Phase 1 includes fuse vaporisation, arc establishment (7.1.1)

Phase 2, arc development (7.1.2), includes factors affecting arc expansion extent and velocity (blade size, plunger inserted/removed, number of turns) and maximum arc current.

Phase 3, arc interruption (7.1.3), includes discussion of time to interrupt.

Section 7.2 discusses the effects of using different polymers on maximum arc expansion and time to interrupt.

7.1 Arc Behaviour

The arc can be divided into three phases in its behaviour, which may be labelled 1, 2 and 3. The first phase corresponds to (A-C) on Figures 4.5, 4.12 and 4.16,

the second phase to D, the third phase to E.

Phase 1, representing arc establishment (Section 7.1.1), includes fuse vaporisation (Melting of Fuse Wire, Figure 7.1) which generates the arc.

Phase 2 (Section 7.1.2) covers the development of the arc up to the point at which it reaches the outer limits of the blades. Factors affecting arc expansion extent and velocity include blade size, presence of the plunger, the number of blade turns and the maximum arc current.

Phase 3 (7.1.3) is the time to interrupt between initial arc establishment and arc extinction.

7.1.1 Phase 1 Fuse Vaporisation and Arc Establishment

The results in chapter 4 illustrate the three distinct phases of arc behaviour. The first is when the fuse wire vaporizes and an arc is established (Figure 4.5) (A-C). During this period, which lasts approximately 1ms, the arc expands rapidly (Figures 4.5, 4.12 and 4.16). The current level is low ($\sim$100A) and this is forced to reduce to an even lower value ($<$10A) whilst the arc's voltage increases to 3.6kV. At this point (C) the instantaneous power from the arc is approximately 36kW for small blades (180mm) and 108kW for the medium PTFE blades and 360kW for the medium PE blades (360mm). During the same period between (A-C) the maximum instantaneous power at point B is about 280kW, 480kW and 360kW respectively for the two sizes of blade. There is a significant reduction in the instantaneous power input for PTFE blades at point C but for the PE blades this remained unchanged.

The arc expansion velocity during this initial period is 80m/s (small blade size) to 100m/s (medium blade size) (Appendix B). This initial rapid acceleration of the arc may be attributed to the vaporization of the fuse wire and by the rapid

heating of the gas during the establishment of an arc. The flow of heated gas on the blade holder side of the arc is restricted by the blocked holes drilled into the former. On the other side of the arc the gas is less restricted and can, therefore, move more freely. The restriction of flow presented by the blade holder produces an increase in pressure which adds to the rapid expansion due this initial period.

7.1.2 Phase 2 Factors Affecting Arc Expansion Extent and Velocity

In the second phase, analysed in Chapter 5, the arc expands less quickly than in Phase 1, at an average speed of between 7m/s (small blades, Figure 5.2) to 22m/s (medium-sized blades, Figure 5.13) for the conditions investigated (small and medium sized blades, Figures 4.5, 4.12 and 4.16), compared with 80m/s to 100m/s in Phase 1.

This lower speed in Phase 2 may well be due to the reduction in arc current limited by the arc at (C) (figure 4.2) which triggers a type of "stall" in the arc's movement. This may be caused by a substantial reduction in the arc's instantaneous power for PTFE blades producing less gas heating and ablation and therefore less gas to aerodynamically drive the arc outwards. There is also a reduction in the Lorentz force acting on the discharge which is proportional to arc current.

The arc's radial expansion velocity and extent are affected by blade size. The blade size factor is discussed in the following paragraph.

7.1.2.1 Blade Size

Three different blade size diameters were used, small (180mm), medium (360mm) and large (500mm).

Blade size is associated with different arc radial expansion velocities. Average velocities are 7m/s for small and 22m/s for medium blades. Increases in blade size cause larger driving forces and therefore higher arc radial expansion velocities are generated.

Blade size may also be expected to influence arc control by means of retaining the arc within the limits of the blades if the blade size is sufficiently large.

Small blades (section 5.1, four PTFE) mainly contained the arc as seen by the high speed camera (Figure 5.1). As the prospective current increases so too does this asymptote, until it reaches around 1130A, where the arc leaves the region of the separating blades whilst still in the rapidly growing phase of its expansion. However, according to the oscilloscope result (Figure 4.3), the arc remains within the blade boundaries only for a short period ($\sim$2ms).

Medium-sized blades (section 5.2 and table 5.1) contained the arc generally with 4 and 5 turns, PE and PTFE. But 3 turns were not sufficient to contain the arc with either PE or PTFE (table 5.1). However, a sufficiently large blade size can contain the arc even with 3 turns (Figures 4.20 (PTFE) and 4.21 (PE)).

In summary, arc control i.e. retaining the arc within the limit of the blades at any arc radial expansion velocity - depends both on sufficiently high number of turns and sufficient blade size.

7.1.2.2 Plunger Removed

From tests on open helical data (sections 4.2.4, 4.2.5 and Figures 5.12 - 5.19) it can be seen that:

(a) The complete helical arc for the hollow core (plunger removed from the former) would not form for less than a certain supply voltage compared to the solid core (Figures 4.9 - 4.10).

(b) The hollow former, by allowing gas to penetrate the wake region of the arc, appears not to have significantly slowed its axial velocity (cf. Figures 5.18, 5.19) although the hollow chamber may have allowed some hot gas to escape the arcing region, into the core of the rod, allowing some expansion cooling of the hot gas in the wake.

(c) With the hollow core, the arc failed to form for $I_{prospective}$ <930A but exhibited current limiting behaviour in the range 930A< $I_{prospective}$ >1130A. Above 930A the fuse vaporised completely within approximately 0.7-1ms, following which the arc expands and remains within the helical structure for up to 10ms.

With the plunger removed, the arc behaviour was not very dissimilar from the behaviour when the plunger was inserted; as the arc was controlled (blade limits were not reached). However, the arc expansion velocities with plunger removed were slower than with the plunger inserted (Figures 5.13 and 5.16).

Generally, however, there is a risk of the arc shorting within the hollow core, which suggests that the plunger should be present.

7.1.2.3 Number of Turns

The number of turns plays a significant role regarding arc length because increasing the number of turns widens the distance between anode and cathode. This effectively distributes the arc power amongst the blades, inter-blade distance remaining constant. Lengthening the arc path and lowering the arc power have a slowing effect on its radial expansion velocity.

The number of blades used varied from 3 to 7, which was an upper limit in terms of practicality. Increasing the number of turns may be seen to reduce

both the radial arc expansion extent and velocity. For example, Figures 5.12 and 5.15 illustrate greater extent, and Figure 5.13 illustrates faster velocity, with 3 turns (blade limits exceeded) rather than with 4 and 5 turns. Figure 5.18 also illustrates faster (axial) arc velocity with 3 turns rather than with 4 and 5.

7.1.2.4 Maximum Arc Current

The maximum arc current is the point at the beginning of Phase 2 (D) when the arc has been established. The average maximum arc current (for PE and PTFE materials taken together on Table 5.1) is 725A (3 turns, 241A per turn), 652A (4 turns, 163A per turn) and 503A (5 turns, 100A per turn), indicating that maximum arc current reduces with the number of turns due to an increase in the arc length. The number of blades which accommodates a max arc length could be used for predicting maximum arc current.

7.1.3 Phase 3

At the end of the second phase the arc discharge may reach or may exceed the edge of the helical blades. In the first case the process is controlled, the current will reach zero and the arc will be extinguished. In the second case the process is uncontrolled if the arc exceeds the outer edge, since at this point inter-turn shorting occurs due to the shorter arc length and there are no additional losses associated with arc/polymer ablation. This results in an increase in current and as a consequence, the arc voltage reduces.

7.1.3.1 Time to Interrupt

Interruption takes place when the arc current reaches zero (E). The time it takes for this to complete (times to interrupt) are compared in Table 5.1 (3, 4 and 5

turns) and Figures 5.20 and 5.21 (4 and 5 turns).

The times to interrupt for (PE and PTFE) 3 turns at medium blade size, 360mm are shorter than with 4 and 5 turns. However, the reason for this is that the arc exceeds the outer limits with 3 turns in all 6 cases, which means that the process has gone out of control at an early stage.

With 4, and especially 5, turns, the arc does not reach the outer limits, so interruption takes place while the process is fully controlled. The additional time interval of 6ms taken with 4 and 5 turns compared with 3 turns is within the range of the overall variation in times to interrupt for each set of tests (e.g. for 4 and 5 turns PTFE). The arc control maintained as the current reaches zero clearly demonstrates the need to keep the arc inside the blades. The effect of different polymers on time to interrupt is discussed separately in section 7.2.

7.2 Effect of Different Polymers

The effects of the two polymers used PTFE and PE, are compared in Table 5.1 (3, 4 and 5 turns) and Figures 5.20 and 5.21 (4 and 5 turns) with regard to the time to reach outer blade limit and time to interrupt. Generally, the arc did not reach the outer blade limit with 4 and 5 turns (except for PTFE 4 turns, 789A) but it did for both PTFE and PE with 3 turns, which suggests that 3 turns and even 4 turns might not be sufficient for controlling the arc. In the 3PTFE turns case, time to reach the outer limit was considerably faster than that of PE. This is due to the lower melting point of PE and higher PE ablation, which slow the radial arc expansion, as compared with lower PTFE ablation, indicating that PE is preferable for these purposes, although there is a disadvantage in terms of material loss with more rapid ablation.

Time to interrupt is of significance when the arc does not reach the outer limits, with 4 and 5 turns. Although PTFE did not keep the arc within limits in all cases (e.g. 1 of 3 cases at 4 turns reached the limits), it nevertheless had a faster time to interrupt than PE in most cases. This is also thought to be due to the relevant properties of PTFE material, compared to that PE which enables faster arc expansion within the blade limits and therefore faster time to interrupt. Arc current variations between the different materials are not considered to be particularly significant.

As PTFE and PE both have relative advantages and disadvantages, a combination of the materials could be beneficial.

7.3 Arc Modelling

Arc modelling calculations were performed in order to compare actual experimental and predicted theoretical results in terms of magnetic, driving and drag forces acting on the arc.

Regarding the magnetic force, the modelling illustrates how the force increases substantially in relative terms with the number of turns and the increase in current (Figures 6.3 and 6.4). It is also slightly higher with the plunger removed ($\sim$10%) than with the plunger inserted but the plunger presence/absence does not appear to have had a major effect on arc control overall. The magnetic force contributes to initial arc radial expansion together with the driving force from temperature/pressure when testing in air.

The modelled driving (and drag) forces are summarised in Table 6.1 for small and medium blades (For the space between 2 PTFE blades in both cases). For the initial expansion period, the driving forces are virtually the same for small

and medium blades.

The actual average radial expansion velocities with the medium blades compared with the smaller blades are ∼3 times faster (7m/s vs. 22m/s, section 7.2.2) although the medium blades controlled the arc better in terms of retaining it within the blade limits. Compared with the modelling results of table 6.1, there appears to be reasonable agreement with the medium blades (8m/s and 22m/s) but there is a mismatch for the small blades (127m/s and 7m/s). A possible explanation for the high relative modelled velocity compared with actual may be related to actual temperature varying in the case of the small blades from the assumed 3,000K. Temprature directly affect pressure which affect driving force which affect the acceleration which affect the radial expansion velocity.

7.4 DC Interruption Process Overview

Using blades to form helical arcs means that relatively long arcs can be produced in a relatively small environment. Arcs which are formed in this device are rapidly accelerated towards the periphery of the blades and in doing so the arc lengthens. This lengthening produces higher arc voltages which may result in current limitation and a "softer" current zero interruption, potentially avoiding current chopping.

Figure 7.1 shows the summary, indicating the composite interactions of mechanisms of the complex interactions took place exposed during this investigation. This model describes the features which have been observed during the experimental tests where the polymeric material and the arc interact and the interrelation between forces.

The flowchart shown in Figure 7.1 provides information on the complex inter-

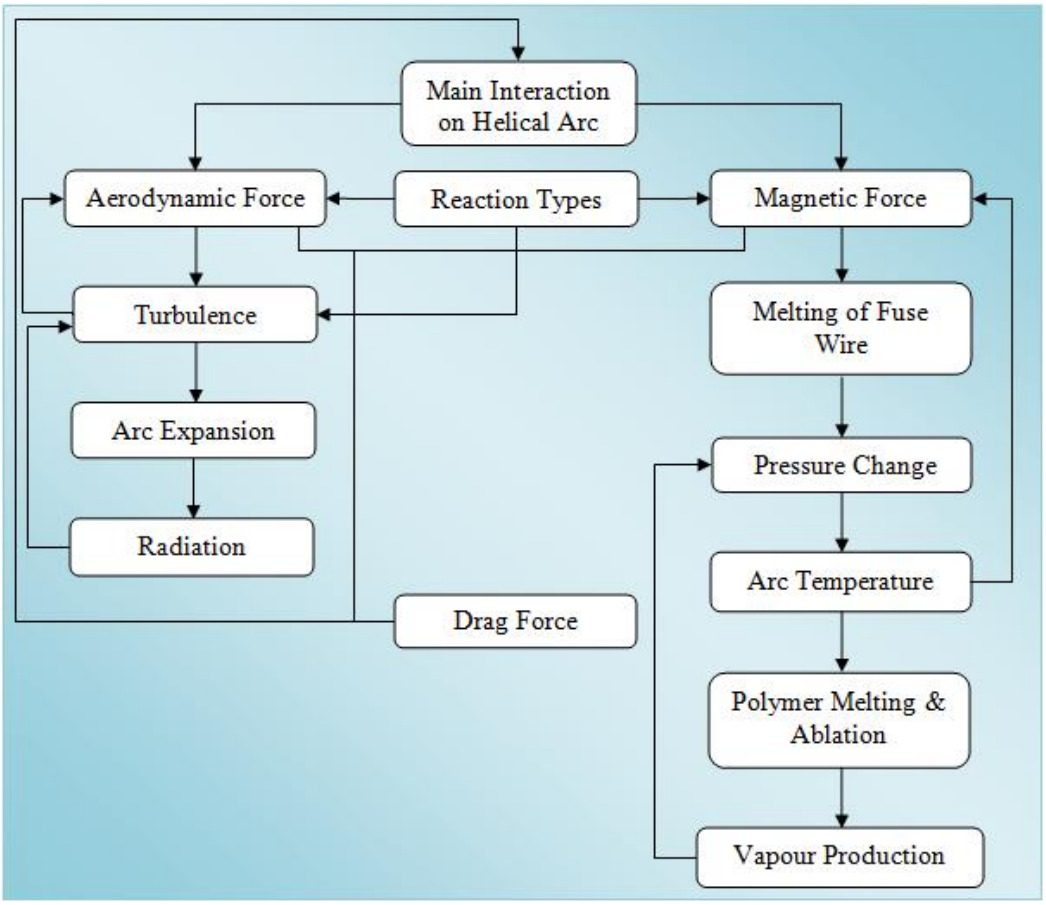

Figure 7.1: Diagram showing processes of the main interaction

action process between helical arc polymers and the high pressure plasma.

The polymer interaction with the arc is involved. After the initiation of the arc from fuse wire the arc interacts with the polymer blades producing a relatively large amount of gas composed of different species which results from various interactions.

There are two driving forces (aerodynamic and magnetic) and two main forces opposing arc movement (drag and friction). Both the aerodynamic and electromagnetic forces serve to drive the arc radially outwards. As the arc moves thus other forces resist its movement. Friction of the arc moving along the blade may not be significant and therefore to a first approximation this is neglected, while

the drag force is the only opposing to the other forces (i.e. aerodynamic and electromagnetic). The drag force (the only left retarding force) is the action of air resistance on the arc, which has the effect of slowing the arc expansion and limiting its radius. The external magnetic field is produced by the arc due to the passage of current through it. The interaction between these forces has an input over the cause and initiation of turbulence which aid in the arc expansion and the radiation of energy consequently. The quantity of the material ablated from the polymer blade is dependent on the ablation from the arc. Hermann et al. [Hermann et al., 1974] derived their model [Hermann and Schade, 1972] in order to approximate the radiation resulted from N_2 (i.e. atmosphere) arcs, which was also employed by Tuma [tuma, 1980].

Exothermic reactions have been observed [Brookes and Spencer, 2010a] to diminish convective cooling and reduce the effect of the temperature gradient between arc and surroundings; an exothermic reaction affects the arc extinction and dielectric recovery negatively by adding thermal energy to the arcing region. On the other hand, endothermic reactions have been concluded [Brookes and Spencer, 2010b] to enhance the energy losses and lead to more efficient cooling of the electrode gap thus aiding the interruption process because of the extraction of thermal energy from the electrode gap; an endothermic reaction affects it positively by removing thermal energy from the arc.

Melting of polymer blades is a change that defines their transition from a solid to an amorphous state and is strongly related to polymer structure. The relationship between polymer melting and reduction in arc temperature as given in the optical spectral analysis by Brookes [Brookes, 2010], which states that they are proportional because polymers consume energy from the thermal plasma to facilitate melting and ablation. Other research by Tanaka [Tanaka et al.,

2008] that uses induction coupled thermal plasma models along with various polymers has confirmed the relationship based on temperature degradation after the reaction of polymers with the arc plasma. The melting of polymers results in production of different kinds of gases depending on the type/composition of polymer. Also, around the arc core irregularly shaped vapor packets as a result of polymer phase change were observed by Brookes [Brookes et al., 2008]. Tanaka [Tanaka et al., 2005] performed computer modelling of polymer arc interaction and concluded that the properties of ablated polymer vapor such as mass density and thermal conductivity can enhance plasma energy losses and aids interruption. Further research also found that in addition to the energy utilized in the change of state, resultant vapor plays an important role in plasma (arc) cooling [tanaka, 2004].

7.5 Summary

This chapter presents the discussion of the results. The overall arc establishment and interruption processes were discussed in terms of 3 phases that can be related to the production and interaction of complex non-physical and physical phenomena modeled in Figure 7.1. Within the 3 phases there are a number of factors that contribute to successful arc control and extinction with acceptable current limitation within acceptable time to interrupt. Notably, with the geometry used, these are blade size, number of turns, and nature of blade material.

The results were presented with plunger removed and plunger inserted, including variation of current limit with time.

The general trend emerging is that it may be possible to plan for sufficiently large blade size (e.g. $\geq$ 500mm) in combination with sufficient number of turns

(e.g. ≥ 4) to optimize the interruption process using PE/PTFE materials, possibly together with copper. Removing the plunger has a negligible advantage but there are potential risks with this strategy regarding arc re-establishment.

The arc modelling appears to give reasonable expansion velocities for the medium blades on the basis of the assumption used but the temperature assumption appears not to fit the case for the small blade arc expansion velocity.

Chapter 9 brings the findings together and draws the conclusions to this work whilst making recommendations for future work.

Chapter 8

Conclusions and future work

This work has been concerned with improving the effectiveness of the DC current interruption principle. This has been achieved by initially studying and detailing the general operation of the electric arc in electromagnetic interrupters, which offers advantages in terms of understanding how the process works and also gives an understanding of controlling the limitation of the current which flows through the helical arc model specifically. The operation of the electric arc in helical interrupter geometries has been studied and found to offer potential advantages for controlling long arcs to produce more efficient arc quenching.

From these studies, it has been possible to hypothesize that the arc control behaviour may be quantified so that further insight may be gained as to how the arc can be utilized for current interruption to better protect the network. This aspect of arc control may have wider industrial applications.

Investigations into these hypotheses were carried out experimentally by enacting the interruption process using helical arcs with the aim of preventing the arc turns from shorting together. A series of tests were undertaken on a device which uses an arrangement of polymeric blades to form helical arcs. These blades

were fabricated from PTFE, copper and PE.

All the experiments with different materials and layouts were recorded by oscilloscope and also optically by High Speed Camera, which can only cover the front view of the experimental setup. However, with fibre optic devices, the rear view was observed. These two methods can be combined to provide 3D view information. By this methodology, more information and analysis was obtained during the arc striking.

Three periods of arc behaviour can be identified from current, voltage and photographic records. Within the 3 periods there are a number of factors that contribute to successful arc control and extinction with acceptable current limitation within acceptable time to interrupt. Notably, with the geometry used, these are blade size and blade material, and number of turns.

It may be concluded from these experiments regarding blade size and materials, that large PTFE blades control the current more effectively and efficiently than the smaller PTFE blades and the large PE blades, despite a slower rate of arc expansion with the large PTFE blades than with the medium and small blades.

Regarding the number of turns, increasing the number of turns may be seen to reduce both the radial arc expansion extent and velocity.

In summary therefore, DC arc control in air i.e. retaining the arc within the limit of the blades at any arc radial expansion velocity - depends both on sufficiently high number of turns (3+) and sufficient blade size (here 500mm PTFE). The materials used (here PTFE or PE) have different advantages and disadvantages over each other. In terms of ablation, it appears that PTFE has particular durability ($\sim$ 5% volume loss over 200 tests, representing expected long term use achievable in practice).

The general trend emerging is that it may be possible to plan for sufficiently large blade size in combination with sufficient number of turns to optimize the interruption process using PE/PTFE materials, possibly together with copper. Removing the plunger has a negligible advantage but there are potential risks with this strategy regarding arc re-establishment.

Calculations of arc area, mass and volume for the initiation period and for the whole expansion period together with arc velocity measurements obtained from the experiments to estimate driving and drag forces on the arc, suggest that results obtained for arc expansion behaviours are within reasonable expectations, in that the driving force on the arc was found to be greater than the drag force, which explains why the arc expands from the centre of the rod towards the extent of the blades. For the medium blades, the calculated expansion velocities appear reasonable but for the small blades it appears that the assumed temperature (3,000K) is higher than would have applied in the experiments in terms of the actual velocities.

Taken together, the results suggest that a sufficiently large blade area in conjunction with sufficient turns to lengthen the arc suffices to retain the arc within the blades for well controlled and rapid arc extinction in spite of increased driving force.

For future work, the conclusions imply that since PTFE and PE have relative advantages and disadvantages, a combination of the two materials could be beneficial and would be worthwhile exploring, potentially using some copper blades with them. Regarding configurations and geometries, it would also be useful to explore a combination of large blades with 4 or more turns to investigate how far arc control and current limitation and the efficiency of the interruption process might be improved.

Appendices

Appendix A

Paper Related to Work Presented in this Thesis

the following page show reprint of conference paper related to work presented in this thesis:

one paper has been accepted for publication in the proceeding of the international conference on gas discharges and their applications/GD 2012/ Sept 2012/ Beijing, China

HELICAL ARC CONTROL FOR CURRENT LIMITATION AND INTERRUPTION OF DC CURRENT

H. ELZAGZOUG, J. E. HUMPHRIES AND J. W. SPENCER

One journal paper to be submitted for publication in IEEE power transaction

DC INTRRUPTION PRINCILE USING A HELICAL ARC ARRANGMENT

H. Y. ELZAGZOUG, J. W. SPENCER AND A. G. DEAKIN

HELICAL ARC CONTROL FOR CURRENT LIMITATION AND INTERRUPTION OF DC CURRENT

H. ELZAGZOUG, J. E. HUMPHRIES AND J. W. SPENCER

CIMS, Department of Electrical Engineering and Electronics, The University of Liverpool, Brownlow Hill, Liverpool, L69 3GJ, UK. joe@liverpool.ac.uk

ABSTRACT

The expansion of a helical arc confined between polymeric helical plates is governed by both electromagnetic and aero-dynamic forces. These arise due to the complex interaction between the individual arc turns, arc helical plate interactions and surrounding media. These interactions can be exploited to control the rate of expansion. During this expansion stage there is a substantial increase in arc voltage which in low voltage systems can limit the current thereby causing current interruption providing the arc quenching conditions are suitable.

1. INTRODUCTION

Electric arc discharges are utilised in circuit breakers to interrupt current in electrical networks [1-3]. The designs of these circuit breakers have been optimised to achieve arc extinction, thereby current interruption, as efficiently as possible to avoid excessive damage to electrodes and nozzles. As well as current interruption, circuit breakers are also designed to withstand the rate of rise of recovery voltage (rrrv) after current zero. In dc current interruption the means of arc extinction is complicated by the lack of a natural current zero.

In dc circuit breakers a forced current zero is created either by the arc voltage exceeding the system voltage (for low voltage system) [4] or through an artificial current zero created by a resonant circuit close to the interrupter (for high voltage systems) [5-6]. Traditionally for high voltages, circuit breakers designed for ac current interruption have been modified and used alongside a resonant circuit. However, such devices only have relatively short arc lengths and therefore have limited applications where there is a requirement to limit the dc fault level current prior to arc extinction in order to lessen the potential for damage.

Helical arc devices have been the subject of research [7-8] as a possible means of limiting the potential for damage to a network when a dc fault develops; achieving successful arc interruption and with the potential of withstanding the rrrv after current interruption due in part to the long arc lengths which can be produced. This contribution extends the scope of previously reported work through tests performed with different helical blades arrangements and various radial sizes and at different current levels. High speed photographs have been used to calculate the arc's velocity as it moves from the centre of the device to edge of the helical plates.

2. EXPERIMENTAL SETUP

2.1 Helical Assembly.

The helical assembly used in this experiment is shown in fig. 1.

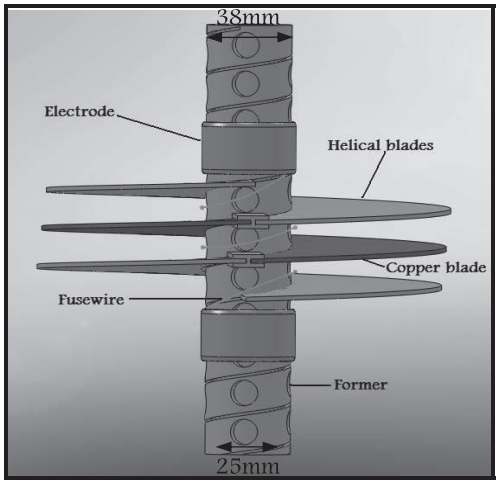

Fig. 1: Schematic of the Helical Arc

The former, or core, of the device has an 18mm pitch thread cut, to allow the helical blades to be screwed onto it as shown in fig. 1. The core is made from tufnol with an outer diameter of 38mm and inner diameter of 25mm. Radial holes (12mm in diameter) are drilled, equally-spaced, through the core, and these are effectively opened or closed by removing or inserting the plunger. Lastly, four Perspex separators were arranged around the outside of the helix to support the blades. The behaviour of the arc was investigated for two different sizes of blades. Five blades were used, four PTFE and one copper, one set was 180mm in diameter and the other was 360mm. Another set was made from polyethylene instead of PTFE for the larger size blades only for comparison.

The arc was initially formed by passing current through fuse wire (0.193mm diameter) which was wound onto the former between the helical plates. The ends of fuse wire are then connected to aluminium rings fitted tightly over the core. The cables delivering the current were also connected to theses rings.

2.2 Power Supply and Measurement Setup.

A capacitor bank was initially charged to between 3.3 and 5.2kV. It was discharged into a fuse wire when triggered using an ignitron switching circuit. The current and voltage were monitored on a digital oscilloscope via a 1mΩ shunt and a 1000:1 probe respectively. Measurements of the arc's helical profile were obtained from high speed photographs from a high speed camera operating at 20,000 frames per second with 50μs between the frames. Fig. 2 shows a schematic of the connection of the power source and the location of the diagnostics relative to the test head.

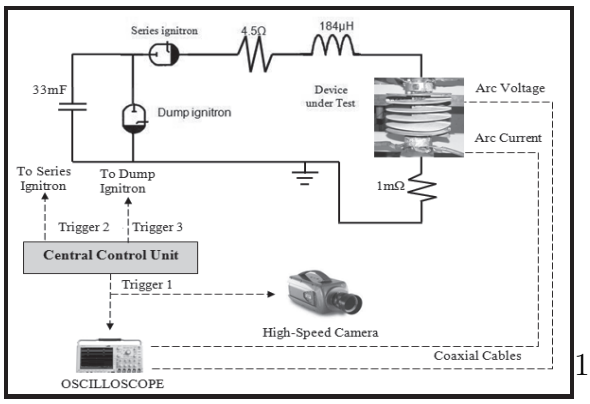

Fig. 2: Layout of Diagnostic Equipment

2.3 Experimental Procedure.

The initial charging voltage on the capacitor bank determined the maximum prospective fault current. The number of the helical blades was kept to five for this set of experiments arranged as two polymeric, one copper and two polymeric blades. The current profile from the capacitor bank with a shorting strap connected across the test unit was pseudo dc waveform decay to 30% of its peak value in 0.148s.

3. RESULTS

3.1 Small Blades Results - 180mm.

Fig. 3 shows typical current and voltage results during the formation of a helical arc. Current starts to flow through the fuse wire at point A. During the period marked B the fuse wire completely vaporises and an arc is established (C). The arc then expands outwards during period D until it reaches the outer edge of the plates where inter turn short circuits occurs. At E the arc is outside of the plates and there is no arc control. The current is limited to approximately 650A with a prospective fault current of 1kA. The arc voltage is approximately 1.2kV when the arc is confined between the helical blades.

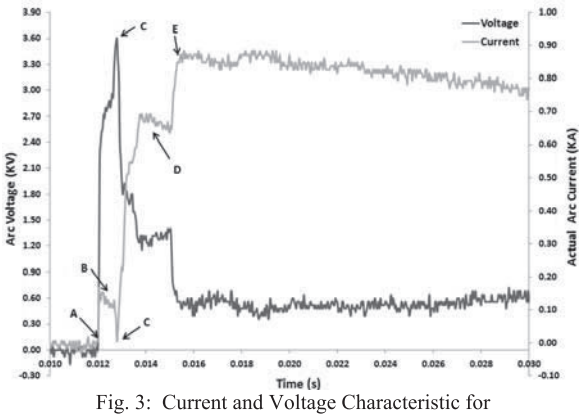

Fig. 3: Current and Voltage Characteristic for 2PTFE, 1 Copper, 2PTFE

Fig. 4 shows some typical frames during the expansion of the helical arc for the 180mm blades, solid-cored device where the expansion velocity is typically 40 m/s.

The interval between each frame shown is 50 μs. In the first frame, the fuse wire is partly vaporised subsequent frames show that it is completely vaporized and an arc is established. This period of fuse action was used to

synchronise the current and voltage waveforms with the high speed film record. Once the arc has fully formed it expanded outwards until it leaves the confines of the helical blades at some stage.

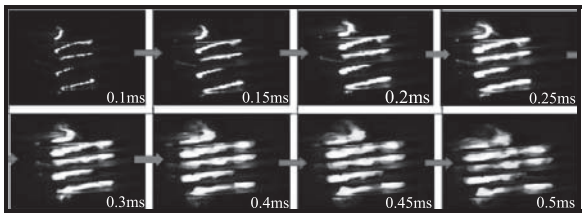

Fig. 4: High Speed Photographs

3.2 Large Blades Results - 360mm.

Fig. 5a shows a test result for the larger size blades used under similar conditions to the smaller blade arrangement. In this result, the arc voltage is 1.6kV which limit the prospective fault current (900A) to an average of 650A. The expansion time is 10ms before the arc leaves the confines of the blades. The average arc velocity is 16m/s.

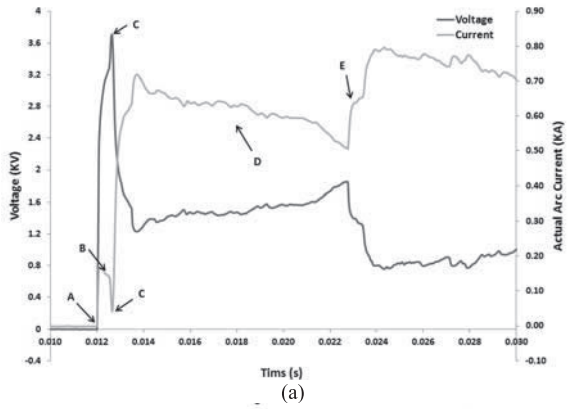

(a)

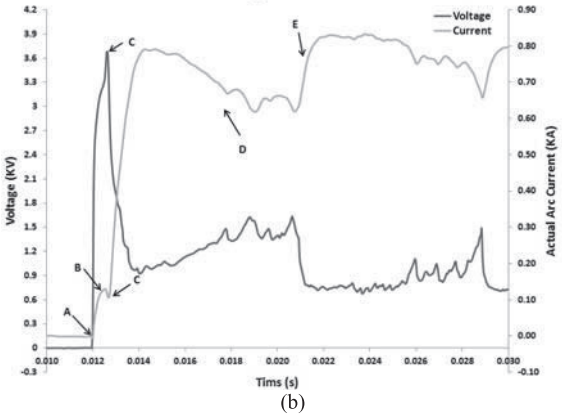

(b)

Fig. 5: Current and Voltage Characteristic for

(a) 2PTFE, 1 Copper, 2PTFE

(b) 2PE, 1 Copper, 2PE

The PTFE blades were replaced by polyethylene (PE) in the same arrangement as for PTFE. Fig. 5b shows the current/voltage characteristic for the PE arrangement. The current is limited to an average of 700A for a prospective fault current of 900A. The maximum arc voltage is 1.5kV and the average arc velocity is 20m/s.

The high speed camera results give an indication of the arc behaviour for the different polymers. Images for each corresponding frame (fig. 6) were taken at the same time period from the arc initiation. The arc behaviour for PTFE arrangement (Fig. 6a) is well define, where as for PE (fig. 6b) the appearance of the arc is less defined and more defuse.

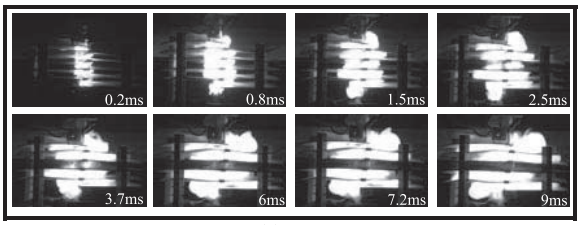

(a)

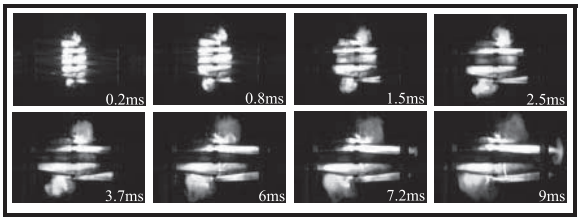

(b)

Fig. 6: High Speed Photographs

4. DISCUSSION

The results show three distinct types of arc behaviour. The first is when the fuse wire vaporises and an arc is established (A-C). During this period, which lasts approximately 1ms, the arc expands rapidly (figures 4 and 6 a, b). The current level is low (~100A) and this is forced to reduce to an even lower value (<10A) whilst the arc's voltage increases to 3.6kV. At this point the instantaneous power dissipation from the arc is approximately 36kW for smaller blades and 108kW for the larger PTFE plates and 360kW for the PE plates. During the same period between (A – C) the maximum instantaneous power is about 280kW, 480kW and 360kW respectively. There is a significant reduction in the instantaneous power input for PTFE blades at

point C but for the PE blades this remained unchanged.

The arc velocity during this initial period is 80m/s to 163 m/s. This initial rapid acceleration of the arc may be attributed to the vaporisation of the fuse wire and by the rapid heating of the gas during the establishment of an arc. The flow of heated gas on the blade holder side of the arc is restricted by the blocked holes drilled into the former. Whereas, on the other side of the arc the gas is less restricted and can, therefore, move more freely. The restriction of flow presented by the blade holder produces an increase in pressure which aids to rapid expansion due this initial period.

In the second phase the arc expands less quickly at an average speed of between 40m/s to 16m/s for the conditions investigated. This lower speed may well be due to the reduction in arc current at C which triggers a type of "stall" in the arc's movement. This may be caused by a substantial reduction in the arc's instantaneous power for PTFE blades producing less gas heating and ablation and therefore gas to aerodynamically drive the arc outwards. There is also a reduction in the Lorentz force acting on the discharge which is proportional to arc current. It is worth noting that the "stall" in arc expansion due to the reduction in the instantaneous power is less significant for the PE blades than for the PTFE plates. Indeed, the arc moves more rapidly when PE is used than PTFE with the arc reaching the edge of the plates (E) approximately 1ms sooner. During this later expansion period (D), the average instantaneous power is 910kW, 960kW and 875kW for the three arrangements (Small PTFE, Large PTFE and Large PE). The level of current during this period was between 700 and 850A. The larger PTFE setup controlled the current (700A) much more effectively than the smaller PTFE or the larger PE arrangements. At the end of the expansion period the current has been reduced to 500A compared to 650A and 620A respectively. Despite the greater rate of expansion for the PE plates this does not appear to provide a significant advantage over PTFE plates in the arrangement under test.

At the end of this second phase the arc discharge will have reached the edge of the helical blades. At this point inter-turn shorting will occur resulting in an increase in current due to the shorter arc length and no losses associated with arc/polymer ablation. As a consequence the arc voltage reduces. The instantaneous power input during this third phase is approximated 400kW, 600kW, 700kW respectively.

5. CONCLUSION

A series of tests have been undertaken on a device which uses an arrangement of polymeric plates to form helical arc. These plates were fabricated from PTFE, copper and PE. Three periods of arc behaviour can be identified from current, voltage and photographs records. The results show that the large PTFE plates control the current more effectively than the smaller PTFE plates and the larger PE plates despite a slower rate of arc expansion.

REFERENCES

[1] Flurscheim, C.H. (Ed.): 'Power Circuit-Breaker Theory and Design' (Peter Perigrinus Ltd, London, 1982)

[2] Ragaller, K.: 'Current Interruption in High Voltage Networks' (Plenum Press, 1978)

[3] Ryan, H.M, and Jones, G.R.: 'SF_6 Switchgear' (peter Perigrinus Ltd,London, 1989)

[4] Browne, Thomas E. Jr. (Ed.): 'Circuit Interruption: Theory and Techniques' (Marcel Dekker Inc, 1984)

[5] Ryan, H.M. (Ed.): 'High Voltage Engineering and Testing' (IEE Publishing, Power series no. 32, 2001, 2nd edn.)

[6] Garrard, C.J.O.: 'High Voltage Switchgear', IEE Proc., 1976, 123, pp. 1053-1080

[7] M.G. Ennis, J.K. Wood, J. Spencer, D.R. Tumer, G.R. Jones, P. Covc:ntry, IEE Proc. A, Vo1.142, No.3, May 1995, pp.201-205

[8] Afanasiev, A.A, Barrault, M.R., Blackburn, T.R., Jones, G.R., and Sethuraman, S.K.: 'Characteristic of electromagnetically driven helix arcs for DC Switching', Proc. IEE 'B', 1981, 128, 950, pp.249-252

[9] Shimomura N, Nagata M, Grabowski C, Akiyama H: IEEE Trans. Plasma Science, Vol.23, No.5, 1995, pp.860-864.

DC Interruption Principle Using a Helical Arc Arrangement

HY Elzagzoug, JW Spencer and AG Deakin
Centre for Intelligent Monitoring Systems,
Department of Electrical Engineering and Electronics, University of Liverpool,
Liverpool L69 3GJ, UK

Abstract — *The expansion of a helical arc confined between polymeric helical blades is governed by both electromagnetic and aerodynamic forces. These arise due to complex interactions between the individual arc turns, arc helical blade interactions and surrounding media. These interactions can be exploited to control the rate of expansion. During this expansion stage there is a substantial increase in arc voltage which in low voltage systems can limit the current thereby causing current interruption providing the arc quenching conditions are suitable. In this investigation current limiting properties of different combinations and sizes of helical blades (metal and polymer) were studied experimentally. Marginal improvement in current limiting properties was found upon substituting (two) outer polymeric blades with copper. Increasing blade count was also beneficial. Blade size was however the most significant factor for enhancing arc control and current limitation, three large polymer blades outperforming all smaller blades, even with lesser blade area.*

Index Terms —

I. Introduction

Electric arc discharges are utilised in AC circuit breakers to interrupt current in electrical networks [1, 2]. The designs of these circuit breakers have been optimised to achieve arc extinction, thereby current interruption, as efficiently as possible to avoid excessive damage to electrodes and nozzles. As well as performing current interruption, which occurs when the current reaches zero, circuit breakers are also designed to withstand the rate of rise of recovery voltage (rrrv). However, in the case of DC current interruption, achieving arc extinction is complicated by the lack of a natural current zero since the DC cycle consists of positive half-cycles compared with AC's positive followed by negative half-cycles.

In DC circuit breakers a forced current zero is created either by the arc voltage exceeding the system voltage (for low voltage systems) [3] or through an artificial current zero created by a resonant circuit close to the interrupter (for high voltage systems) [4, 5]. Traditionally, for high voltages, circuit breakers designed for AC current interruption have been modified and used alongside a resonant circuit. However, such devices only have relatively short arc lengths and therefore have limited applications where there is a requirement to limit the DC fault level current prior to arc extinction in order to lessen the potential for damage.

Helical arc devices have been the subject of research [6, 7] as a possible means of limiting the potential for damage to a network when a DC fault develops. They achieve successful arc interruption and have the potential of withstanding the rrrv after current interruption due in part to the long arc lengths which can be produced in the helix. The present contribution aims to extend the scope of previously reported work through tests performed with different helical blade arrangements and various radial sizes and different current levels. Technical improvements in high speed cameras have also enabled photographs to be used to calculate the arc's velocity as it moves from the centre of the device to edge of the helical blades.

With the aim of improving DC current interruption by means of controlling the arc and limiting the fault current, we present a novel experimental set up by 1) using metal-polymer blade combinations in a helical arc assembly, 2) by using sufficiently large sized blades in a helical arc assembly and 3) by increasing the number of turns of the blades.

II. EXPERIMENTAL SETUP

A. Helical Assembly

The helical assembly used in this experiment is shown in Figure 1.

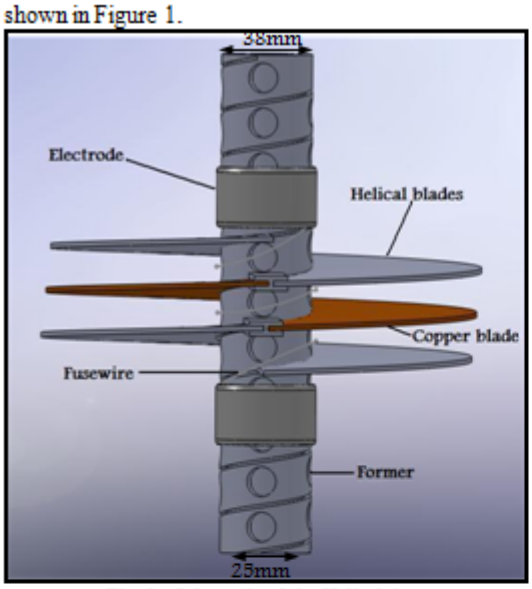

Fig. 1: Schematic of the Helical Arc

The former, or core, of the device has an 18mm pitch thread cut to allow the helical blades to be screwed onto it as shown in Figure 1. The core is made from tufnol with an outer diameter of 38mm and inner diameter of 25mm. Radial holes (12mm in diameter) are drilled, equally-spaced, through the core, and these are effectively opened or closed by removing or inserting the plunger. Lastly, four Perspex separators were arranged around the outside of the helix to support the blades. The behaviour of the arc was investigated for three different sizes of blades.

The arc was initially formed by passing current through fuse wire (0.193mm diameter) which was wound onto the former between the helical blades. The ends of the fuse wire are then connected to aluminium rings fitted tightly over the core. The cables delivering the current were also connected to theses rings.

B. Power Supply and Measurement Setup

A capacitor bank was initially charged to between 3.3 and 5.2kV. It was discharged into the fuse wire when triggered using an ignitron switching circuit. The current and voltage were monitored on a digital oscilloscope via a 1mΩ shunt and a 1000:1 probe respectively. Measurements of the arc's helical profile were obtained from high speed photographs from a high speed camera operating at 20,000 frames per second with 50μs between the frames. Figure 2 shows a schematic of the connection of the power source and the location of the diagnostics relative to the test head.

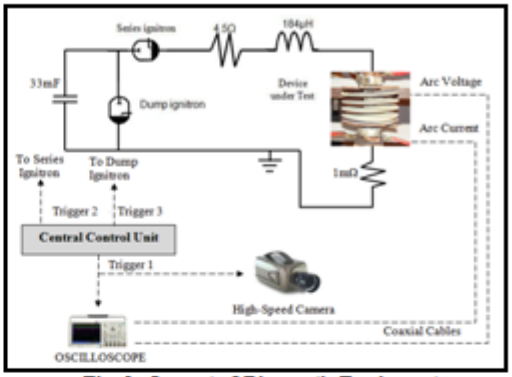

Fig. 2: Layout of Diagnostic Equipment

C. Experimental Procedure

The initial charging voltage on the capacitor bank determined the maximum prospective fault current. The number of helical blades used was between 4 and 7 for the set of experiments arranged for small and medium blade sizes with blade material being polymeric for 4 or 5 blades plus 1 or 2 additional copper blades in all but one case. For large blade sizes three polymeric blades were used. The diameter of the polymeric and copper blades was changed from 180 to 360 and 500mm (Small - Medium - Large). Two different types of polymer (PTFE, PE) were used for the blades in order to determine their effect on the arc behaviour and interruption performance.

III. RESULTS

A. Small Blades Results - 180mm

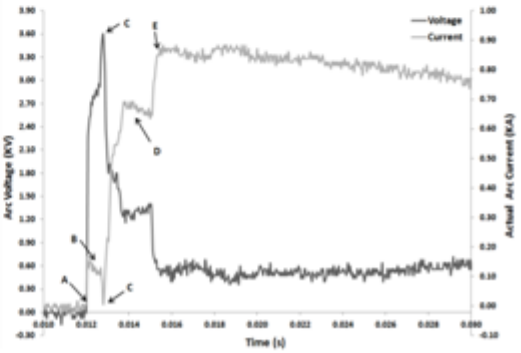

Fig. 3: Current and Voltage Characteristic for 2PTFE, 1 Copper, 2PTFE

Figure 3 shows typical current and voltage results during the formation of a helical arc. Current starts to flow through the fuse wire at point A. During the period marked B the fuse wire completely vaporises and an arc is established (C). The arc then expands outwards during period D until it reaches the outer edge of the blades (E) where inter turn short circuits occur. At E the arc is outside the confines of the blades and there is no arc control (this labelling of the phases A to E is used on all subsequent figures). The current is limited to approximately 650A during phase D with a prospective fault current of 1.11kA. The arc voltage is approximately 1.2kV when the arc is confined between the helical blades.

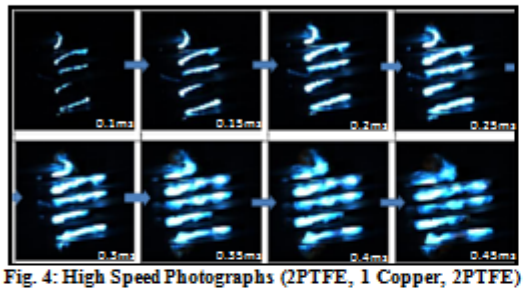

Fig. 4: High Speed Photographs (2PTFE, 1 Copper, 2PTFE)

Figure 4 shows some typical frames during the expansion of the helical arc for the 180mm blades, solid-cored device where the expansion velocity is typically 40m/s during period D. The interval between each frame shown is 50μs. In the first frame, the fuse wire is partly vaporized. Subsequent frames show that it is completely vaporized and an arc is established. This period of fuse action was used to synchronise the current and voltage waveforms with the high speed film record. Once the arc has fully formed it expands outwards until it eventually leaves the confines of the helical blades at some stage.

B. Medium Blades Results - 360mm

Figure 5a shows a test result for the Medium size PTFE blades used under similar conditions to the smaller blade arrangement. In this result, the arc voltage during period D is 1.6kV which limits the prospective fault current (1050A) to an average of 650A. The expansion time is 10ms before the arc leaves the confines of the blades. The average arc velocity is 16m/s.

The PTFE blades were replaced by polyethylene (PE) in the same arrangement as for PTFE. Figure 5b shows the current/voltage characteristic for the PE arrangement. The current is limited to an average of 700A for a prospective fault current of 1050A. During period D the maximum arc voltage is 1.5kV and the average arc velocity is 20m/s.

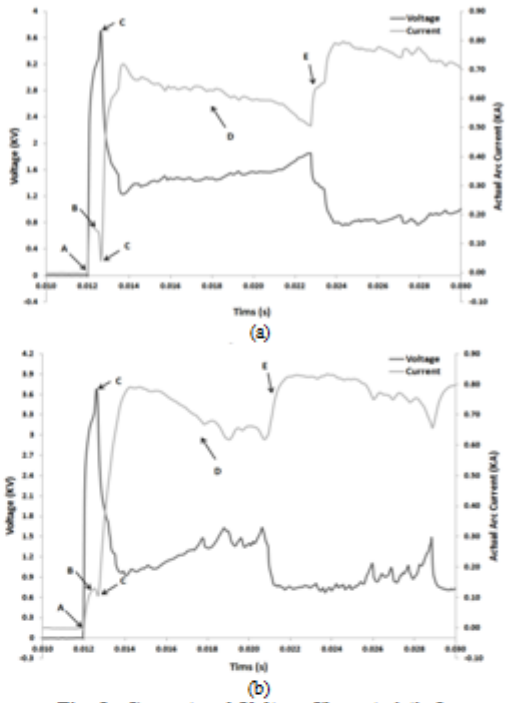

Fig. 5: Current and Voltage Characteristic for
(a) 2PTFE, 1 Copper, 2PTFE
(b) 2PE, 1 Copper, 2PE

The high speed camera results give an indication of the arc behaviour for the different polymers. Images for each corresponding frame (Figure 6) were taken at the same time period from the arc initiation. The arc behaviour for PTFE arrangement (Figure 6a) is well defined, whereas for PE (Figure 6b) the appearance of the arc is less defined and more diffuse.

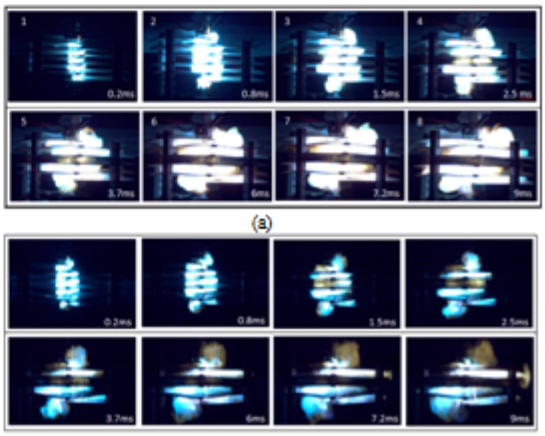

(b)

Fig. 6: High Speed Photographs for
(a) 2PTFE, 1 Copper, 2PTFE
(b) 2PE, 1 Copper, 2PE

C. Large Blades Results - 500mm

Large blades were inserted into the test rig and tested. Two blade arrangements were used. The first test used a blade arrangement of 3PTFE turns. The second arrangement consisted of 3PE blades. These were selected to determine the effect that different materials have on arc movement within the helical arrangement. High speed photographs also provide information on the arc expansion.

PTFE Result

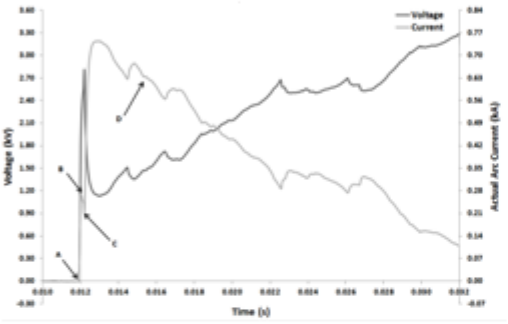

Fig. 7: Current and Voltage characteristic for 3PTFE

The arc current and voltage waveforms for 3PTFE blades are shown in Figure 7. As may be seen in Figure 7, vaporisation time is shorter here (~0.5ms) than with the medium and small blades (~1ms) but it is not considered to be a significant difference as it did not affect control of the arc by means of keeping it within the blade limits. (This applies also with the test shown on Figure 9). The result for this arrangement is similar to those seen before, a rise in arc voltage during the evaporation of the fuse wire and thus a sharp decline as the arc established. Once the arc establishes there is an increase in voltage as the arc expands outwards, with a few small falls in voltage during the overall rise. The fault current was limited to an average of 420A with the prospective fault current being 1050A.

The arc current also shows the same trend as before. The high speed film images shown in Figure 8 are a selection of images during the arcing period for a 3PTFE turns test.

Frames 14, 15 and 16 show the initiation of the arc and its formation. In the frames which follow, 20 to 60, the arc column is seen to expand outwards with the arc roots attached to the electrodes. The shaping of the fuse wire pre-disposes the helical shape of the arc. The last few frames 65, 70 and 80 show that the arc remains within the limit of the blades.

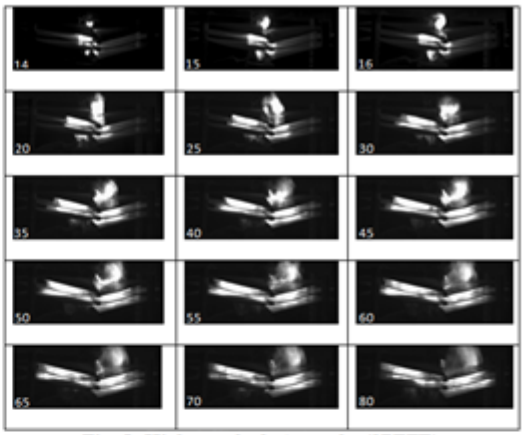

Fig. 8: High speed photographs (3PTFE)

PE Result

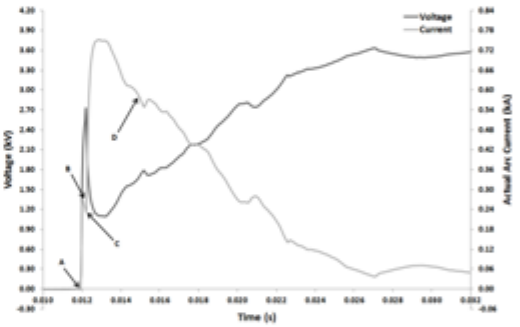

Fig. 9: Current and Voltage characteristic for 3PE

Figure 9 shows arc current and voltage waveform for 3PE turns. With 3PE turns the fault current reduces to near zero within 14ms and the arc stays within the limit of the blades. The prospective arc current of 1050A has been successfully reduced and controlled. The fault current was limited to an average of 420A.

The high speed camera photographs shown in Figure 10 are for a 3PE blades test. In frames 20, 25, 30 and 35 the helical turn appears in a complete form. Frames 40, 45, 50 and 55 show that the arc remains within the limit of the blades. In the last few frames the helical turns do not persist for a long time but start to collapse as the current reduces due to the arc limiting it. This decay of the arc has been observed by Spencer [8] and Kolacinski et al. [9] for rotary arcs and indicates the non-homogeneity in the cooling along the arc.

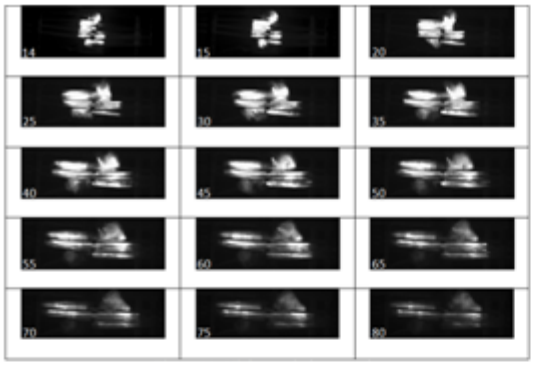

Fig. 10: High speed photographs (3PE)

Table 1: Summary table

Blade Size	No. of Turns	Blade Arrangement	% of Current Limit	Time arc exceeds blades (ms)
Small 180	4	4PTFE	33	15
	5	2PTFE + 1Copper + 2PTFE	50	15
	7	1Copper + 2PTFE + 1Copper + 2PTFE + 1Copper	52	16
	6	1Copper + 4PTFE + 1Copper	46	15.5
	7	1Copper + 5PTFE + 1Copper	58	16
Medium 360	5	2PTFE + 1Copper + 2PTFE	38	23
	6	2PTFE + 2Copper + 2PTFE	48	22
	6	1Copper + 4PTFE + 1Copper	66	27
	5	2PE + 1Copper + 2PE	31	21
	6	2PE + 2Copper + 2PE	47	23
	6	1Copper + 4PE + 1Copper	47	Did not reach
Large 500	3	3 PTFE	60	Did not reach
	3	3 PE	65	Did not reach

Table 1 shows, for the three blade sizes used and for all blade configurations tested, the average actual current during the current limitation phase (D) as a percentage of the fixed prospective current applied from the capacitor bank, calculated as (prospective current - actual limited current) / prospective current. It also shows the time instant (E) at which the arc leaves the confines of the blades where appropriate.

As limiting the actual current and keeping the arc within blade confines are both useful, the utility of the blade sizes and configurations may be compared in the Table.

IV. DISCUSSION

The results show three distinct types of arc behaviour [10]. The first is when the fuse wire vaporises and an arc is established (A-C). During this period, which lasts approximately 1ms, the arc expands rapidly (Figures 4 and 6 a, b). The current level is low (~100A) and this is forced to reduce to an even lower value (<10A) whilst the arc's voltage increases to 3.6kV. At this point the instantaneous power dissipation from the arc is approximately 36kW for small blades, 108kW for the medium PTFE blades and 360kW for the medium PE blades, and 600kW for large PTFE and 648kW for large PE blades. During the same period A – C the maximum instantaneous power is about 280kW, 480kW, 360kW, 696kW and 648kW respectively. There is a significant reduction in the instantaneous power input for medium and large PTFE blades at point C but for the medium and large PE blades this remained unchanged.

The arc velocity during this initial period is 80m/s to 100m/s. This initial rapid acceleration of the arc may be attributed to the vaporisation of the fuse wire and the rapid heating of the gas during the establishment of an arc. The flow of heated gas on the blade holder side of the arc is restricted by the holes drilled into it whereas on the other side of the arc the gas is less restricted and can therefore move more freely. The restriction of flow presented by the blade holder produces an increase in pressure which aids rapid expansion during this initial period.

In the second phase the arc expands less quickly at an average speed of 7m/s to 22m/s. This lower speed may well be due to the reduction in arc current at C which triggers a type of 'stall' in the arc's movement. This may be caused by a substantial reduction in the arc's instantaneous power with PTFE blades producing less gas heating and ablation, and therefore gas, to aerodynamically drive the arc outwards. There

is also a reduction in the Lorentz force acting on the discharge which is proportional to arc current. It is worth noting that the 'stall' in arc expansion due to the reduction in the instantaneous power is less significant for the PE blades than for the PTFE blades. Indeed, the arc moves more rapidly when PE is used than PTFE with the arc reaching the edge of the blades (E) approximately 1ms sooner for medium blades. During this later expansion period (D), the average instantaneous power is 910kW, 960kW, 875kW, 960kW and 924kW for the five arrangements (Small PTFE, Medium PTFE, Medium PE, Large PTFE and Large PE). The level of current during this period was between 700 and 850A. The large PE blades setup controlled the current (740A) much more effectively than the smaller PTFE or the medium PTFE and medium PE arrangements. At the end of the expansion period, with large PE blades the current has been reduced to 5A compared to 650A, 500A and 620A respectively (smaller PTFE, medium PTFE and medium PE). Despite the greater rate of expansion for the PE blades this does not appear to provide a significant advantage over PTFE blades in the arrangement under test. At the end of this second phase the arc discharge will have reached the edge of the helical blades for the small and medium blade sizes. At this point inter-turn shorting occurs resulting in an increase in current due to the shorter arc length and no losses associated with arc/polymer ablation. As a consequence, the arc voltage reduces. The instantaneous power input during this third phase is approximately 400kW, 600kW, and 700kW respectively. The large PE/PTFE blades do not have a phase 3 since the arc is under control and stays within the limits of the blades.

Table 1 highlights the factors of blade size, number of turns, blade arrangement and material, that may be expected to affect the performance of the arc control, and enables them to be compared.

Regarding blade material, the selection of PE vs. PTFE does not appear to have a significant effect by itself when comparing the same number of turns (3) of large blade size in terms of the percentage of current limit reached (60% vs. 65%) and the time the arc is retained within the blades (equal). There is however an example in medium blades with 6 turns where replacing the central 4 PTFE with PE blades reduced the percentage of current limit reached from 66% to 47% but it instead gave additional arc control, achieving "did not reach outer limit" compared with 27 seconds for the arc to leave the blade confines with PTFE. Replacing a polymeric blade with a copper blade appears to have only a marginal effect (e.g. Small, 7 turns, 1Copper + 2PTFE + 1Copper + 2PTFE + 1Copper with 52% vs. 1Copper + 5PTFE + 1Copper with 58%).

More significant effects are achieved by varying the arrangements so that copper blades are on the outside (e.g. medium blades, 2PTFE + 2Copper + 2PTFE with 48% vs. 1Copper + 4PTFE + 1Copper with 66%). Also, whilst not changing the percentage of current limit reached, moving 2 medium copper to the outside of 4 PE gave additional arc control, achieving "did not reach outer limit" from 23 seconds for the arc to leave the blade confines.

Major effects are however produced by increasing the number of turns and increasing the blade size. Regarding the number of turns, increasing the number of turns for small and for medium blade sizes may be generally seen to reduce both the radial arc expansion extent and velocity.

Regarding blade size, large blades control the current and the arc more effectively and efficiently than medium blades, both large blade tests achieving 60%-65% current limitation and full arc control. There is evidence that a similar effect occurs when comparing medium and small blade sizes as well in terms of the percentage of current limit reached and the time the arc is retained within the blade confines. Overall, the large blades outperformed the medium and small blade sizes with just 3 turns compared with increasing turns up to 6 or 7 for the smaller blade sizes, indicating that blade size may therefore be the most significant factor affecting performance and that the other factors are secondary considerations. Notably, blade area with 3 large polymer turns is lower than for 6 medium turns which include 1 or 2 copper blades.

V. CONCLUSIONS

A series of tests have been undertaken on a device which uses an arrangement of metal/polymeric or polymeric blades to form helical arcs. These blades were fabricated from PTFE, Copper and PE. Three periods of arc behaviour can be identified from current, voltage and photographic records. Within the 3 periods there are a number of factors that contribute to successful arc control and extinction with acceptable current limitation within acceptable time to interrupt. Notably, with the geometry used, these are blade size, blade material, and number of turns.

Regarding blade material, the choice of polymeric material (PE vs. PTFE) appears to be mainly dependent on the desired level of durability. Replacing a polymeric blade with a copper blade has

a marginal effect but arranging for 2 copper blades to be outside polymer blades, rather than the polymer blades on the outside, is beneficial.

Regarding the number of turns, increasing the number of turns may be generally seen to reduce both the radial arc expansion extent and velocity and increase the percentage of the current limit that may be achieved.

Major advantages are however gained by increasing the blade size in particular. Turn for turn, large blades control the current and the arc more effectively and efficiently than medium blades and similarly the medium more than the small blades. In fact the large blades outperformed the smaller blades sizes with just 3 turns compared with 6 or 7 turns for medium and small blades and blade size may therefore be considered to be the most significant factor.

In conclusion therefore, DC arc control in air i.e. retaining the arc within the limit of the blades at any arc radial expansion velocity appears to depend both on a sufficient number of turns (3+) and sufficient blade size (here 500mm). It is possible that further improvements may be achievable by adding turns and including copper blades outside the stack. Selection of polymeric blade materials PE vs. PTFE has a lesser role but their different durabilities are a significant consideration for long-term performance.

REFERENCES

[1] Flurscheim, C. (1982). Power circuit breaker theory and design, volume 1. Inspec/Iee.

[2] Ragaller, K. (1978). Current interruption in high-voltage networks, volume 5. Plenum Publishing Corporation.

[3] Browne, T. (1984). Circuit Interruption: theory and techniques. M. Dekker.

[4] Ryan, H. (2001). High voltage engineering and testing. Number 32. Inst of Engineering & Technology.

[5] Garrard, C. (1976). High-voltage switchgear. Proceedings of the Institution of Electrical Engineers, 123(10):1053-1080.

[6] Ennis, M. G., Turner, D. R., Spencer, J., Jones, G. R., Wood, J. K., and Coventry, P. (1995). Helical arcs in electromagnetic interrupters. In IEE Colloquium on Physics of Power Interruption, pages 201-205. IET.

[7] Afanasiev, A., Barrault, M., Jones, G., Sethuraman, S., and Blackburn, T. (1981). Characteristics of electromagnetically driven helix arcs for dc switching. IEE Proceedings B: Electric Power Applications, 128(5):249-252.

[8] Spencer, J. W. (1987). Some investigations of the behaviour of a rotating arc discharge.

[9] Kolacinski, Z., Campbell, L., and Zdanowicz, L. (1992). Spiral arc quenching. IEEE Transactions on Power Delivery, 7(2):822-828.

[10] Elzagzoug, H. Humphries, J. E. and Spencer, J. W. (2012). Helical arc control for current limitation and interruption of dc current. In 19th International Conference on Gas Discharges and their Applications, pages 98-101, China, Beijing.

Appendix B

Calculations

B.1 calculations of the driving (F) and drag (F_D) for medium blade(360 mm diameter)

B.1.1 Arc Volume and pressure for the whole expansion period

$$V_{total} = L \times \pi \times (r_2^2 - r_1^2) \tag{B.1}$$

$$V_{total} = 0.016 \times \pi \times (0.157^2 - 0.017^2)$$

$$V_{total} = 0.00122m^3$$

Loss of PTFE is approximately 2.3g for 80 shot, so the loss of PTFE per shot = 2.3g/80 = 28.7mg.

Number of moles base on loss of PTFE per shot = 28.7mg/50 = 0.57m moles

From equation 6.3 pressure is

$$P = nRT/V_{total}$$

$$P = 0.57 \times 10^{-3} \times 8.314 \times \frac{3000}{0.00122}$$

$P = 11.7$kPa

B.1.2 Arc volume and pressure for initiation period

$$V_i = L \times \pi \times (r_2^2 - r_1^2) \tag{B.2}$$

$$V_i = 0.016 \times \pi \times (0.034^2 - 0.017^2)$$

$$V_i = 0.0000436m^3$$

From equation 6.3 the pressure is

$$P = nRT/V_i$$

$$P = 0.133 \times 10^{-3} \times 8.314 \times \frac{3000}{0.0000436}$$

$P_i = 76.5$kPa for the specific area.

B.2 Forces on Arc

B.2.1 Whole expansion period

The aerodynamic force, the acceleration of the driving force, and the drag force for the whole expansion period may be calculated as follows.

To calculate the aerodynamic force (equation 6.6):

$$F = PA \tag{B.3}$$

where

P = 11.7 $\times 10^3 Pa$

$A = 2\pi \times 5 \times 10^{-3} \times 16 \times 10^{-3} = 5 \times 10^{-4} m^2$

$F = 11.7 \times 10^3 \times 5 \times 10^{-4} = 5.9N$

To calculate the acceleration A_c of driving force:

$$F = m_t \times A_c(SolidState) \tag{B.4}$$

Where m_t is the total mass which $= m_p + m_c$

m_p = mass of hot gas (g)

m_c = mass of cold gas (g)

$$\begin{aligned} m_p &= V_{total} \times Density \\ &= 0.00122 \times 0.2293 \\ &= 2.807 \times 10^{-4} kg \end{aligned}$$

Now the cold gas volume of V_2 can be calculated as

$$\begin{aligned} V_2 &= L \times \pi \times (r_3^2 - r_2^2) \\ &= 0.016 \times \pi \times (0.180^2 - 0.157^2) \\ &= 0.000389m^3 \end{aligned}$$

Density at 300K open air = 1.1738 (kg/m^3) [Tanaka, 2004]

$$\begin{aligned} m_c &= V_2 \times Density \\ &= 0.000389 \times 1.1738 \\ &= 4.573 \times 10^{-4}kg \end{aligned}$$

$m_t = 2.807 \times 10^{-4} + 4.573 \times 10^{-4} = 7.381 \times 10^{-4}$kg

$$\begin{aligned} A_c &= F/m_t \\ &= 5.9/7.381 \times 10^{-4} \\ &= 7.963 \times 10^3 m/s^2 \end{aligned}$$

The drag force for a solid body is given by:

$$F_D = \frac{1}{2}\rho v^2 C_D A \tag{B.5}$$

$$\begin{aligned}\rho &= 1.1738(kg/m^3)\\ v &= A_c \times t\\ &= 7.963 \times 10^3 \times 1 \times 10^{-3}\\ &= 7.963m/s\end{aligned}$$

The drag force may therefore be calculated as:

$$F_D = \frac{1}{2} \times 1.1738 \times (7.963)^2 \times 0.47 \times \pi \times (8 \times 10^{-3})^2 = 3.5mN$$

Since the calculated driving force F is greater than the drag force F_D, it explains why the arc keeps expanding away from the centre rod.

B.2.2 Initiation period

The aerodynamic force, the acceleration of the driving force, and the drag force for the initiation period may be calculated as follows.

To calculate the aerodynamic force (equation 6.6):

where

P = 76.5 $\times 10^3 Pa$

$A = 2\pi \times 5 \times 10^{-3} \times 16 \times 10^{-3} = 5 \times 10^{-4} m^2$

$F = 76.5 \times 10^3 \times 5 \times 10^{-4} = 38.5N$

To calculate the acceleration A_c of driving force:

$$\begin{aligned} m_p &= V_i \times Density \\ &= 0.0000436 \times 0.2293 \\ &= 9.99 \times 10^{-6} kg \end{aligned}$$

Now the cold gas volume of V_2 can be calculated as

$$\begin{aligned} V_2 &= L \times \pi \times (r_3^2 - r_2^2) \\ &= 0.016 \times \pi \times (0.180^2 - 0.034^2) \\ &= 0.00157 m^3 \end{aligned}$$

$$\begin{aligned} m_c &= V_2 \times Density \\ &= 0.00157 \times 1.1738 \\ &= 1.84 \times 10^{-3} kg \end{aligned}$$

$m_t = 9.99 \times 10^{-6} + 1.84 \times 10^{-3} = 1.85 \times 10^{-3}$kg

$$\begin{aligned} A_c &= F/m_t \\ &= 38.5/1.85 \times 10^{-3} \\ &= 2.075 \times 10^4 m/s^2 \end{aligned}$$

$$\begin{aligned} v &= A_c \times t \\ &= 2.075 \times 10^4 \times 1 \times 10^{-3} \\ &= 20.75 m/s \end{aligned}$$

$$F_D = \frac{1}{2} \times 1.1738 \times (20.75)^2 \times 0.47 \times \pi \times (8 \times 10^{-3})^2 = 23.9 mN$$

B.3 The Calculation of the Arc Initiation

The diameter of the former (rod) is 38mm where half of it is equal to 17mm. For the small blades (180mm) the arc expand to 51mm from 19mm in 0.4ms (Figure 4.6)

Arc expansion velocity = 32/0.4=80m/s.

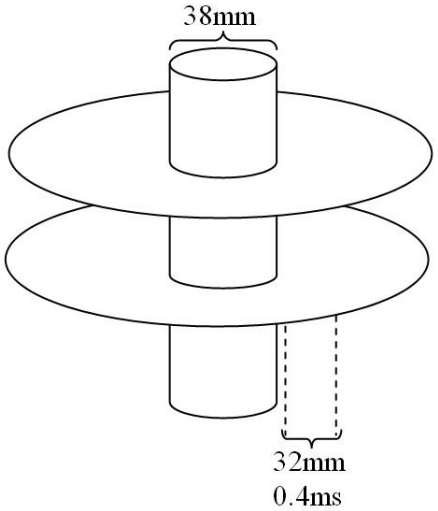

Figure B.1: Diagram showing the arc expansion (small blade)

For the medium blades (360mm) the arc expand to 79mm from 19mm in 0.6ms

(Figure 4.13)

Arc expansion velocity = 60/0.6=100m/s.

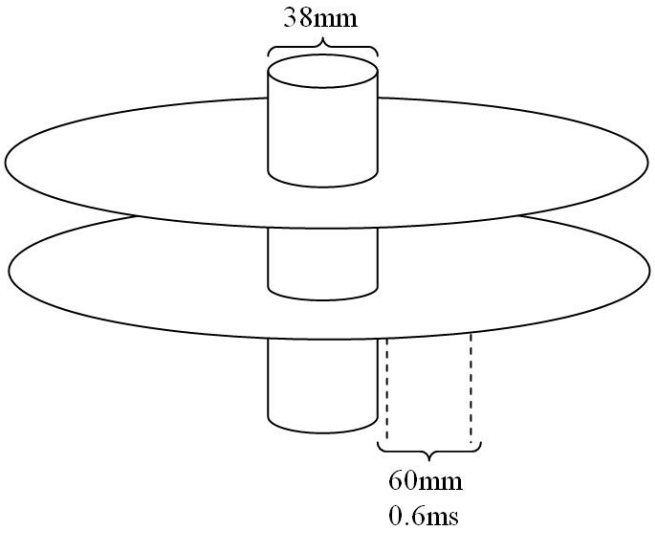

Figure B.2: Diagram showing the arc expansion (medium blade)

Appendix C

Sketches of Helical Arc Material Design

The following pages show the sketches of helical arc design related to work presented in this thesis:

1. Small blades with siding piece design (measurements)
2. Rod and plunger(measurements)
3. Collimate tube for fibre optic(measurements)
4. Comb(measurements)
5. Supporter(measurements)
6. Medium blade(measurements)

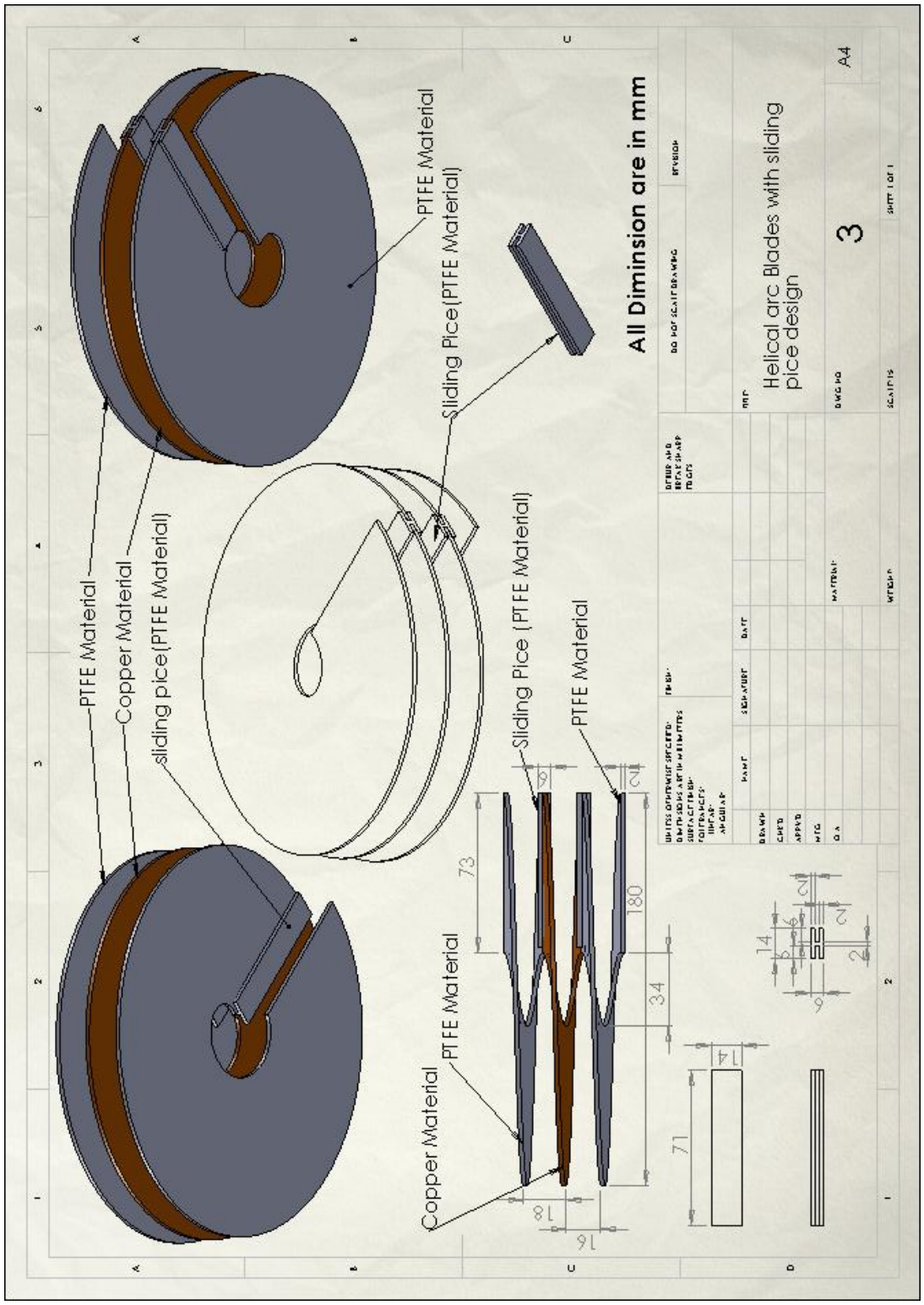

Figure C.1: Small blades with siding piece design (measurements)

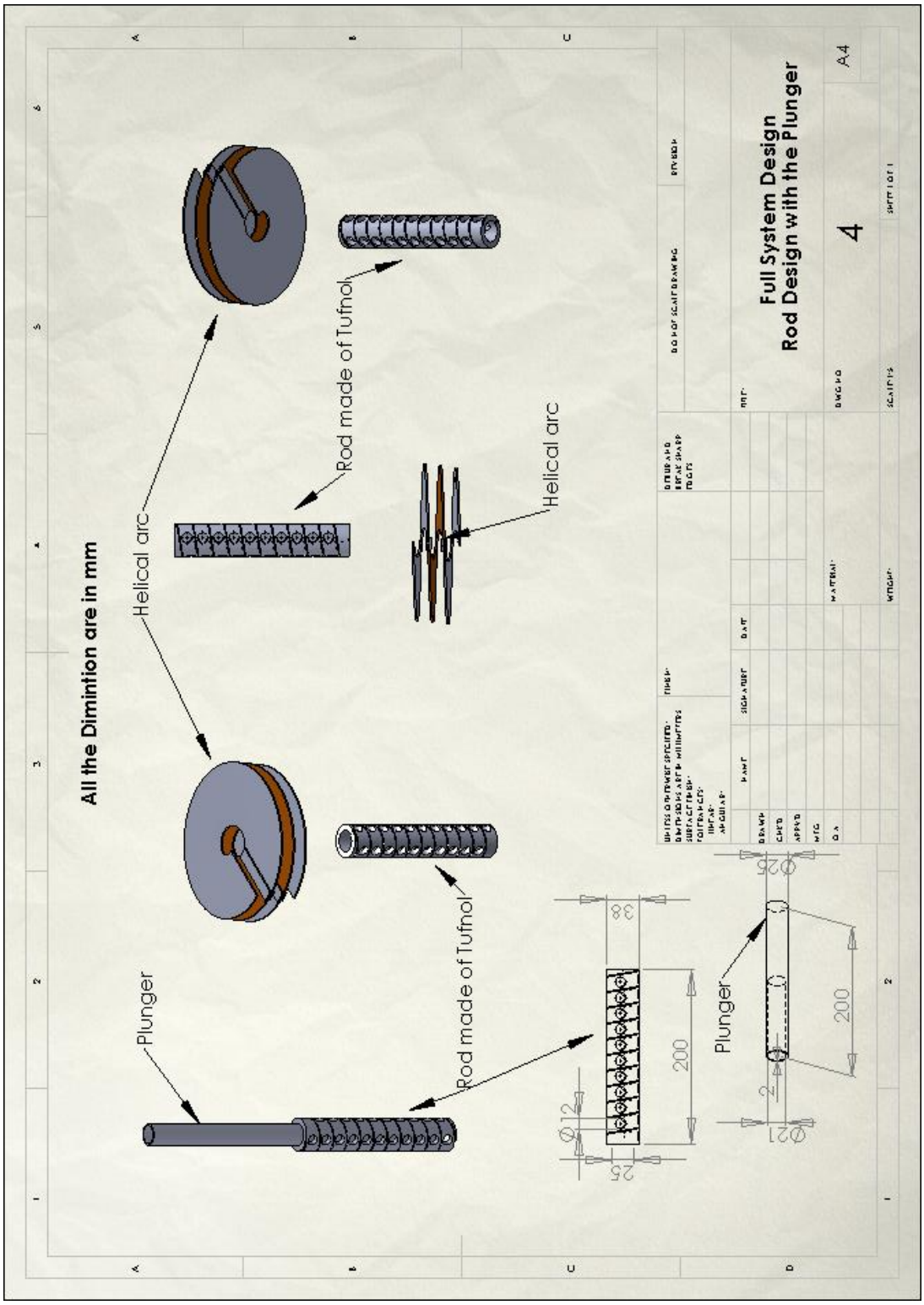

Figure C.2: Rod and plunger(measurements)

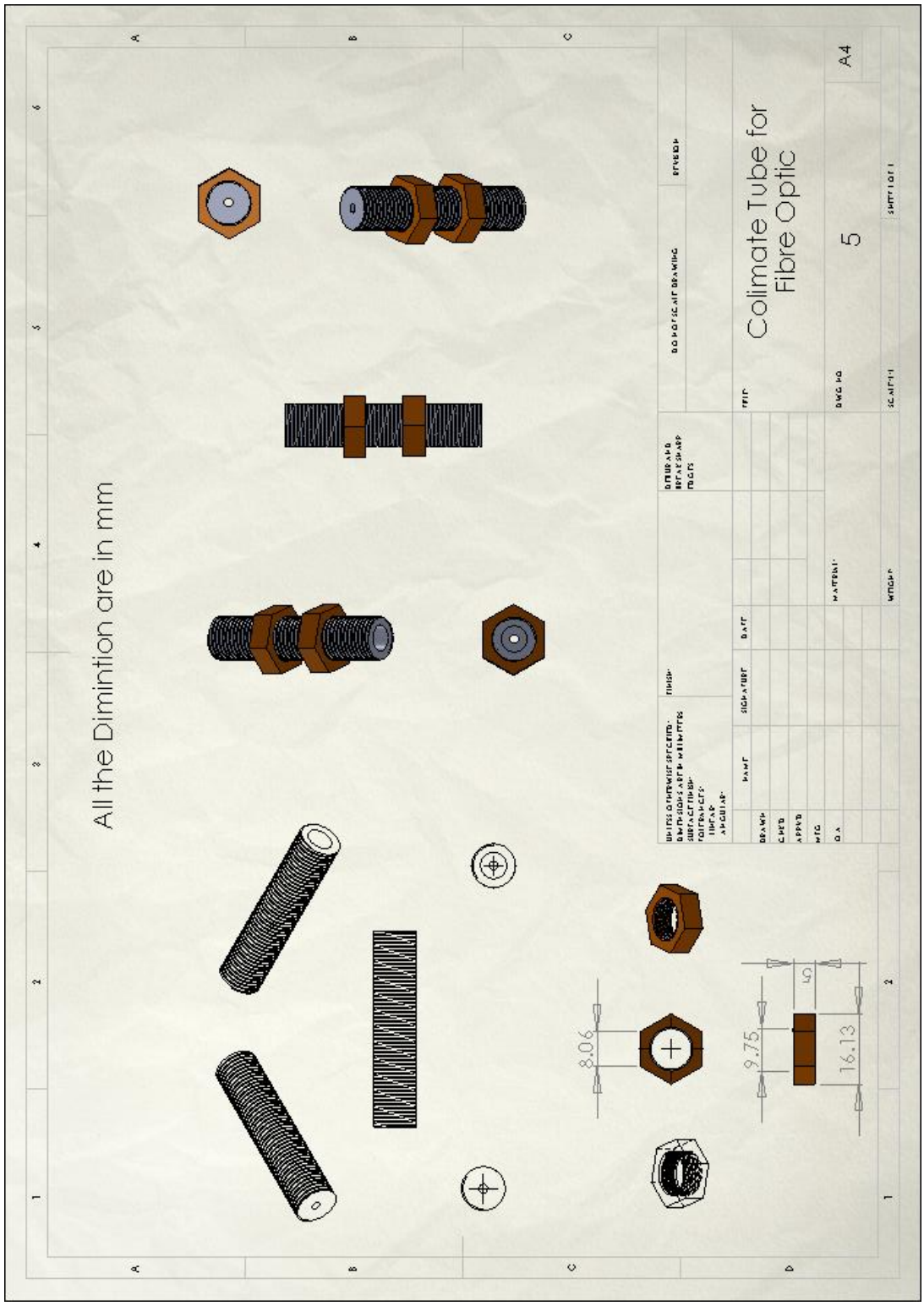

Figure C.3: Collimate tube for fibre optic(measurements)

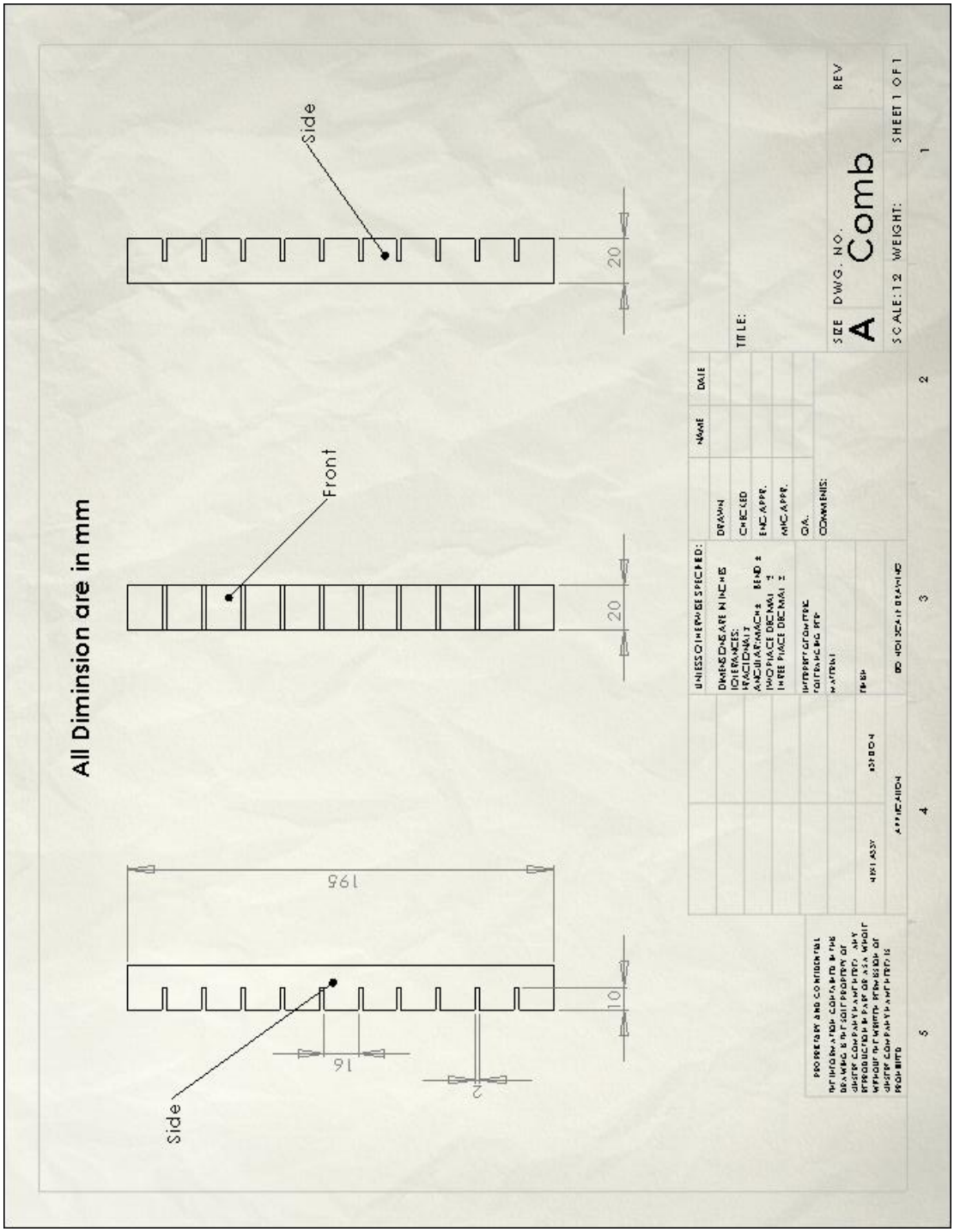

Figure C.4: Comb(measurements)

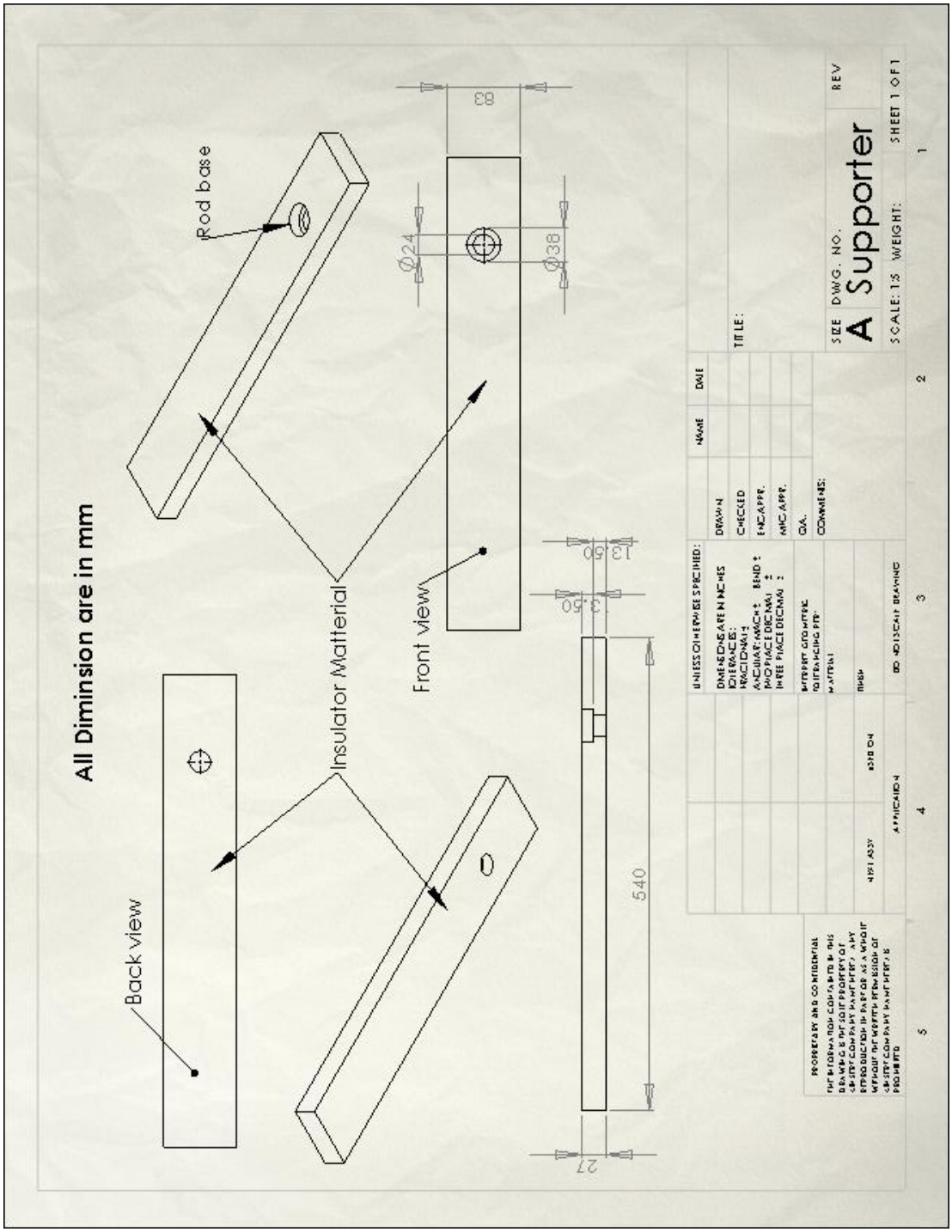

Figure C.5: Supporter(measurements)

Figure C.6: Medium blade(measurements)

Bibliography

[Adam, 1963] Adam, V. W. (Sept. 1963). Technical Note Aero 2915.

[Afanasiev et al., 1981] Afanasiev, A., Barrault, M., Jones, G., Sethuraman, S., and Blackburn, T. (1981). Characteristics of electromagnetically driven helix arcs for dc switching. *IEE Proceedings B: Electric Power Applications*, 128(5):249 –252.

[Ali, 2001] Ali, S. (2001). Switchgear design, development and service. *IEE Power and Energy Series*, 32:301–334.

[Bernard et al., 1990] Bernard, G., Girard, A., Malkin, P., and Scarpa, P. (1990). An sf6 autoexpansion breaker: the correlation between magnetic arc control and critical current. *IEEE Transactions on Power Delivery*, 5(1):196 –201.

[Brookes, 2010] Brookes, R. J. (2010). *Exploration of polymer replacements for SF6 in circuit breakers*. PhD thesis, University of Liverpool.

[Brookes et al., 2008] Brookes, R. J., Looe, H. M., and Spencer, J. W. (2008). Investigation using atomic spectroscopy for the analysis of arc discharges in switchgear operating with polymeric replacements for sf6. In *17th International Conference on Gas Discharges and Their Applications*, pages 121 –124.

[Brookes and Spencer, 2010a] Brookes, R. J. and Spencer, J. W. (2010a). Influence of combustion on polymer arc interrution. In *18th International Conference on Gas Discharges and their Applications*, pages 102–105, Germany.Greifswald.

[Brookes and Spencer, 2010b] Brookes, R. J. and Spencer, J. W. (2010b). Pressurisation characterisitics of polymeric interruption media. In *18th International Conference on Gas Discharges and their Interactions*, pages 70–73, Germany.Greifswald.

[Browne, 1984] Browne, T. (1984). *Circuit Interruption: theory and techniques*. M. Dekker.

[Browne, 1948] Browne, T. E. (1948). A study of a-c arc behavior near current zero by means or mathematical models. *Transactions of the American Institute of Electrical Engineers*, 67(1):141 –153.

[Carabok et al., 1994] Carabok, M., Miller, P., and Partridge, B. (1994). The methodology, results and implications following the risk assessment of the installation, operation and maintenance of switchgear. In *Trends in Distribution Switchgear, 1994., Fourth International Conference on*, pages 116 –120.

[Cassie, 1939] Cassie, A. M. (1939). A new theory of arc rupture and circuit-breaking. CIGRE 10. pp. 102.

[Chen and Lieberman, 1984] Chen, F. and Lieberman, M. A. (1984). *Introduction to plasma physics and controlled fusion/Francis F.* Plenum Press, New York.

[Cobine, 1958] Cobine, J. D. (1958). *Gaseous conductors: theory and engineering applications*. Dover New York.

[Cowley, 1974] Cowley, M. (1974). Integral methods of analysing electric arcs: I. formulation. *Journal of Physics D: Applied Physics*, 7(16):2218.

[Cullwick, 1966] Cullwick, E. (1966). *Fundamentals of electro-magneticsm*. Cambridge University press, 3rd edition.

[Desaulniers-Soucy and Meunier, 1999] Desaulniers-Soucy, N. and Meunier, J. (1999). A study of magnetically rotating arc stability using fluctuations in voltage, velocity and emission line intensity. *Journal of Physics D: Applied Physics*, 28(12):2505.

[Djakov and Bakardjiev, 1976] Djakov, B. E. and Bakardjiev, V. (1976). Electric characteristics of a magnetically driven arc on circular electrodes. In *Proceedings of International Conference on Gas Discharges, Swansea*, volume 1, pages 315–318.

[Drobny, 2001] Drobny, J. (2001). Technology of fluoropolymers, 2001. *CRC Press*, 200:14.

[Elzagzoug et al., 2012] Elzagzoug, H., Humphries, J. E., and Spencer, J. W. (2012). Helical arc control for current limitation and interruption of dc current. In *19th International Conference on Gas Discharges and their Applications*, pages 98–101, China, Beijing.

[Ennis et al., 1995] Ennis, M. G., Turner, D. R., Spencer, J., Jones, G. R., Wood, J. K., and Coventry, P. (1995). Helical arcs in electromagnetic interrupters. In *IEE Colloquium on Physics of Power Interruption*, pages 9–1. IET.

[Fang, 1983] Fang, M. T. C. (1983). A review of gas blast circuit breaker arc modelling. Arc research report, Liverpool University. ULAP-T69.

[Flurscheim, 1965] Flurscheim, C. (1965). Chairman's address: Power division. development in power engineering. *Proceedings of the Institution of Electrical Engineers,*, 112(1):55 –61.

[Flurscheim, 1982] Flurscheim, C. (1982). *Power circuit breaker theory and design*, volume 1. Inspec/Iee.

[Gallagher and Pearmain, 1983] Gallagher, T. J. and Pearmain, A. J. (1983). *High voltage measurment, testing and design.* a wiley-Interscience.

[Gangal, 1989] Gangal, S. V. (1989). Encyclopaedia of polymer science and technology. *John Wiley & sons, New York*, 16.

[Garrard, 1976] Garrard, C. (1976). High-voltage switchgear. *Proceedings of the Institution of Electrical Engineers*, 123(10):1053–1080.

[Garzon, 2002] Garzon, R. (2002). *High voltage circuit breakers: design and applications*, volume 114. CRC.

[Grant and Phillips, 1997] Grant, I. and Phillips, W. R. (1997). *Electromagnetism.* Wiley-Blackwell, Manchester, UK, 2nd edition.

[Harrison, 2005] Harrison, K. (2005). Polytetrafluoroethylene (ptfe), teflon. *Chemistry, structures & 3D molecules from 3Dchem.*

[Heberlein et al., 1984] Heberlein, J., KIMBLIN, C., and LEE, A. (1984). Nature of the electric arc. *Circuit Interruption: Theory and Techniques*, 21:135.

[Hermann et al., 1974] Hermann, W., Kogelschatz, U., Niemeyer, L., Ragaller, K., and Schade, E. (1974). Experimental and theoretical study of a stationary high-current arc in a supersonic nozzle flow. *Journal of Physics D: Applied Physics*, 7(12):1703–1722.

[Hermann and Schade, 1972] Hermann, W. and Schade, E. (1972). Radiative energy balance in cylindrical nitrogen arcs. *Journal of Quantitative Spectroscopy and Radiative Transfer*, 12:12571282.

[Ito et al., 2002] Ito, H., Sakuta, T., and Kobayashi, T. (2002). Measurement of arc properties and spectrum intensity in ac arcs surrounded by plastics. *Electrical Engineering in Japan*, 140(1):38–47.

[Jiles, 1998] Jiles, D. (1998). *Introduction to magnetism and magnetic materials*. CRC.

[Jones, 1984] Jones, G. (1984). Predicting pressure transients due to arcing in two pressure, puffer and rotary arc interrupters. *Proc. IEE Symp. On Trends in modern switchgear design 3.3-150kV*, pages 8.1–8.5.

[Jones, 1988] Jones, G. (1988). *High pressure arcs in industrial devices: diagnostic and monitoring techniques*. Cambridge University Press Cambridge.

[Jones, 2001] Jones, G. (2001). Gas filled interrupters-fundamentals. *IEE Power And Energy Series*, 32:273–298.

[Jones and Fang, 1980] Jones, G. and Fang, M. (1980). The physics of high-power arcs. *Reports on Progress in Physics*, 43(12):1415.

[Kolacinski et al., 1992] Kolacinski, Z., Campbell, L., and Zdanowicz, L. (1992). Spiral arc quenching. *IEEE Transactions on Power Delivery*, 7(2):822–828.

[Kraus, 1991] Kraus, J. (1991). *Electromagnetics*. McGraw Hill, pg, 4th edition.

[Langeac and Barrault, 1987] Langeac, D. and Barrault, M. (1987). Optical diagnostics in the design and development of rotary autoexpansion sf6 circuit breakers. *Journal of Physics D: Applied Physics*, 20(5):602–607.

[Leclerc et al., 1980] Leclerc, J., Smith, M., and Jones, G. (1980). Pressure transients in a model gas-blast circuit breaker operating at extra high current levels. *IEEE Transactions on Plasma Science*, 8(4):376–384.

[Lee and Kim, 2007] Lee, J. C. and Kim, Y. J. (2007). Sf6 arc plasmas modelling for compact and environmental-friendly gas circuit breakers. *Surface and Coatings Technology*, 201(911):5641 – 5645. Proceedings of the Fifth Asian-European International Conference on Plasma Surface Engineering.

[Lide, 2004] Lide, D. R. (2004). Crc handbook of chemistry and physics: a ready-reference book of chemical and phyical data. CRC press, 85th edition.

[Liebermann and Lowke, 1975] Liebermann, R. and Lowke, J. (1975). Radiation emission coefficients for sulfur hexafluoride arc plasmas. *Journal of Quantitative Spectroscopy and Radiative Transfer*, 16(3):253–264.

[Looe et al., 2008] Looe, H. M., Yan, J. D., and Spencer, J. W. (2008). Development of a non-sf¡ inf¿ 6¡/inf¿ self-blast type interrupter unit. In *Gas Discharges and Their Applications, 2008. GD 2008. 17th International Conference on*, pages 117–120. IEEE.

[Lythall and Worth, 1972] Lythall, R. and Worth, C. (1972). *The J. & P. switchgear book: An outline of modern switchgear practice for the non-specialist user*. Newnes-Butterworths.

[Mayr, 1943] Mayr, O. (1943). *On the theory of the electric arc and its extinction*. Number 64. ETZ.

[Mendis et al., 1996] Mendis, S. R., Bishop, M. T., and Witte, J. F. (1996). Invistigations of voltage flicker in electric arc furnace power systems. *IEEE Industry Applications Magazine*, 2:28–34.

[Minoo et al., 1995] Minoo, H., Arsaoui, A., and Bouvier, A. (1995). An analysis of the cathode region of a vortex-stabilized arc plasma generator. *Journal of Physics D: Applied Physics*, 28(8):1630.

[Molyneaux et al., 2003] Molyneaux, I., Ebnesajjad, S., and Fluoroproducts, D. (2003). Environmental aspects of ptfe based laminates in relation to halogen-free.

[Naidu and Kamaraju, 1996] Naidu, M. S. and Kamaraju, V. (1996). *High voltage engineering*. McGraw-Hill, 2 edition.

[Pansini and Smalling, 1994] Pansini, A. and Smalling, K. (1994). *High voltage power equipment engineering*. Fairmont Press.

[Plessl and Poole, 1987] Plessl, A. and Poole, D. (1987). A new sf6 self-extinguishing mv distribution circuit-breaker. Technical report, Brown Boveri Review. vol. 3, pp.150-153.

[Plunkett, 1941] Plunkett, R. (1941). Tetrafi. US Patent 2,230,654.

[Purcell, 2011] Purcell, E. (2011). *Electricity and magnetism*. Cambridge University Press.

[Ragaller, 1978] Ragaller, K. (1978). *Current interruption in high-voltage networks*, volume 5. Plenum Publishing Corporation.

[Reynolds and Jones, 2010] Reynolds, Q. G. and Jones, R. T. (2010). High speed photography and modelling of direct current plasma arcs. In *29th International Congress on High-Speed Imaging and Photonics*.

[Ryan, 2001] Ryan, H. (2001). *High voltage engineering and testing*. Number 32. Inst of Engineering & Technology.

[Ryan, 2012] Ryan, H. (2012). *High voltage engineering and testing*. Inst of Engineering & Technology, 3 edition.

[Ryan and Jones, 1989] Ryan, H. and Jones, G. (1989). *SF6 switchgear*, volume 10. Peter Peregrinus Limited.

[Schupp et al., 2000] Schupp, J., Fischer, W., and Mecke, H. (2000). Welding arc control with power electronics. In *8th International Conference on Power Electronics*, number 475, pages 443–450.

[Shiba et al., 2011] Shiba, Y., Morishita, Y., Kaneko, S., Okabe, S., Mizoguch, H., and Yanabu, S. (2011). Study of d.c. circuit breaker of h2-n2 gas mixture for high voltage. In *Electrical Engineering in Japan*, volume 174, pages 9–17.

[Shimomura et al., 1995] Shimomura, N., Nagata, M., Grabowski, C., et al. (1995). Mechanism of unstable behavior of parallel fuses as an opening switch. *IEEE Transactions on Plasma Science*, 23(5):860–864.

[Shpanin, 2006] Shpanin, L. M. (2006). *Electromagnetic arc control for current interruption*. PhD thesis, University of Liverpool.

[Solver, 2002] Solver, C. (2002). Electric arcs and arc interruption. *Chalmers University of Technology, Gotenburg, Sweden, EEK*, 195.

[Spencer, 1987] Spencer, J. (1987). *Some Investigations of the Behaviour of a Rotating Arc Discharge*. PhD thesis, University of Liverpool.

[Spencer, 2012] Spencer, J. (2012). Private Communication.

[Tanaka, 2004] Tanaka, Y. (2004). Two-temperature chemically non-equilibrium modelling of high-power ar–n2 inductively coupled plasmas at atmospheric pressure. *Journal of Physics D: Applied Physics*, 37(8):1190.

[Tanaka, 2005] Tanaka, Y. (2005). Influence of copper vapor contamination on dielectric properties of hot air at 300-3500 k in atmospheric pressure. *IEEE Transactions on Dielectrics and Electrical Insulation*, 12(3):504–512.

[Tanaka et al., 2005] Tanaka, Y., Numada, T., Kaneko, S., and Okabe, S. (2005). Thermodynamic and transport properties of arcs thermal plasmas with polymer ablated vapors and influence of their inclusions on plasma temperature. *Journal Series B: JSME International*, 48(3):417–424.

[Tanaka et al., 2008] Tanaka, Y., Takeuchi, Y., Sakuyama, T., Uesugi, Y., Kaneko, S., and Okabe, S. (2008). Numerical and experimental investigations on thermal interaction between thermal plasma and solid polymer powders using induction thermal plasma technique. *Journal of Physics D: Applied Physics*, 41(2):025203.

[Tekletsadik and Campbell, 1995] Tekletsadik, K. and Campbell, L. C. (1995). Optical fibre investigation of the arc dynamics of a spiral arc current limiting interrupter. In *IEE Proceedings- Generation, Transmission and Distribution*, volume 142, pages 608–612. IET.

[Tuma, 1980] Tuma, D. (1980). A comparison of the behavior of sf6 and n2 blast arcs around current zero. *IEEE Transactions on Power Apparatus and Systems*, (6):2129–2137.

[Uchii, 2011] Uchii, T. (2011). Private Communication.

[Von Engel, 1983] Von Engel, A. (1983). Electric plasmas-their nature and uses. *London, Taylor and Francis, Ltd., 1983, 254 p.*, 1.

[Yan et al., 2004] Yan, J. D., Zhang, J. L., Kweon, K. Y., Dixon, C. M., and Fang, M. T. C. (2004). Computer simulation of high voltage circuit breakers. In

The XVth International Conference on Gas Discharges and their Applications, Toulouse, France, pages 1025–1034.

[Zhang et al., 2002] Zhang, J., Yan, J., Murphy, A., Hall, W., and Fang, M. (2002). Computational investigation of arc behavior in an auto-expansion circuit breaker contaminated by ablated nozzle vapor. *IEEE Transactions on Plasma Science*, 30(2):706–719.